Scaling relations between structure and rheology of ageing casein particle gels

Michel Mellema

Promotoren:	dr. ir. P. Walstra emeritus hoogleraar in de Zuivelkunde
	dr. E. van der Linden hoogleraar in de Fysica en fysische chemie van levensmiddelen
Co-promotoren:	dr. ir. T. van Vliet universitair hoofddocent bij Levensmiddelenleer, department Agrotechnologie en voedingswetenschappen
	dr. J. H. J. van Opheusden universitair docent bij de sectie Wiskunde

Scaling relations between structure and rheology of ageing casein particle gels

Michel Mellema

Proefschrift
ter verkrijging van de graad van doctor
op gezag van de rector magnificus
van Wageningen Universiteit,
dr. ir. L. Speelman,
in het openbaar te verdedigen
op vrijdag 10 november 2000
des namiddags om half twee in de Aula

The study presented in this thesis was part of the European Union project FAIR CT96-1216, on 'Structure, Rheology and Physical Stability of Aggregated Particle Systems containing Proteins and Lipids' and was performed at Wageningen University, Food Physics Group, which participates in the Graduate School Food Technology, Agrobiotechnology, Nutrition and Health Sciences (VLAG), accredited by the Royal Netherlands Academy of Arts and Sciences (KNAW).

WAGENINGEN UNIVERSITY

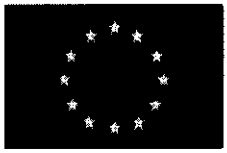

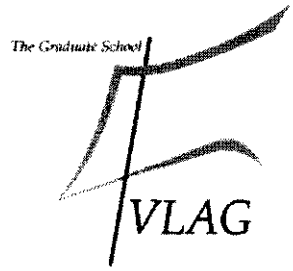

Mellema, M., 'Scaling relations between structure and rheology of ageing casein particle gels', PhD Thesis, Wageningen University, 2000
('Schalingsrelaties tussen structuur en reologie van verouderende caseïne-deeltjesgelen', proefschrift, Wageningen Universiteit)

140 + 12 pages, references by chapter, English and Dutch summaries

Keywords: colloid / structure / rheology / casein / rennet / gel / fractal / scaling / simulation / microscopy

ISBN 90-5808-302-0

Cover art: S. Mellema-Manschot
Sponsored by: ir. J. J. Manschot
Printed by: Universal Press, Veenendaal

Stellingen behorende bij het proefschrift 'Schalingsrelaties tussen structuur en reologie van verouderende caseïne-deeltjesgelen', Michel Mellema, Wageningen Universiteit, 10 november 2000.

1. Op basis van het werk van Fuchs is de geschiktheid van de naar hem genoemde parameter met betrekking tot de voorspelbaarheid van de fractale structuur van deeltjesgelen, verassend.
   - Fuchs, N.A.: *Z Phys* **89**, 736 (1934)
   - dit proefschrift, hoofdstuk 2

2. Bos heeft onvoldoende aandacht besteed aan het belang van de keuze van de grijswaarde-drempel voor de waarde van de fractale structuurparameters afgeleid uit confocale microscopie-plaatjes.
   - Bos, M.T.A.: *PhD Thesis*, WAU (1997)
   - Thill, A. *et al.*: *J Coll Interf Sci* **204**, 357 (1998)
   - dit proefschrift, hoofdstuk 3

3. Hoewel de afleidingen van de schalingsrelaties van Shih *et al.* en Bremer verschillen, is het resultaat identiek.
   - Shih, W. H. *et al.*, *Phys Rev A* **42**, 4772 (1990)
   - Bremer, L. G. B.: *PhD Thesis*, WAU (1992)
   - dit proefschrift, hoofdstuk 4

4. Het stadium van veroudering van met leb gestremde caseïnegelen is gerelateerd aan de gemiddelde grootte van de compacte bouwstenen van het gel.
   - dit proefschrift, hoofdstuk 5

5. De veelvuldig gebruikte 'verklaring' voor het aggregeren van para-caseïnemicellen in termen van het opheffen van repulsie, is geen verklaring.

6. Het gebrek aan algemeen aanvaarde definities van de begrippen 'gelpunt' en 'zwichten' werkt remmend op het ontwikkelen van reologische inzichten.

7. De populariteit van het gebruik van fractale modellen voor de beschrijving van de relatie structuur-reologie van deeltjesgelen wordt mede veroorzaakt door de afwezigheid van alternatieven.

8. De interpretatie van grensvlakreologische metingen is moeilijker dan die van bulkreologische.

9. De dimensionaliteit van de weg die een persoon aflegt in een drukke winkelstraat, is gerelateerd aan zijn/haar persoonlijkheid en niet aan fysische wetten.

10. Besturen om te besturen levert niet de beste sturing.

11. Een ultieme consequentie van het doel om steeds meer water en lucht in levensmiddelen te verwerken, is het 'vluchtig toetje'.

Abstract

The relation between (colloidal) interactions, structure and rheology of particle gels is discussed, with emphasis on the properties and the spontaneous ageing behavior of rennet-induced casein(ate) or skim milk gels.

Methods involved were Brownian dynamics simulations, confocal microscopy, permeametry and rheometry (large- and small deformations). A categorization of relevant (fractal) scaling models and types of structural rearrangements (particularly those affecting the rheological properties) for particle gels has been made, and applied to experimental data of rennet-induced casein gels.

Using Brownian dynamics simulations, the relation between colloidal particle interactions and gel structure was obtained. The simulation model used, included a repulsive barrier between the particles; the bonds formed were irreversible. The aggregation was delayed by a long-range repulsive barrier, and a high fractal dimensionality of the gels (2.4-2.5) resulted. This value was independent of the details of the interactions and volume fraction of particles in the range of 3-10 vol% particles. The simulation results agreed well with experimental results on rennet-induced aggregation and gelation in skim milk.

The (fractal) structure of rennet-induced casein gels, as studied by confocal scanning laser microscopy and permeametry was monitored during aging, at various pH values (5.3-6.65) and temperatures (20-30°C). At low pH, a gradual coarsening of the structure was observed; the size of the pores and compact structures increased. This was reflected in a decrease in apparent fractal dimensionality (from 2.4 to 1.7), and in an increase in pore size and lower cut-off length of the fractal regime (from 0.5 to 1.5 μm).

A scaling model was developed for the rheological behaviour of particle gels as a function of structure and particle volume fraction. The main structural parameters are the fractal dimensionality, the size of the compact building blocks and two parameters describing the number of deformable links in the strands and the dominating type of deformation of these links. Application to rheological data (storage modulus, maximum linear strain, yield stress) as a function of volume fraction (5-9 vol%) showed that rennet-induced casein gels contain straight, elastic strands.

Application of the model to results of measurements of the storage modulus during ageing, showed that at low pH rearrangements induce a dramatic increase in compact building block size and early disappearence of the fractal structure. It is concluded that the main types of rearrangements in rennet-induced casein gels after gelation, are particle fusion and stretching and breaking of strands.

Contents

No single thing abides; but all things flow.
Fragment to fragment clings - the things must grow
Until we know and name them. By degrees
They melt, and are no more the things we know.

Titus Lucretius Carus (Roman Poet, 99/94-55 BC)
translated by W.H. Mallock, 1900

Chapter 1

Introduction

1.1 Aim of this study

Structure and rheological properties of complex gel systems, which are found e.g. in foods, paints and sludges, are well described. However, the understanding of the relationship between these two and their changes in time (ageing), is insufficient. The main complicating factor is that several parameters, like pH, temperature, and concentration of salts, enzymes and other agents, affect the structure and rheological properties at a wide range of length and time scales.

In the case of food gels, understanding of the relationship between structural and rheological properties and their changes in time, may help to control texture. Texture is considered here to include both perceivable inhomogeneities as well as rheological and fracture properties. It relates primarily to eating characteristics, and affects manufacture, eating properties and physical ageing (shelf-life).

In this thesis, relations between structure and rheology of ageing rennet-induced casein particle gels are discussed. The reason for chosing casein gels is that they serve as a model example of complex particle gels, which are important for the food industry. These gels are studied as a function of pH, temperature and volume fraction of casein. Their rheology is determined by properties of structural elements at a range of length scales, from the macroscopic length scales down to the internal (molecular) structure of the particles (*i.e.* the 'casein micelles') themselves.

The structure-rheology relations obtained can in principle help to improve manufacture and quality of dairy products like cheese and quarg. Moreover, a major part of the conclusions are of a generic nature.

The thesis contains four main chapters. Figure 1.1 gives a general overview of the whole thesis in terms of the main aspects studied (particle-particle interactions, aggregate and gel matrix structure, and macroscopic rheology) and the main tools to study these aspects as a function of time (rheometry, confocal microscopy, computer simulations and scaling theory).

In sections 1.4-1.7 an introduction to the subject of each of the above chapters is given. First a short introduction is given to the experimental system (1.2) and to the concept of fractal aggregation (1.3), which is often used in this thesis.

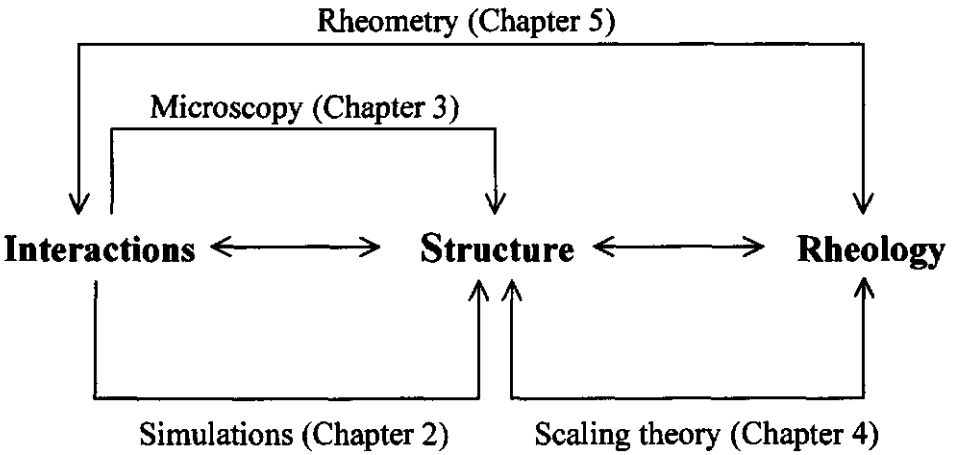

Figure 1.1. General overview of the thesis in terms of its main aspects (bold) and tools used.

1.2 Casein gels

This section gives an introduction on (the formation of) rennet-induced casein particle gels.

The fact that casein in milk is not present in solution but in micelles has important consequences for the properties of milk and any products derived from milk. For overviews more specifically centred on the properties of casein micelles, see Walstra (1990), Dalgleish (1998), Holt and Horne (1996). Almost all caseinate in fresh uncooled milk is present in approximately spherical particles of 40-300 nm in diameter (Note: the term 'caseinate' means 'casein in the ionic form', *i.e.* including counterions. From now on, the term 'casein' will be used for both casein and caseinate). On average, the micelles comprise approximately 10^4 casein molecules, of which κ-casein mainly resides at the surface. The casein micelles also contain inorganic matter, mainly micellar or colloidal calcium phosphate (MCP or CCP). The CCP plays an important part in the internal stability of the micelles. The micelles are voluminous, holding approximately 60% water. The surface has a negative charge. This, combined with the hairy layer formed by the C-terminal parts of the κ-casein molecules, makes the micelles electrostatically and sterically protected against aggregation.

In the first stages of cheese making, the main component of the rennet, chymosin, cuts off the C-terminal part of the κ-casein, thereby removing the protective hairy layer ('brush') on the casein micelles (rennet activity: **stage 1**). Casein micelles after renneting are called para-casein micelles. As a result, attractive interactions cause these micelles to aggregate (aggregation: **stage 2**). As the aggregates grow, they will ultimately touch, a network of particles fills all space available and a gel is formed (gelation: **stage 3**). The structure of the aggregates and the gel network may change in time (rearrangements: **stage 4**), until eventually the gel matrix shrinks and liquid is expelled (syneresis: **stage 5**). A schematic representation of the stages is shown in figure 1.2.

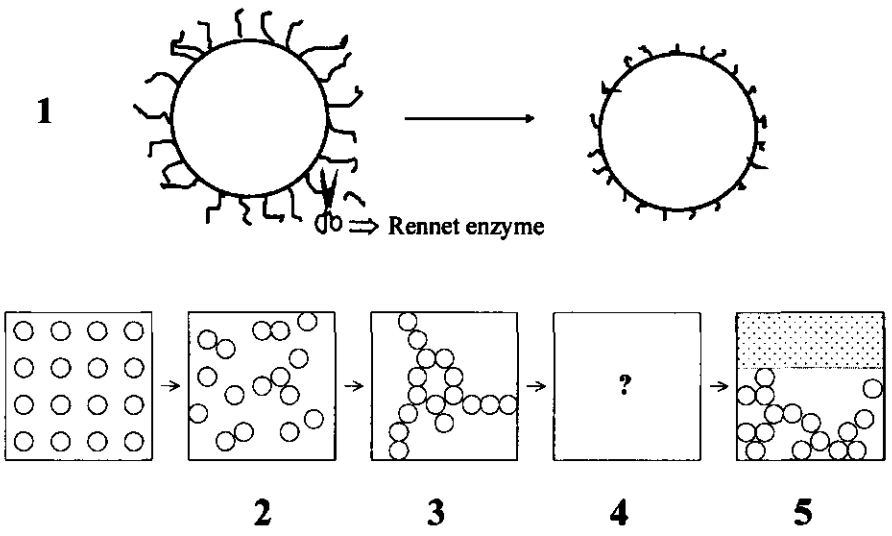

Figure 1.2. Model sequence of events during gelation. (1) Cutting off 'hairs' → electrostatic and steric repulsion decreases, (2) aggregation, (3) full gelation as large clusters form a continuous network, (4) microstructural rearrangements and (5) syneresis. The hairs are not drawn to scale: in reality they are much smaller and are present at a much higher number density.

The structural changes as a result of rearrangements (stage 4) are mostly unknown. Stage 4 is the one this thesis will mainly deal with.

The early stages or processes shown in figure 1.2, are illustrated in figure 1.3.

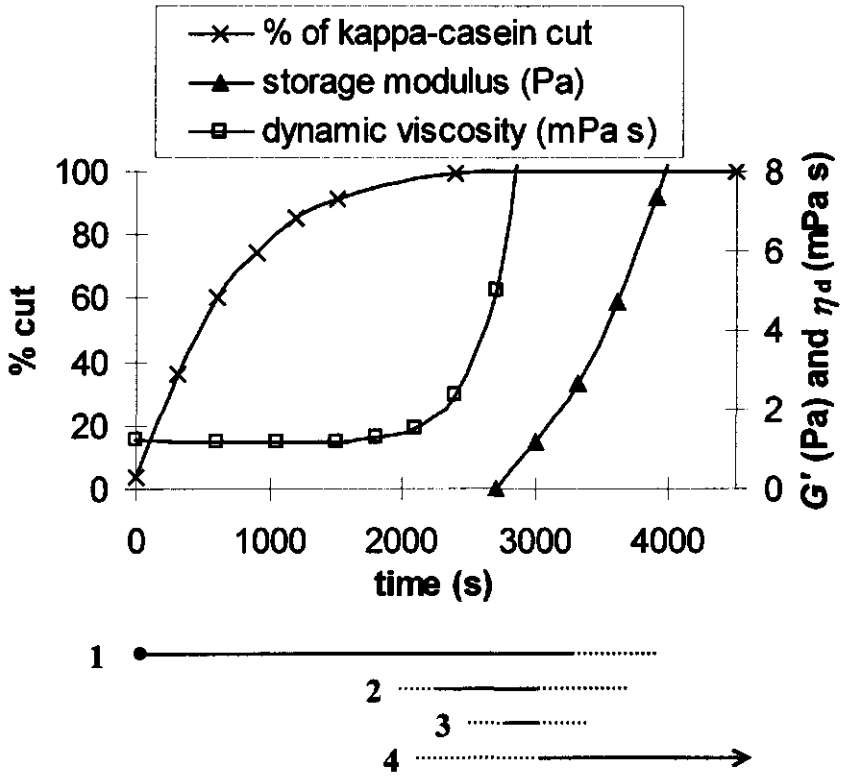

Figure 1.3. Scheme of events taking place during the renneting (0.02 vol%) of an average sample of skim milk at 30°C and pH = 6.65. Shown are the storage modulus G', dynamic viscosity η_d and % of κ-casein cut. Taken from Mellema *et al.* (1999). For explanation of numbers, see figure 1.2.

With respect to stage 2, van Hooydonk and Walstra (1987) showed that considerable repulsive forces remain present even after complete cutting of the hairs. This results in slow aggregation.

Besides by cutting the hairs using rennet, aggregation can also be induced by adding acid (which decreases the electrostatic potential of the particles, causing a collapse of the hairy layer) or ethanol (which decreases solvent quality, presumably leading to a collapse of the hairy layer). The attractive forces during aggregation probably result from calcium (Walstra (1990)), and casein (Mellema *et al.* (1999)) mediated bridging, and hydrophobic interactions. Van der Waals forces are insufficient to account for the attraction during aggregation (Payens (1979)).

1.3 Fractal aggregation

The particle aggregates that are formed during the aggregation of colloidal particles, can be considered *fractal* if the geometry is scale-invariant, which implies that the structure is similar when viewed at a reasonably large range of magnifications. Best known are the so-called deterministic fractals, *i.e.* fractals that can be described using a constant algorithm. Such very regular structures are rarily found in real life. Particle gels, like casein gels, can have *stochastic* fractal features over a certain range of length scales. These features are a product of the random Brownian motion involved in the aggregation. Scaling relations apply to both types of fractals. In the present case, the 'fractal scaling regime' holds approximately over a length scale between the size of the particles (a) and the size of the cluster (R). The following equation applies:

$$N = \left(\frac{R}{a}\right)^{D_f}, \qquad (1.1)$$

where N is the number of particles in the aggregate and D_f is the fractal dimensionality.

Fractal aggregation in relation to particle gels in general, and to casein dispersions in particular, has been thoroughly discussed by *e.g.* Bremer (1992) and Bos (1997) and references therein. Bremer *et al.* (1989) were the first to point to the formation of fractal (hence tenuous) aggregates, as a prerequisite for the formation of a space-spanning network.

The fractal nature of casein particle gels allows application of so called *scaling* theory. This thesis discusses the consequences and limitations of such scaling analyses.

1.4 Simulations

Chapter 2 deals with the results of Brownian dynamics (BD) simulations of aggregation. The effect of colloidal particle interactions on aggregate structure during formation of the gels was studied. The simulations were tuned to give an accurate description of fresh casein particle gels, taking the fairly high fractal dimensionalities and slow aggregation rates found for this system into account.

Pioneering work on the subject of fractal aggregation studied by simulation was performed by Meakin (1988). He fully discussed the differences between various types of simulation algorithms (ballistic,

diffusion-limited, reaction-limited, cluster-cluster types of simulations). The applicability of a combination of fractal concepts and simulations for engineers was discussed by Dickinson (1990). He also developed a (2D) Brownian dynamics simulation model to study the effect of interactions on aggregate structure (see *e.g.* Dickinson (1994)). A similar simulation model in three dimensions was tested for various types of interactions by Bijsterbosch *et al.* (1995) and Bos (1997).

The state-of-the-art in simulating particle gels was recently discussed by Dickinson (2000). In the near future, most progress on the subject of (fractal) aggregation and formation of particle gels can be expected from computer simulations. Scientists are especially looking forward to realistic simulations of the rheological properties of particle gels and suspensions, of which those by Whittle and Dickinson (1997) and Lodge and Heyes (1999) are a first attempt.

1.5 Microscopy

In Chapter 3 structural changes of rennet-induced casein gels during aging, as observed by confocal scanning laser microscopy (CSLM) and permeametry, are discussed. A fractal approximation was applied to the results. Parameters varied include pH and temperature. The structural aging effects as given in this chapter, are related to changes in *e.g.* storage modulus and maximum linear strain in chapter 5.

Microscopy is the most direct and therefore an obvious technique for studying particle gels. Transmission electron microscopy was applied to rennet–induced casein gels by Knoop and Peters (1975). The high resolution of this technique, allowed direct visualization of the (aggregated state) of the paracasein micelles. Scanning electron microscopy gives a more complete impression of the 3D structure of a gel matrix. Recent examples include a study on acid casein gels by Lagoueyte *et al.* (1994). In these electron microscopy studies, particle fusion effects have been observed.

At the end of the 1980s, confocal scanning laser microscopy (CSLM) was introduced. Even though the optical aspects of this technique were already known for decades, the full development was made possible by computer-directed laser beams and computer-mediated image analysis. The first CSLM on casein gels was performed by Bremer (1992), who showed that these gels have a fractal structure with relatively high dimensionality. Bos (1997) developed a deconvolution scheme to obtain a higher resolution of confocal images. This is especially important if the fractal structures of interest are small. Thill *et al.* (1998) showed that the choice of gray scale threshold is also very important in determining fractal parameters. Bremer

(1992) and Auty *et al.* (1999) were among the first to study the ageing of casein gel structures using CSLM.

1.6 Scaling theory

In chapter 4 a simplified version of existing scaling models is presented which relates the structure of particle gels to their rheology. In the model, the gels contain stress-carrying strands with a certain flexibility and curvature. A variety of possible scaling exponents is categorized. During aging of a gel, the appropriate scaling exponent can change. In this way, a scaling model can be a helpful tool in determining structural rearrangements, which is done in chapter 5.

Scaling modeling of the rheological properties of particle gels is not widely used among food engineers. One reason for this is the high complexity of the gel structures found in e.g. foods and paints. The other reason has to do with the relatively high complexity of the models presented in the literature.

One of the first scaling models suitable for describing the rheology of particle gels was given by Kantor and Webman (1984). They identified a relation between the structure of a random chain of elements and its elasticity and conductivity. Later, Shih *et al.* (1990) showed that practical systems can be found that obey the scaling laws incorporating two extreme values of the scaling exponents. At this point, fractal scaling was explicitly incorporated into the Kantor and Webman model. Recent applications of this model to complex protein gels include those by Ikeda *et al.* (1999).

At about the same time, Bremer (1989, 1992) developed an alternative fractal scaling model, that showed the existence of two intermediate scaling exponents that were considered relevant for casein gels.

1.7 Rheometry

In Chapter 5 the results of rheometry are presented. By combination of the experimental data with structural data from chapter 3 and the scaling model of chapter 4, information can be obtained on rearrangements taking place during aging of rennet-induced casein gels. A systematic overview or categorization of types of rearrangements is made, which accounts for the large diversity of rearrangements involved in the aging of particle gels in general. Emphasis is placed on rearrangements after gelation.

Although the importance of the dynamic nature of the structure of particle gels has fully been recognized for decades now, quantitative studies of the non-equilibrium or transient structure of particle gels are still rather

difficult. This is mainly because of the large number of parameters that are involved.

'Transient' (see a review by Poon (1998)) is a term mainly used for gel structures that are (temporarily) formed by reversible aggregation. The same thermodynamical considerations cannot be used to describe the breakdown of gels formed by irreversible aggregation. These gels do not change their structure by reversibility of particle-particle junctions, but by flexibility of these junctions or by deformation of the particles themselves. We use the term 'rearrangements' for all types of changes that lead to distinct changes in the structure and rheology of aging particle gels, including those formed by irreversible aggregation.

For most particle gels, the final consequence of (coarsening) rearrangements is endogenous syneresis, i.e. the spontaneous separation of liquid due to shrinkage of the gel matrix. For casein gels, relations have been identified between changes in pore size (van Dijk and Walstra (1986)) and rheological properties like tan δ (van Vliet *et al.* (1991)) with the rate of syneresis.

An interesting theoretical approach to the transient behavior or 'collapse' of particle (or emulsion) gels is given by Tanaka (1999). He introduces a simple mathematical desciption of the lifetime of a gel in terms of the competition between cluster growth and phase separation.

Knowledge obtained on the exact nature of the rearrangements will allow a more direct 'tuning' of the rearrangements. For casein gels, tuning can be achieved *e.g.* by adding certain agents to the milk, like carrageenan, calcium, formic acid, EDTA etc. A recent example of such tuning is the addition of crosslinking enzymes to milk prior to yogurt formation, by Lorenzen *et al.* (1999). Action of microbial transglutaminase was shown to increase gel firmness and reduce syneresis. Another option is a special pretreatment of the milk. High pressure- or heat-treatment of milk prior to rennet addition, increases gel firmness.

1.8 References

Auty, M. A. E.; Fenelon, M. A.; Guinee, T. P.; Mullins, C.; Mulvihill, D. M., "Dynamic confocal scanning laser microscopy methods for studying milk protein gelation and cheese melting," Scanning **21**, 299 (1999).

Bijsterbosch, B. H.; Bos, M. T. A.; Dickinson, E.; van Opheusden, J. H. J.; Walstra, P., "Brownian dynamics simulation of particle gel formation: from argon to yoghurt," Faraday Discuss **101**, 51 (1995).

Bos, M. T. A., "The structure of particle gels as studied with confocal microscopy and computer simulations," , PhD Thesis, Wageningen Agricultural University (1997).

Bremer, L. G. B., "Fractal aggregation in relation to formation and properties of particle gels," , PhD Thesis, Wageningen Agricultural University (1992).

Bremer, L. G. B.; van Vliet, T.; Walstra, P., "Theoretical and experimental study of the fractal nature of the structure of casein gels," J Chem Soc Faraday Trans 1 **85**, 3359 (1989).

Dalgleish, D. G., "Casein micelles as colloids: surface structures and stabilities," J Dairy Sci **81**, 3013 (1998).

Dickinson, E., "Particle gels," Chem Ind **1 Oct**, 595 (1990).

Dickinson, E., "Computer simulation of particle gel formation," J Chem Soc Faraday Trans **90**, 173 (1994).

Dickinson, E., "Structure and rheology of simulated gels formed from aggregated colloidal particles," J Coll Interf Sci **225**, 2 (2000).

Holt, C.; Horne, D. S., "The hairy casein micelle: evolution of the concept and its implications for dairy technology," Neth Milk Dairy J **50**, 85 (1996).

Ikeda, S.; Foegeding, E. A.; Hagiwara, T., "Rheological study on the fractal nature of the protein gel structure," Langmuir **15**, 8584 (1999).

Kantor, Y.; Webman, I., "Elastic properties of random percolating systems," Phys Rev Lett **52**, 1891 (1984).

Knoop, A.-M.; Peters, K.-H., "Structural changes of rennet curds during aging," Kieler Milchwirtschaftliche Forschungsberichte **27**, 315 (1975).

Lagoueyte, N.; Lablee, J.; Lagaude, A.; Tarado de la Fuente, B., "Temperature affects microstructure of renneted milk gel," J Food Sci **59**, 956 (1994).

Lodge, J. F. M.; Heyes, D. M., "Rheology of transient colloidal gels by Brownian dynamics simulation," J Rheol **43**, 219 (1999).

Lorenzen, P. C.; Mautner, A.; Schlimme, E., "Effect of enzymatic crosslinking of milk proteins on the resulting properties of yoghurt products," Kieler Milchwirtschaftliche Forschungsberichte **51**, 89 (1999).

Meakin, P., "Fractal aggregates," Adv Coll Interf Sci **28**, 249 (1988).

Mellema, M.; Leermakers, F. A. M.; de Kruif, C. G., "Molecular mechanism of the renneting process of casein micelles in skim milk, examined by viscosity and light-scattering experiments and simulated by model SCF calculations," Langmuir **15**, 6304 (1999).

Payens, T. A. J., "Casein micelles: the colloid-chemical approach," J Dairy Res **46**, 291 (1979).

Poon, W. C. K., "Phase separation, aggregation and gelation in colloid-polymer mixtures and related systems," Current Opinion Coll Interf Sci **3**, 593 (1998).

Shih, W. H.; Shih, W. Y.; Kim, S. I.; Lui, J.; Aksay, I. A., "Scaling behavior of the elastic properties of colloidal gels," Phys Rev A **42**, 4772 (1990).

Tanaka, H., "Viscoelastic model of phase separation in colloidal suspensions and emulsions," Phys Rev E **59**, 6842 (1999).

Thill, A.; Veerapaneni, S.; Simon, B.; Weisner, M.; Bottero, J. Y.; Snidaro, D., "Determination of structure of aggregates by confocal scanning laser microscopy," J Coll Interf Sci **204**, 357 (1998).

van Dijk, H. J. M.; Walstra, P., "Syneresis of curd: 2. One-dimensional syneresis of rennet curd in constant conditions," Neth Milk Dairy J **40**, 3 (1986).

van Hooydonk, A. C. M.; Walstra, P., "Interpretation of the kinetics of the renneting reaction in milk," Neth Milk Dairy J **41**, 19 (1987).

van Vliet, T.; van Dijk, H. J. M.; Zoon, P.; Walstra, P., "Relation between syneresis and rheological properties of particle gels," Coll Polym Sci **269**, 620 (1991).

Walstra, P., "On the stability of casein micelles," J Dairy Sci **73**, 1965 (1990).

Whittle, M.; Dickinson, E., "Brownian dynamics simulation of gelation of soft sphere systems with irreversible bond formation," Mol Phys **5**, 739 (1997).

Chapter 2

Relating colloidal particle interactions to gel structure using Brownian dynamics simulations and the Fuchs stability ratio*

2.1 Summary

Brownian dynamics simulations of aggregation of hard-sphere dispersions at intermediate volume fractions (φ ~3-10 vol%) have been performed. A long-range activation energy for aggregation was incorporated. The bonds formed were irreversible and flexible. Cluster growth rate and fractal properties of the gel matrix could be related to particle interactions by using a Fuchs stability ratio W_F. Although this approach is expected to apply only to the very early stages of gelation, W_F was shown to be a useful parameter, especially for predicting gel matrix parameters like the fractal dimensionality D_f (which is a measure of the 'compactness' of the clusters in the intermediate or fractal length scale regime) and the correlation length ξ (which is a measure of the average gel pore size). The number of aggregates, N_{agg}, was found to be a convenient measure of the stage of aggregation for the range of volume fractions and interactions studied. For high values of W_F, the value of D_f was more generic (i.e. less dependent on W_F or φ). In addition, the fractal parameters were less dependent on W_F at higher φ. These observations can be explained by the limited formation of (diffusion-kinetics type) depletion zones in the presence of repulsive barriers compared to purely attractive systems.

J Chem Phys **111**, 13, 6129 (1999)

2.2 Introduction

In recent years, several Brownian Dynamics (BD) simulation studies have been published on the formation and properties of particle gels [1-8]. The various studies differ with respect to the interaction potential used, the freedom for rearrangement, volume fraction *etc*. Here we present a study on aggregation and gelation of spherical particles at intermediate volume fractions (around 3-10 vol%), using a BD simulation model with short-range irreversible bonding and intermediate-range repulsive pair-interactions. We will focus on the effect of delayed aggregation due to an incorporated repulsive barrier for aggregation on the evolution of the fractal structure [3,9] of the aggregates and gel matrix, at different volume fractions. Even though in practical systems, *e.g.* casein gels, often a repulsive barrier at intermediate distances is present during aggregation, this aspect has not been thoroughly studied before.

The simulation results are compared to rennet-induced gelation of skim milk. In milk, casein particles are present which are protected against aggregation by a hairy layer comprising of the C-terminal ends of κ-casein molecules. The hairs can be 'removed' by rennet enzymes [10], and attractive forces become operative.

A gel is only obtained if the aggregation is irreversible or above a certain percolation threshold volume fraction [11]. For casein micelle gelation no threshold value can be found [12], hence the aggregation is probably largely irreversible. Aggregation rates found in casein dispersions and milk are low, probably because a 'hairy layer' remains even after renneting [13-15]. Subsequently the gel fractal dimensionalities are relatively high [16,9,17] (even higher than expected for reaction-limited aggregation [18]). It may thus be illustrative to incorporate (high) repulsive barriers in the simulations.

We will show that the Fuchs stability ratio [19] can be a useful parameter in predicting the fractal characteristics of the simulated gels. The relevant characteristics of the particle interactions can be approximated by this 'stickiness' parameter if only limited rearrangements are allowed. Furthermore, by pointing out some differences between results from the simulations and from experiments on milk gels, we will show the importance of gel matrix rearrangements.

2.3 Theory

2.3.1 Brownian dynamics model

The BD model is based on a Langevin-type equation of motion for each of the macroscopic particles with a fluctuating random force added to account for the thermal collisions of the solvent molecules with the particle. The solvent is considered as a continuum. We keep track of N hard-core spheres in a cubic box with edges set equal to R, using periodic boundary conditions. All parameters corresponding to sizes or distances are normalised to the radius of one spherical particle and all parameters corresponding to energies are normalised to units of kT.

The resulting force on a particle i, F_{res}, is given by the Langevin equation [20]

$$F_{\text{res}} = m\frac{\mathrm{d}^2}{\mathrm{d}t^2}r_i = \sum_j F_{ij}(r_{ij}) + R_i + H_i \qquad (2.1)$$

where t is the time, F_{ij} is the net force of interaction between the pair of particles i and j, R_i is the random (Brownian) force, H_i is the Stokes friction force acting on particle i and r_i is the position of particle i and r_{ij} is the relative position of particle i to particle j.

The particle pair-interactions (represented by F_{ij}) are described using a potential $u(r)$. The force F_{ij} is taken to be constant over a centre-to-centre distance $2.1 < r < D$

$$u(r) = \begin{cases} 0 & r \geq D \\ F_{ij}(r - D) & D_{\text{bond}} < r < D \\ 0 & 2 < r < D_{\text{bond}} \end{cases} \qquad (2.2)$$

where D_{bond} is the bonding distance (always set to 2.1) and D is the maximum interaction distance (ranging from 2.1 to 3.3). In this study, the parameter F_{ij} ranges from 0 to -25, implying the interactions are repulsive. Note that the hard core repulsion implies $u(r) = \infty$ that for $r < 2$.

Once a bond is formed it is irreversible. The points at which the bonds are attached to the particle surfaces are fixed and the angles between all bond attach-points on the same particle are fixed too. The relative particle motion is restricted such that the surface-to-surface bond length does not exceed the maximum specified bond length $D_{\text{string}} = 0.1$, but it can be less also, which gives a certain bond 'flexibility' (see ref. [8] or the appendix).

The liquid drag force, H_i, is proportional to the particle velocity

$$H_i = \frac{\mathrm{d}r_i}{\mathrm{d}t}\gamma \tag{2.3}$$

where $\gamma\ (= 6\pi\eta_0)$ is the Stokes drag and η_0 is the solvent shear viscosity. Note that the particle radius a = 1. Many-body hydrodynamic interactions are neglected.

Equation (2.1) is solved numerically to extract the movement of the particles, using a constant timestep Δt. We chose this Brownian timestep much larger than the relaxation time of the particle velocity, but small enough to ensure that the interaction forces do not change significantly during one timestep. Using the Euler forward method [20] to solve the remaining first-order differential equation, we arrive at

$$\Delta r_i(t+\Delta t) = \frac{\Delta t}{\gamma}\left(\sum_j F_{ij}(t) + R_i(t)\right) \tag{2.4}$$

The effect of the random force R_i is a translational displacement which, on the average, obeys Einstein's law for an isolated particle. For instance in the x-direction this gives us

$$\Delta x_i^{\mathrm{R}}(t+\Delta t) = N_{\mathrm{s}}\sqrt{6D_{\mathrm{c}}\Delta t} \tag{2.5}$$

where D_{c} (=$1/\gamma$) is the diffusion coefficient, which is normalised to 1. The parameter N_{s} is a uniform random number on (-1,1), so its variance is 1/3. The dimensionless root-mean-square displacement in the absence of interactions is $\langle|\Delta x_i^{\mathrm{R}}|\rangle = \sqrt{(2D_{\mathrm{c}}\Delta t)}$. For all simulations we fixed $\sqrt{(2D_{\mathrm{c}}\Delta t)}$ at 0.004, which is small enough also for the steeper potentials. If the number of particles is N, in one timestep $3N$ numbers corresponding to all three directions (x,y,z), are drawn. This means that we have uncorrelated distributions (i.e. no hydrodynamic interactions between the particles) for F_{ij} = 0. The number of steps which the simulation has passed, is given by $N_{\Delta t}$. The parameter $N_{\Delta t}$ is a direct measure of time.

Apart from the translational diffusion the individual particles also undergo rotational diffusion. The rotational motion is governed by a diffusion coefficient D_R. (particle radius a = 1, kT = 1)

$$D_R = \frac{3D_c}{4} \tag{2.6}$$

The implementation of the rotational diffusion is quite similar to that of translational diffusion, with small uniformly random rotations of each particle as to satisfy equation (2.6). Rotational diffusion of the clusters is generated by the different translations of the individual particles combined with the constraints. These constraints, both the hard core repulsion and the finite length strings, which may be violated by the particle displacements, are satisfied by a SHAKE-like procedure [20], iteratively running over all violated constraints, and removing these by moving and rotating the involved particles.

2.3.2 Aggregation kinetics*

Meakin [21] defined two types of aggregation which differ with respect to the 'probability of bonding' due to different particle interactions. In Diffusion-Limited Cluster Aggregation [22] (DLCA) each particle (or cluster) encounter leads to bonding. For Reaction-Limited Cluster Aggregation [18] (RLCA), there is a low chance of bonding (upon particle encounter) so on average a large number of particle encounters are needed for bonding.

A higher degree of reaction-limitation causes a delay in the aggregation process and the structures formed are usually more compact, i.e. have higher fractal dimensionality [23]. In order to quantify the relation between particle interactions and fractal gel structure, we introduce the Smoluchowski [24] and Fuchs [19] concept of the stability ratio W, which measures the effectiveness of a potential barrier in preventing colloidal particles from aggregating. The basic definition of W is given by Smoluchowski (for repulsive hard spheres)

$$W = \frac{\textit{average time for bonding with repulsion}}{\textit{average time for bonding without repulsion}} \tag{2.7}$$

The reciprocal of W (= $1/W$) is the sticking probability of the encountering particles. For our simulations, this theory can only be expected to apply to the first few aggregation steps or, equivalently, to a few times the time required for the number of separate particles to be reduced to half of the initial value. After this 'Smoluchowski-regime' the shape and dimensions of the aggregates formed will influence the rate of the ongoing aggregation.

*see also the appendix

According to Smoluchowski [24,25], the particle flux for dimerisation of a single pair of identical hard spheres equals

$$J_0 = 2aD_c\varphi \tag{2.8}$$

where φ is the particle bulk volume fraction. According to Fuchs [19,25], the particle flux for a single pair of identical spheres *with* a potential force between the particles equals

$$J = \frac{D_c\varphi}{\int_{2a}^{\infty} \frac{1}{r^2} e^{u(r)/kT} dr} \tag{2.9}$$

where r is the particle distance. The probability of bonding, which Fuchs originally called κ, equals J/J_0. We now introduce a Fuchs stability ratio $W_F=1/\kappa$:

$$W_F = 2a\int_{2a}^{\infty} \frac{1}{r^2} e^{u(r)/kT} dr \tag{2.10}$$

The integral can be approximated numerically for any shape of the repulsive barrier $u(r)$, defined by the value of the parameters F_{ij} and D (see ref. [8] or the appendix). In our case (equation (2.2)) the interaction force (F_{ij}) and range (D) are the important parameters, the bond length (D_{bond}) has only minor influence. This 'theoretical' W_F will be related to 'experimental' fractal parameters obtained from the simulations.

2.3.3 Power-law behavior

For an ideal fractal aggregate, the following scaling relation can be written [26,16]

$$\varphi_c = \left(\frac{R}{a}\right)^{D_f-3} \tag{2.11}$$

where φ_c is the density or volume fraction inside the aggregate of size R and D_f is the fractal dimensionality. A 3D homogeneous object would give $D_f = 3$, which means that φ_c is independent of cluster size. For $D_f < 3$ the density drops

with increasing cluster size. At the 'gel point' t_{gel} we assume $\varphi_c = \varphi$ and define $R = R_{gel}$. Rewriting equation (2.11) leads to

$$R_{gel} = a_{eff}\varphi^{\frac{1}{D_f - 3}} \tag{2.12}$$

where a_{eff} is a prefactor equal to an effective particle radius [12].

In experiments t_{gel} is roughly defined at the point at which the storage modulus G' is systematically larger than the loss modulus G''. The change of the actual R_{gel} with the bulk volume fraction φ is a central subject in the fractal analysis of rheological and permeability data [16,27].

The mass distribution of an object or an image of the object can be probed by evaluating a pair correlation function $g_2(r)$. In computer simulations all particle positions are known, so $g_2(r)$ is exactly defined. For estimating an effective D_f from the simulations, it is convenient to smooth out short-range oscillations in $g_2(r)$ by integration, leading to [3,9]

$$n \propto \tilde{n}\left(\frac{r}{2a}\right)^{D_f}; \qquad 2a \le r \le \xi \tag{2.13}$$

where n is the average number of particles within range r of another particle and ξ is the correlation length. The correlation length ξ is an important parameter because at t_{gel}, it should equal R_{gel}. The prefactor $\tilde{n}$ is defined as the effective average number of particles at $r = 2a$. The procedure of the linear fitting according to equation (2.13) is shown in figure 2.3, which is a plot of $\log(n)$ versus $\log(r)$ and shows how D_f, $\tilde{n}$ and ξ are derived.

The gel matrix is only fractal over a limited range of length scales. The parameter ξ is the upper cut-off length of the fractal regime (or the lower cut-off length of the homogeneous regime at large length scales; $D_f = 3$). In a dispersion of separate particle clusters ξ corresponds to the average cluster separation. In a gel matrix ξ corresponds to the average radius of the gel pores. The values of $\tilde{n}$ gives information on the compactness of the gel matrix at small length scales.

Scaling laws can also be applied to quantify the kinetics of the cluster growth. The kinetics of aggregation can be described by a simple scaling relation between the average radius of gyration R_g and the time t [4]

$$R_g \propto t^{\alpha} \tag{2.14}$$

where α is a constant depending on sticking probability and volume fraction. In theories on droplet coalescence, the value of α is predicted to be 1/3 (Lifshitz-

Slyozov) or 0.2 (Binder-Stauffer). Generally the exponent is in the range ~0.2-0.4. For diffusion-limited growth α equals $1/D_f$ and for reaction-limited growth $R_g \propto e^{\beta t}$, where β is a constant [28].

Assuming that ξ is proportional to R_g, we should be able to relate the parameter α to the Fuchs stability ratio W_F. In addition, if we define $\xi(t_{gel}) = R_{gel}$, we can derive how R_{gel} relates to W_F or the volume fraction and compare this to experimental results. Especially the relation between R_{gel} and φ is important in the fractal analysis (see equation (2.12)) of permeability or rheology data.

2.4 Results and discussion

Simulations have been performed for various values of D and F_{ij}. For each combination of D and F_{ij}, a value of W_F was calculated. Note that several combinations of D and F_{ij} can lead to the same value of W_F.

A value for W can be derived from the evolution of the total number of bonds in the system, N_{bonds}, with the number of timesteps $N_{\Delta t}$ ($N_{\Delta t}$ is proportional to the time), according to the method described earlier (see ref. [8] or the appendix). In that paper, we have also shown that W_F and W are equivalent. This supports the validity of the approach, at least in the early stages of aggregation.

At the start of a simulation, the total number of aggregates $N_{agg} = 1000$ and $N_{bonds} = 0$. During a simulation, N_{bonds} increases, N_{agg} decreases and subsequently the number of free (non-bonded) particles decreases (figure 2.1) and the average number of particles per aggregate increases (figure 2.2). From figure 2.1 we see that at $N_{agg} = 10$ the number of free particles is approximately zero. So any bonds formed after $N_{agg} = 10$, can be assumed to be inter- or intracluster. The figure also illustrates the generic behavior of the aggregation process, since the results of simulations of a variety of combinations of φ, F_{ij} and D ($\varphi = 0.034$ or 0.065, $W_F = 1$, 20 or 40) nearly coincide on a straight 'mastercurve' on a double log-scale.

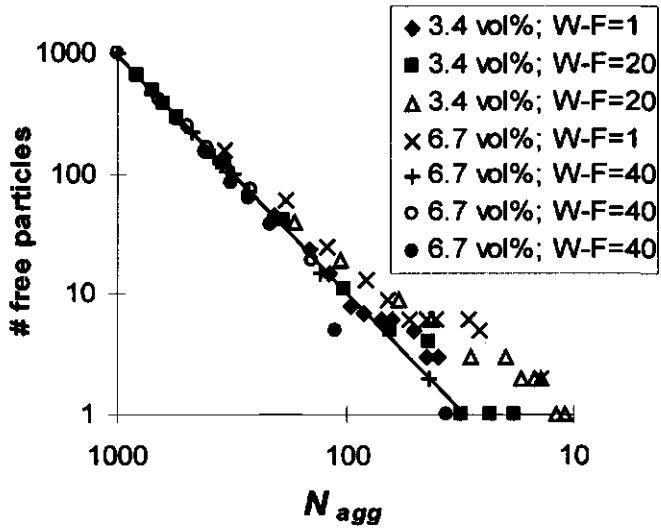

Figure 2.1. Number of free (non-bonded) particles as a function of the number of aggregates, N_{agg}, for several combinations of F_{ij} and D.

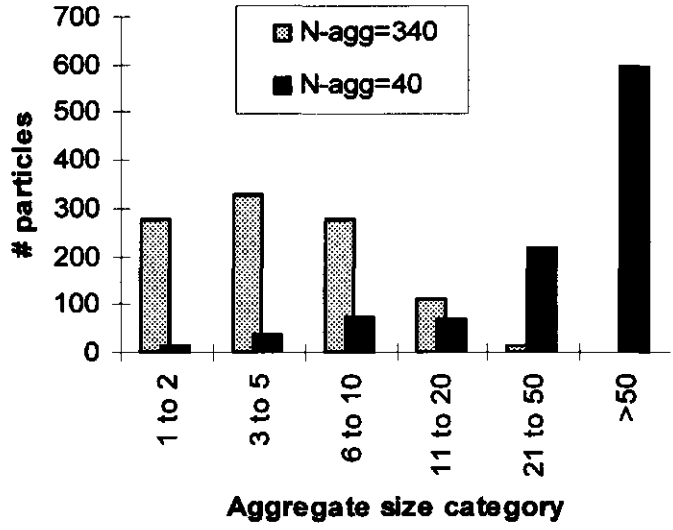

Figure 2.2. Size distribution of the average total number of particles in aggregates at two stages during aggregation (at N_{agg} = 340 and 40).

We clearly see from figure 2.2 that already at a stage at which N_{agg} = 340, most of the particles are in small aggregates of a size 3 to 5. This

presence of a limited amount of single particles during the aggregation process is certainly not unusual for cluster-cluster aggregation. Figure 2.2 is an average of the results of four simulations, namely $\varphi = 0.034$ ($W_F = 1$ and 20) and $\varphi = 0.065$ ($W_F = 1$ and 40); surprisingly, there was no systematic difference between these simulation results. Any difference in R_{gel} at different φ or W_F is probably due to the formation of more tenuous or dense aggregates, and not to a different distribution of the particles over the aggregates (see below). Both figures 2.1 and 2.2 suggest that the parameter N_{agg} is a good measure of the stage of aggregation for the full range of values of φ and W_F studied.

In figure 2.3 we give an example of the number density correlation function $n(r)$, to indicate how the fractal parameters were derived. Usually the simulated gel structures have a fractal regime over roughly half a decade. The size of the fractal regime decreases as φ increases, because the clusters are smaller at the moment a gel is formed.

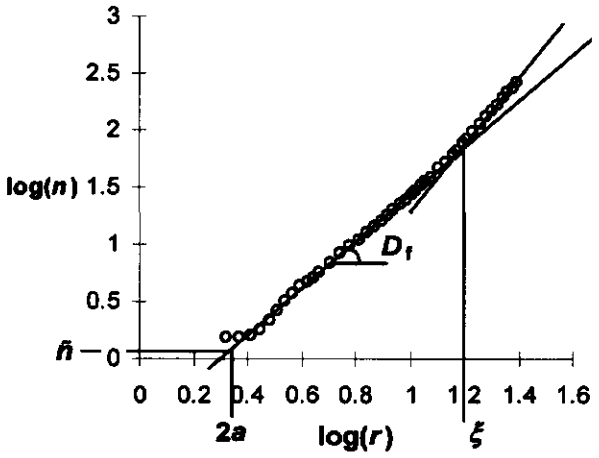

Figure 2.3. Example of a determined number correlation function $n(r)$, indicating how the fractal parameters are derived. Volume fraction $\varphi = 3.4$ vol%.

An example of the development of the parameters D_f, $\tilde{n}$ and ξ during a simulation (one simulation data set; $W_F = 1$, $\varphi = 0.034$) is given in figure 2.4. We see that D_f gradually decreases with the decrease in N_{agg}, while $\tilde{n}$ increases. The parameter $\tilde{n}$ can be smaller than 2, because it is derived by extrapolation from the fractal regime.

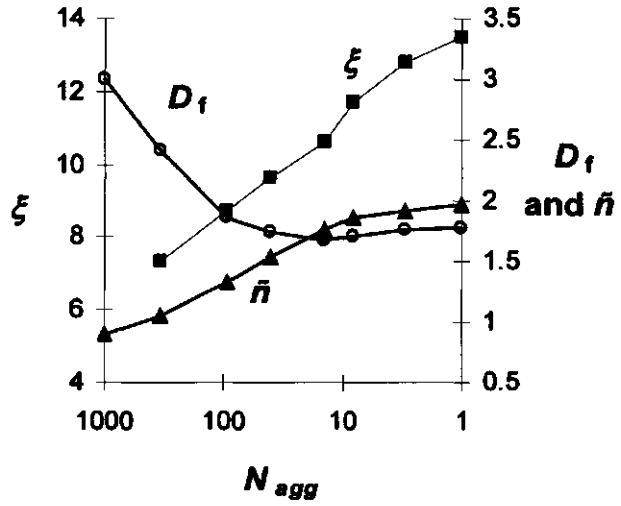

Figure 2.4. Evolution of D_f, $\tilde{n}$ and ξ at $W_F = 1$ and $\varphi = 0.034$.

The evolution of ξ with $N_{\Delta t}$ is shown in figure 2.5 on a log-log scale. It is clear that ξ increases with time. A value for α can be derived from each line (see below, figure 2.6), assuming that $\xi = R$. We found that a semilogarithmic plot ($\log(R_{gel})$ as a function of t, not shown) of figure 2.5 did not give a linear behavior. So the aggregate radius does not grow exponentially, as expected for pure RLCA [18].

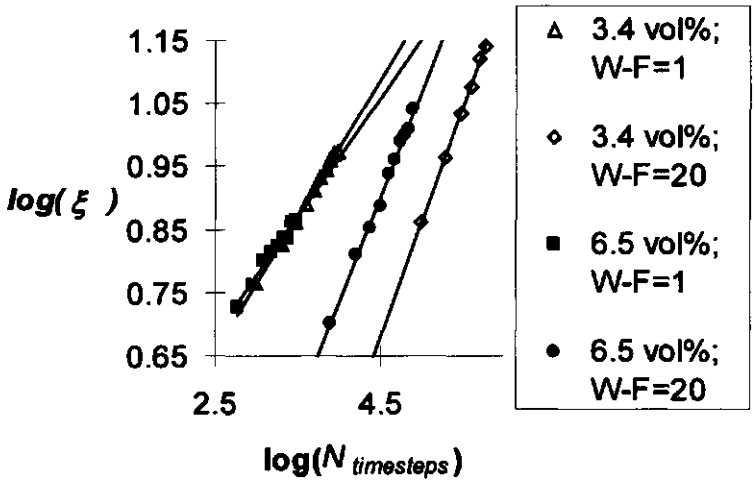

Figure 2.5. Log(ξ) as a function of log($N_{\Delta t}$) at $\varphi = 0.034$ (W_F=1 and 20) and $\varphi = 0.065$ (W_F=1 and 20). The slope is equal to α.

The relation between α and W_F (for several combinations of F_{ij} and D) is shown in figure 2.6, for three different values of the volume fraction. The values obtained for α do not systematically depend on φ and are in the same range as generally found. The parameters W_F and α are expected to be related, because the (early-stage) growth of the clusters as a function of time, should depend on an effective stickiness of the particles. However, from the figure this is not clear. Maybe, there is a leveling off of α at high values of W_F. The limit of $W_F \rightarrow 1$ corresponds to diffusion-limited behavior, so we can calculate a value of D_f according to $\alpha = 1/D_f$ [21]. This leads to irrealistically large values for D_f, indicating that our situation is more complicated. Interestingly, we see from figure 2.6 that α is independent of W_F, at high (9.8 vol%) values of φ. The reason for this may have to do with limited formation of depletion zones at high φ, which we will discuss later.

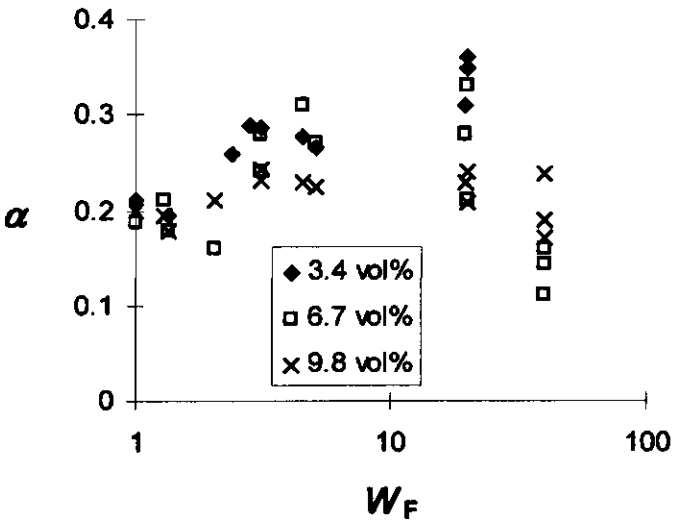

Figure 2.6. The cluster growth exponent α as a function of W_F, at different volume fractions. Each data point corresponds to one simulation. Several combinations of F_{ij} and D were tested.

In figures 2.7a and 2.7b we show projected images of the resulting structure of simulations performed at respectively $W_F = 1$ and $W_F = 20$. In both cases $N_{agg} = 10$. Usually more than 90% of all particles are part of the largest aggregate at this stage of the aggregation process, so we speak of a gel. The images are projections along the z-axis. Shading is used as depth cueing. For more clear visualization, the particles are depicted at half their original size and a link is shown where a bond is present. The most clear difference between the images is that the pores in the gel seem larger at $W_F = 20$, which

is confirmed by a higher value of ξ. The two systems also have distinctly different D_f, but this is less clear from the image, probably because the fractal regime is relatively small.

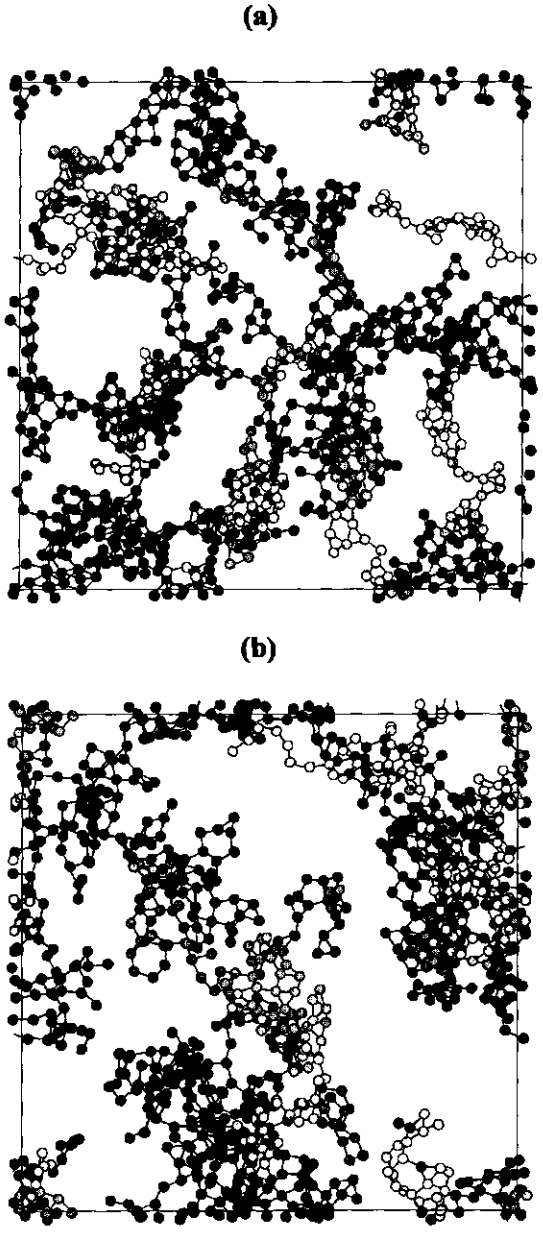

Figure 2.7. Projected images of simulated gels: (a) $W_F = 1$; $D_f = 1.7$; $\xi = 11.5$ and (b) $W_F = 20$; $D_f = 2.1$, $\xi = 22.3$.

In figure 2.8, the value of D_f at $N_{agg} = 10$ is plotted against W_F for three different volume fractions. Each data point corresponds to one simulation with a certain value for D and F_{ij}. As we saw before [8], D_f is related to W_F. At high W_F, D_f is systematically larger. At $W_F > 5$ we see a leveling off of the curve. Important to note is that in the interaction range studied, no systematic relation was found between the shape of the repulsive barrier and D_f. The fractal dimensionality D_f was not systematically higher or lower than the average behavior shown in figure 2.8, for e.g. short-range repulsion.

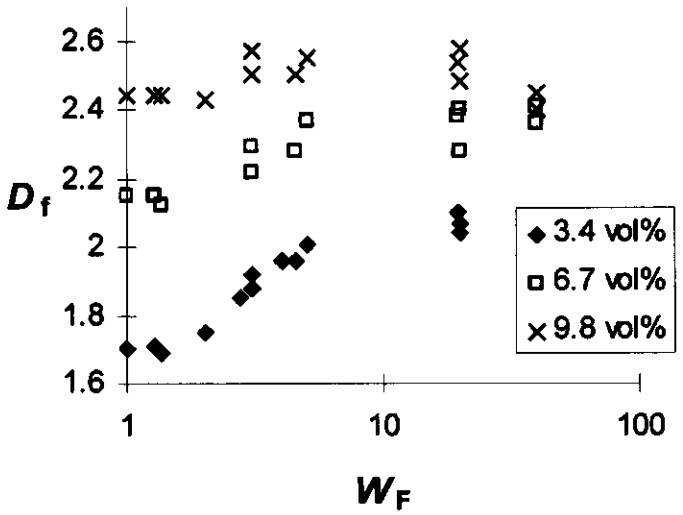

Figure 2.8. The fractal dimensionality D_f at $N_{agg} = 10$ as a function of W_F, at different volume fractions. Each data point corresponds to one simulation. Several combinations of F_{ij} and D were tested.

In figure 2.9, the value of ξ at $N_{agg} = 10$ ($\propto R_{gel}$) is plotted against W_F for three volume fractions. The correlation length ξ, and consequently R_{gel}, is larger at low φ, because gelation is reached at a later stage and the clusters are allowed to grow longer before they touch. In figure 2.9, we see a similar leveling off behavior as in figure 2.8. Not shown in the figure is that ξ is slightly higher for short-range repulsive barriers; i.e. most of the data points that are higher than the averages presented in figure 2.9, correspond to similations incorporating a relative small value for the interaction range D.

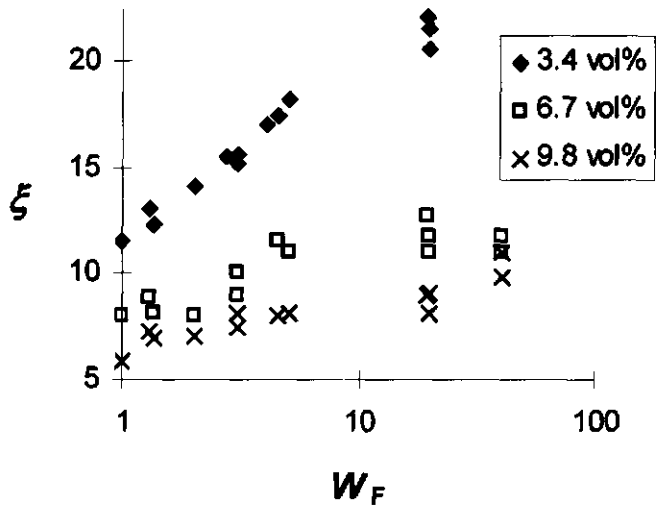

Figure 2.9. The cluster radius at gelation, R_{gel}, as a function of W_F, at different volume fractions. Each data point corresponds to one simulation. Several combinations of F_{ij} and D were tested.

The levelling-off behavior of figures 2.8 and 2.9 and the decreased dependency of D_f and ξ on W_F at high values of W_F (and high φ) may be due to a.) larger fractal regimes at high W_F (and high φ), and therefore more justified or accurate determination of these fractal parameters, or b.) the limited formation of 'depletion zones' around the clusters compared to purely attractive systems. Maybe at high W_F (and high φ) such depletion zones can hardly develop.

We do not mean depletion zones due to an (entropic) volume exclusion effect, but due to a (kinetic) diffusion gradient effect. We expect that above a certain level of aggregation delay, there would be no depletion zones anymore. Similarly, fractal theory is mean-field and may therefore only work properly if no strong density gradients are present at the surface of the clusters due to a reaction taking away particles (e.g. by aggregation) which is faster than the supply by diffusion. However, we have not checked explicitly for the existence of this type of depletion zones around clusters. Note that $n(r)$, which gives the average density distribution around fractal clusters, is always below the average bulk volume fraction φ near ξ, without showing clear depletion zones.

The decreased dependency of the fractal parameters on W_F at high W_F, means that if we want to simulate, for instance, casein gels that are formed at a much slower rate than according to fast Smoluchowski kinetics we probably

do not have to incorporate the correct (very high) value for W_F to obtain reliable results, at least for the structural parameters discussed above.

At high W_F, the clusters formed and the pores in the gel are larger, but $\tilde{n}$ only increases slightly (implying that D_f is larger). Consequently, we find that the fractal scaling region is larger. In fact, $\tilde{n}$ decreases by about 10% for W_F (1 $\rightarrow$ 20), and is especially low at high D. The latter observation is in accordance with results of Meakin [29]. The decrease with increasing φ (e.g. 0.034 $\rightarrow$ 0.098) is larger, namely by about 25% (data not shown). With increasing W_F, the structures are more tenuous at small length scales, and relatively homogeneous at intermediate (fractal) and large length scales.

We now define R_{gel} as the plateau value (i.e. at high W_F) of ξ at N_{agg} = 10. In figure 2.10, we plotted this R_{gel} as a function of φ. Also plotted are the values of ξ from CSLM experiments on acid casein gels [9], and a prediction using the fractal theory on R_{gel} according to equation (2.12), incorporating a_{eff} = 1. We clearly see that the simulation and experimental results both have a scaling behavior predicted by incorporating D_f = 2.1, which is a realistic value. In addition, the figure shows that ξ at N_{agg} = 10 is smaller than may be expected, but rougly proportional to ξ determined in a fully developed gel. In addition, a larger value for a_{eff}, which is more realistic for casein systems [30,31], leads to a much better agreement between theoretical and experimental data.

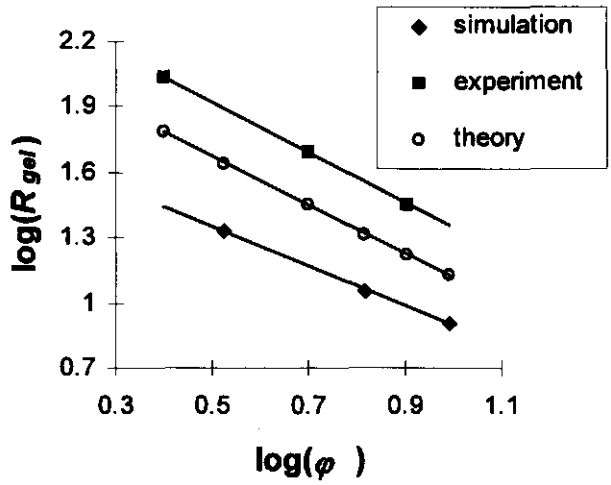

Figure 2.10. Simulated R_{gel} as a function of φ. Also shown are lines according to equation (2.12) and experiments [9].

In the simulations, rearrangements can only take place to a limited extent. This may account for differences in results between the simulations

and experiments on practical systems. In our simulations (and other studies [23]), rearrangements such as rolling or bending are accompanied by an increase in short-range compactness. Rheological and confocal experiments on rennet casein gels [17,31] show that extensive rearrangements induce syneresis and make the structures non-fractal, and this can not happen in the simulations. These aging effects occur especially at low pH and high T (i.e. high particle affinity) and to simulate it, we probably have to incorporate particle fusion and breakage of strands [32,33,31].

2.5 Conclusions

The cluster growth rate and the fractal properties of the gel matrix can be related to the particle interactions, by approximating the simulation activation energies by a Fuchs stability ratio W_F.

Although the Fuchs approach would only apply to the very early stages of gelation, W_F was shown to be a useful parameter to obtain gel matrix parameters like the fractal dimensionality D_f and the correlation length ξ. The fractal parameters D_f and ξ systematically increase with W_F.

Interestingly, for high values for W_F, the value of D_f was more generic (i.e. less dependent of W_F or φ), possibly due to the limited formation of (kinetic) depletion or density gradient zones, compared to purely attractive systems. This is confirmed by the observation that also ξ and the cluster growth time scaling exponent α, are less dependent of W_F at higher φ.

The distribution of the particles over the aggregates for the range of volume fractions and interactions studied was found to depend only on the number of aggregates, N_{agg}. We therefore conclude that the parameter N_{agg} is a good measure of the stage of aggregation, if we compare results of simulations at the same number of particles.

The results obtained cannot fully explain the behavior of rennet-induced casein gels and similar systems, probably because in this case other rearrangements than allowed in this study, like particle fusion and breaking of strands, are important in determining the final (fractal) structure.

2.6 Appendix: Aggregation kinetics*

In reaction-limited aggregation (RLA) a parameter P_{bond} is introduced that determines the propability that a bond is formed upon contact of the hard spheres. Only for very small P_{bond} one has real RLA. The parameter P_{bond} is always set to 1 in our simulations. Instead of a bonding probability we used a repulsive force of finite extent which has a similar but subtly different effect. In that sense the simulations are of RLA type, albeit with still rather high effective bonding probability. The interactions are schematically presented in figure 2.A1a. We show hard sphere particles diffusing translationally and rotationally. Interesting to notice is the difference between the effect of P_{bond} and u at the level of particle encounters, which is shown in figure 2.A1b. If one particle encounters a doublet, the effects of u will add up. The effect of P_{bond} is separate for both particles in the doublet. At the same 'bonding probability' a high u is expected to lead to more stringy structures than a low P_{bond}.

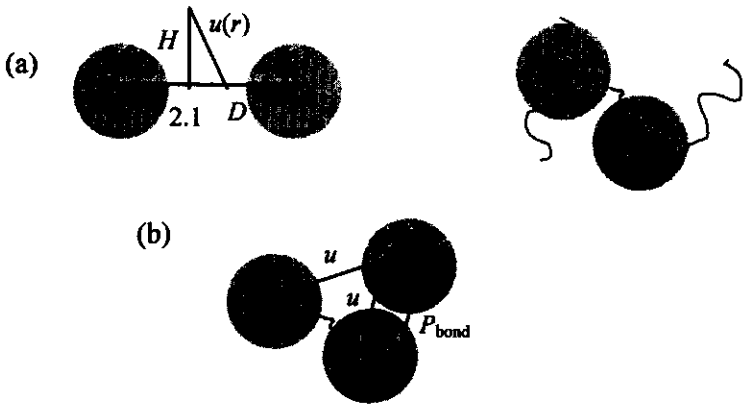

Figure 2.A1. (a) Schematic representation of the close encounter (left) and the resulting bonding (right) of two colloidal particles. (b) Representation of the close encounter of a doublet and a single particle. Arrows illustrate the difference in the effect of P_{bond} and $u(r)$.

Different bonding probabilities as a result of a repulsive barrier $u(r)$, lead to different stability ratios of the dispersion. In an actual simulation-'experiment', the stability ratio can be defined as:

* part of *Food emulsions and foams: interfaces, interactions and stability*, pages 176-191, Royal Society of Chemistry, Cambridge (1999)

$$W_S = \frac{\left(\frac{\delta N_{bonds}}{\delta N_{\Delta t}}\right)_{u>0}}{\left(\frac{\delta N_{bonds}}{\delta N_{\Delta t}}\right)_{u=0}} \qquad (2.A1)$$

where $\delta N_{\Delta t}$ is the 'time' elapsed since the zero point random configuration. The reciprocal W_S ($=1/W_S$) is a measure of the stickiness of the particles. For our simulations, the theory only applies to the first few aggregation steps or a few times the time required for the number of aggregates, N_{agg}, to be reduced to half of the initial value. In this approach, a single particle is considered an aggregate of radius 1. After this 'Smoluchowski-regime' the shape and dimensions of the aggregates formed influence the rate of the ongoing aggregation. Actually, the Smoluchowski theory deals with coalescence rather than aggregation. Hence the inapplicability of the theory to later stages in aggregation.

Fuchs modified Smoluchovski's theories for diffusion in a force field. The Fuchs ratio W for a single pair of particles, having an interaction potential $u(r)$, is given by equation (2.10). Rewriting this integral incorporating the potentials we used, leads to the theoretical Fuchs ratio of our system, W_F:

$$W_F = 2\int_{D_{bond}}^{D} \exp\left(H\left[\frac{D-r}{D-D_{bond}}\right]\right)\frac{dr}{r^2} + \frac{2}{D} + 1 - \frac{2}{D_{bond}} \qquad (2.A2)$$

where $H = F_{ij}(r = D_{bond})$. This integral can be approximated numerically for any given H and D and one can use this 'theoretical' W_F to compare to the 'experimental' W_S.

The Fuchs approach is one concept which describes the aggregation rate for hard core spheres in suspension. It is specifically only applicable to the early aggregation stage. There may be other parameters describing the rate at different stages during the aggregation process. As a comparison, we included the Boltzmann factor e^H and the quantity $(D - 2.1)\Delta H$ (the surface area of the potential) as a measure of the aggregation retardation in the discussion of our results. Note that quantities like $(D - 2.1)\Delta H$, W_F, and e^H are not equivalent. For instance, this means that two simulations can be done at the same ratio $(D - 2.1)\Delta H$, while $1/W_F$ is different and *vice versa.*

In a simulation the number of bonds N_{bonds} increases and the number of aggregates N_{agg} decreases with $N_{\Delta t}$. For several simulations this is shown in figure 2.A2. It is clear that incorporation of large repulsive forces decreases the initial rate of bonding. In the very early stage, the bonding rate is influenced by

the specific initial random configuration. After $N_{\Delta t}$=1000 the shape and dimensions of the aggregates formed start to influence the bonding rate.

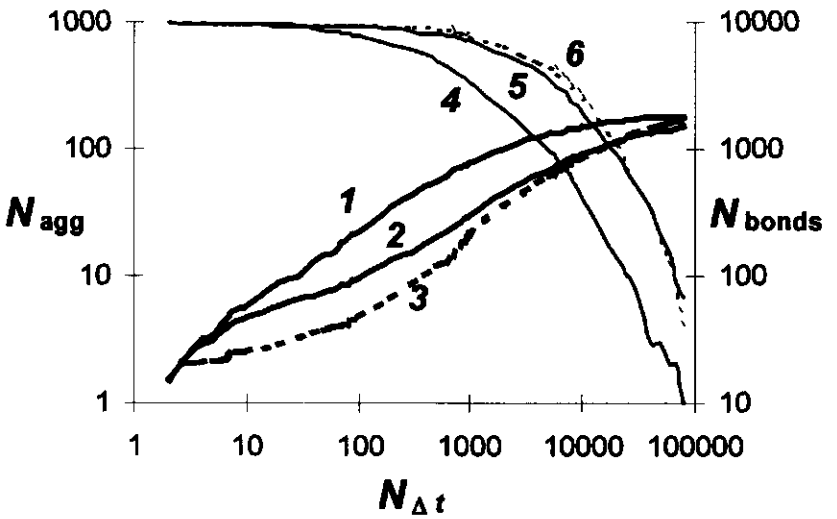

Figure 2.A2. The quantities N_{agg} and N_{bonds} as a function of $N_{\Delta t}$ for three simulated systems. (1) N_{agg}; $W_F = 1$, (2) N_{agg}; $W_F = 2.4$, $D = 3$, $H = 2.7$, (3) N_{agg}; $W_F = 2.4$, $D = 2.4$, $H = 3.9$, (4) N_{bonds}; $W_F = 1$, (5) N_{bonds}; $W_F = 2.4$, $D = 3$, $H = 2.7$, (6) N_{bonds}; $W_F = 2.4$, $D = 2.4$, $H = 3.9$.

From the increase in N_{bonds} with $N_{\Delta t}$ (up to $N_{\Delta t}$=1000), we derived a value for the Smoluchowski stability ratio W_S, using equation (2.A1). Each value of W_S is derived from one simulation at $u \neq 0$ and one using the same set of parameters except that $u = 0$ (for normalisation). We can approximate W_F, incorporating u in equation (2.A2). We performed simulations at four chosen values of W_F, but at a different slope of the potential. A weak, long range potential can have the same value for W_F as a strong, short range potential. Hence (D-2)/H may serve as a distinction beween different barriers with equal effective repulsion. The reciprocal of both W's is plotted in figure 2.A3, along with the ratio $(D - 2)/H$. From this figure we see that W_F predicts the aggregation rate as given by W_S, very well. For $D < 2.2$, W_S was usually smaller than expected from the value of W_F. This is due to the short time spent by the particle in the interaction range. This simulation artefact can be corrected by using smaller timesteps, but this increases the total simulation time significantly.

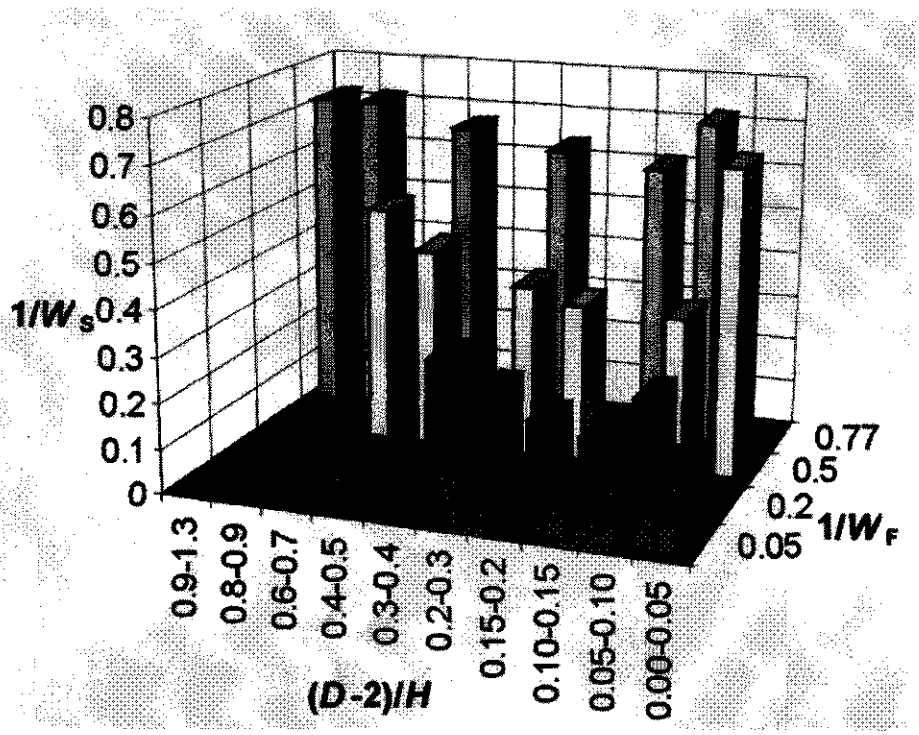

Figure 2.A3. The quantity W_S as a function of W_F and $(D\text{-}2)/H$ for various simulated systems.

We also studied the influence of the interaction properties e^H and $(D\text{-}2.1)\Delta H$ on the value of W_S. We found that especially e^H is very poor in predicting the actual bonding rate as given by W_S. Also for $(D\text{-}2.1)\Delta H$ there is poor correlation with W_S (see figure 2.A3).

Figure 2.A4a and 2.A4b show the influence of respectively $(D\text{-}2.1)\Delta H$ and e^H on the value of D_f and ξ derived for several simulations at $N_{agg} = 10$. We can see clearly that these parameters have no predictive value for both fractal parameters.

There is a general importance of the net bonding rate on the properties of the structures formes. In this appendix, we have shown that the theoretical Fuchs stability ratio W_F calculated from the interactions $u(r)$, can be used to predict the early bonding rate of the aggregates. The predictive value of W_F is considerably higher than the Boltzmann factor e^H or the integral over the potential curve.

(a)

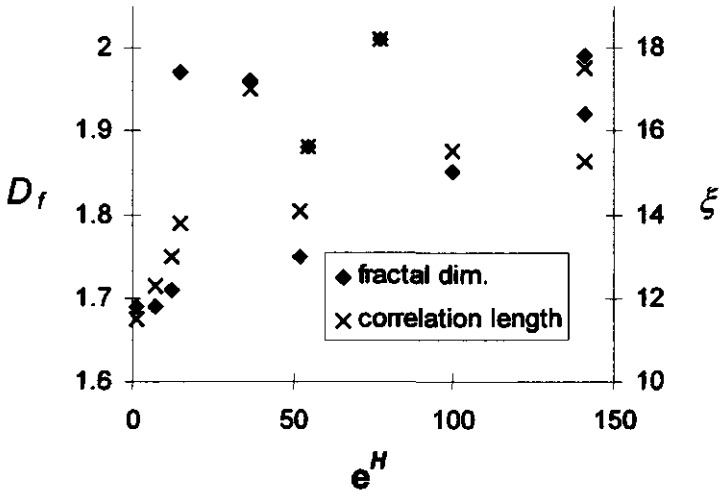

(b)

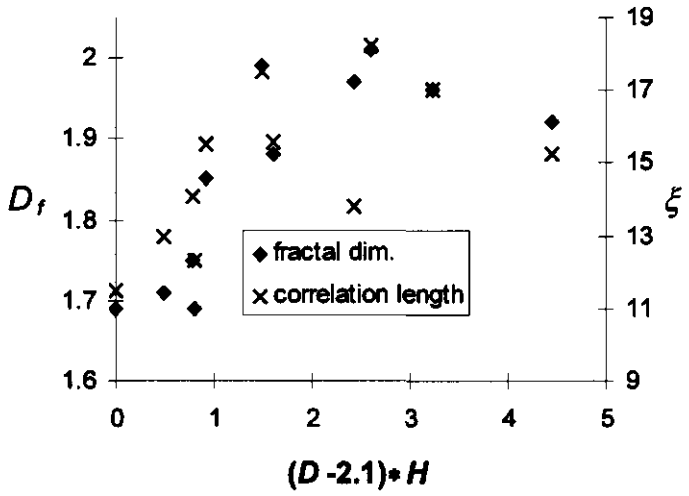

Figure 2.A4. Quantities D_f and ξ as a function of (a) e^H and (b) $(D\text{-}2.1)\times H$ for several systems with different $(D\text{-}2)/H$.

2.7 References

[1] Dickinson, E., *J Chem Soc Faraday Trans* **90**, 173, (1994)
[2] Bijsterbosch, B. H.; Bos, M. T. A.; Dickinson, E.; van Opheusden, J. H. J.; Walstra, P., *Faraday Discuss* **101**, 51, (1995)
[3] Bos, M. T. A.; van Opheusden, J. H. J., *Phys Rev E* **53**, 5044, (1996)
[4] Lodge, J. F. M.; Heyes, D. M., *J Chem Soc Faraday Trans* **93**, 437, (1997)
[5] Whittle, M.; Dickinson, E., *Mol Phys* **5**, 739, (1997)
[6] Wijmans, C. M.; Dickinson, E., *J Chem Soc Faraday Trans* **94**, 129, (1998)
[7] Lodge, J. F. M.; Heyes, D. M., *J Rheol* **43**, 219, (1999)
[8] Mellema, M.; van Opheusden, J. H. J.; van Vliet, T. In *Food Emulsions and Foams: Interfaces, Interactions and Stability*; Dickinson, E., Rodríguez Patino, J. M., Eds.; Royal Society of Chemistry: Cambridge, 1999.
[9] Bos, M. T. A., PhD Thesis, Wageningen Agricultural University, 1997.
[10] Holt, C.; Horne, D. S., *Neth Milk Dairy J* **50**, 85, (1996)
[11] Haw, M. D.; Sievwright, M.; Poon, W. C. K.; Pusey, P. N., *Adv Coll Interf Sci* **62**, 1, (1995)
[12] Bremer, L. G. B. PhD Thesis, Wageningen Agricultural University, 1992.
[13] Payens, T. A. J., *Biophys Chem* **6**, 263, (1977)
[14] van Hooydonk, A. C. M.; Walstra, P., *Neth Milk Dairy J* **41**, 19, (1987)
[15] Mellema, M.; Leermakers, F. A. M.; de Kruif, C. G., *Langmuir* **15**, 6304, (1999)
[16] Bremer, L. G. B.; Bijsterbosch, B. H.; Walstra, P.; van Vliet, T., *Adv Coll Interf Sci* **46**, 117, (1993)
[17] this thesis, chapter 3
[18] Lin, H. Y.; Lindsay, H. M.; Weitz, D. A.; Ball, R. C.; Klein, R.; Meakin, P., *Phys Rev A* **41**, 2005, (1990)
[19] Fuchs, N., *Z Physik* **89**, 736, (1934)
[20] Allen, M. P.; Tildesley, D. J. *Computer Simulation of Liquids*; Oxford Science Publications, 1987.
[21] Meakin, P., *Adv Coll Interf Sci* **28**, 249, (1988)
[22] Meakin, P., *Heterogeneous Chem Rev* **1**, 99, (1994)
[23] Meakin, P.; Jullien, R., *J Physique* **46**, 1543, (1985)
[24] Smoluchowski, M., *Z Physik Chem* **92**, 129, (1917)
[25] Tadros, T. F., *Adv Coll Interf Sci* **68**, 97, (1996)
[26] Mandelbrot, B. B. *The Fractal Geometry of Nature*; Freeman: New York, 1983.
[27] Dickinson, E. In *Food Colloids: Proteins, Lipids and Polysaccharides*; Dickinson, E., Bergenståhl, B., Eds.; Royal Society of Chemistry: Cambridge, 1997.

[28] Carpineti, M.; Giglio, M., *Adv Coll Interf Sci* **46**, 73, (1993)
[29] Meakin, P., *J Coll Interf Sci* **134**, 235, (1990)
[30] van Vliet, T.; Lucey, J. A.; Grolle, K.; Walstra, P. In *Food Colloids; Proteins, Lipids and Polysaccharides*; Dickinson, E., Bergenståhl, B., Eds.; Royal Society of Chemistry: Cambridge, 1997.
[31] this thesis, chapter 5
[32] Roefs, S. P. F. M.; van Vliet, T.; van den Bijgaart, H. J. C. M.; de Groot-Mostert, A. E. A.; Walstra, P., *Neth Milk Dairy J* **44**, 159, (1990)
[33] van Vliet, T.; van Dijk, H. J. M.; Zoon, P.; Walstra, P., *Coll Polym Sci* **269**, 620, (1991)

Chapter 3

Structure and scaling behavior of aging rennet-induced casein gels examined by confocal microscopy and permeametry*

3.1 Summary

A study is presented on the structure of rennet(-induced) casein or skim milk gels at three pH values (5.3, 6.0 and 6.65) and temperatures (20, 25 and 30°C). The structure was examined by confocal scanning laser microscopy and permeametry. Deconvolution was applied to the microscopic images. A fractal scaling analysis has been applied to the images and permeametry results. In this analysis, the fractal dimensionality (D_f), lower cut-off length (R_0) and apparent pore size (P) of the linear scaling regime were calculated from the microscopical data. The D_f and apparent pore size were also calculated from the permeametry data. During aging of the gels, a coarsening of the structure was observed; the pore size increased and the clusters became more compact. This was reflected in the fractal parameters: R_0 and P increased during gel aging. Their values are generally high (0.5-1.5 and 5.0-15 μm, respectively) compared to data obtained by computer simulations. The D_f value is also high (~2.2-2.6), which is an indication of slow aggregation or rearrangements during aggregation. The gel aging effects are probably mainly due to rearrangements like particle fusion and strand fracture, which rates increase with increasing temperature, and even more pronouncedly, with decreasing pH.

*_Langmuir_ **16**, 17, 6847 (2000)

3.2 Introduction

Aging of rennet-induced casein gels is accompanied by specific changes in the (fractal) structure. The nature and the rate of these changes is quantified using confocal scanning laser microscopy (CSLM) and permeametry. The structure is determined by the properties of the caseinate particles or casein 'micelles', which have been varied by changing pH and temperature. Knowledge obtained in the relation between the properties of the casein and the structure of the gel matrix can help to improve dairy products or add new fundamental physical insight.

Casein gels, or more correctly, caseinate gels can be formed by adding rennet enzyme to milk, as occurs in the early stages of cheesemaking. The gel matrix of rennet(-induced) casein gels is built of aggregates of caseinate particles or para-casein micelles. A casein micelle (radius ~25-125 nm) is a roughly spherical particle formed by association of casein molecules. The main casein proteins are α_{s1}-, α_{s2}-, β- and κ-casein. The outer layer of a casein micelle mainly consists of the hydrophilic parts of the κ-casein protruding in the solution like 'hairs'. The rennet enzyme specifically splits off the κ-casein hairs and para-casein micelles are formed. This reduces the (steric and electrostatic) repulsion between the micelles and the suspension mostly becomes unstable.

The structural and rheological properties of rennet-induced casein gels depend on the behavior of the (para-)casein micelles of which they are built. The micelles are probably held together by a combination of hydrophobic and electrostatic interactions. From this it can be expected that both pH and temperature can influence properties of the micelles. For instance, a lowering of the pH from the physiological level (~6.65) to 5.3 increases the relative importance of hydrophobic interactions (because the system is closer to the pI). Moreover, calcium phosphate goes into solution, which causes the micelles to swell. The temperature also influences the voluminosity of the micelles. An overview on the behavior of casein micelles is e.g. given by Horne [1] and references therein.

The rate of aggregation of the micelles increases with decreasing pH and increasing temperature [2]. In addition, the rate of rearrangement in the aggregates and gel matrix is probably also increased. Occurrence of rearrangements is an important phenomenon in particle gels, because the rearrangements determine the changes in the rheology and some other properties of the system.

In this paper only rearrangements of the system *at rest* (not induced by external forces) are discussed. Rearrangements in rennet-induced casein aggregates or gels have been studied by permeametry [3,4] light scattering [5], electron microscopy [6,4] and rheology [7]. Gel aging processes in acid(-

induced) casein gels have also been studied [8-11]. All types of rearrangements are expected to give rise to local matrix compactifications, and the formation of larger gel pores. Eventually the solvent (whey) may be expelled due to contraction of the gel matrix; this process is called syneresis [12].

The structure of particle gels at volume fractions in the range of approximately 1 to 10 vol%, can be characterized using a fractal scaling approximation. This type of structural description, based on the density variation in a gel at various length scales, has proven to be a useful tool for relating structure to rheology of casein(ate) gels [13] and for describing food structure in general [14]. The scaling behavior can be described by a fractal dimensionality (D_f) and a lower cut-off length (R_0) of the fractal regime, and an apparent (maximum) pore size (P). Gel aging gives rise to changes in these fractal parameters.

3.3 Theory

3.3.1 Confocal microscopy

Confocal Scanning Laser Microscopy (CSLM) has a number of advantages over conventional light microscopy techniques for studying foods [15] and colloids in general [16]. With such a microscope one can obtain an image of the structure of a region internal to a sample without having to slice it. To obtain an image with enhanced resolution, a three-dimensional volume is scanned by moving the sample relative to the microscope, and the resulting stack of images is subjected to a deconvolution procedure. In this way, the distortion of the images due to the finite lens aperture can be reduced. It enhances the resolution of the images, most importantly the axial resolution (perpendicular to the optical plane of the lens), and will lead to more realistic values for the fractal parameters. The main aspects of the image analysis procedure used are discussed by Bos and van Opheusden [17,18].

A CSLM experiment involves the following: laser light of wavelength λ_{ex} emanates from a pinhole. The light is focused onto a point in the sample where it excites fluorescent molecules (rhodamine). These then re-emit the light at a wavelength λ_{em}. This light is focused by the same lens onto a pinhole-detector. Because of the finite lens aperture (NA) the focal 'point' actually constitutes a intensity distribution, both for the incident and emitted light. The combined effect is described by a three-dimensional point spread function (PSF). This is a systematic effect. It can be removed from the raw data, a digital 3-D matrix of intensities over a 3-D block in the sample, using Fourier techniques. In practice we measure a 512 × 512 × 16 block of voxels

(the 3-D equivalent of a pixel), of which after deconvolution only the middle plane is used for further analysis.

Apart from the systematic optical distortion of the image, which can be removed by deconvolution, there is also a random noise component in the signal, which can be suppressed by smoothing. The extent of the noise suppression in the deconvolution, is given by a parameter κ. Larger values of κ give the deconvolved image a smoother appearance, whereas smaller values give it a more grainy appearance. A value of κ between 1 and 10 was found to be optimal for fractal analysis [17].

In addition to the deconvolution procedure, a background signal (e.g. resulting from rhodamine in the whey liquid) is removed by choosing a threshold gray scale value ρ_t. All gray scale information below ρ_t is omitted before the density correlation analysis. The choice of ρ_t is briefly discussed by Bos [17]. The choice of a threshold gray scale is not straightforward; it will influence the values of the resulting fractal parameters (see ref.[19] and Results and Discussion section of this study).

3.3.2 Scaling behavior

For clusters formed by fractal aggregation, the scaling of the density, φ_c, with the radius R_c is described by [20,21]

$$\varphi_c \propto R_c^{D_f-3} \tag{3.1}$$

where D_f is the fractal dimensionality, which can be seen as a measure of the compactness of the aggregates at fractal length scales.

At the gel point t_{gel}, the following approximations are made: $\varphi_c = \varphi$ (where φ is the total volume fraction of casein in the bulk) and $R_c = R_{gel}$. This approximation assumes that the gel is formed from growing fractal clusters of size R_{gel}, when they reach a density identical to that of the suspension. In addition, an effective building block size, a_{eff}, of the matrix is introduced as prefactor [17,9]. Note that a_{eff} need not be identical to the (average) micelle size. Rewriting relation (3.1) and incorporation of this assumptions, leads to

$$R_{gel} = a_{eff}\varphi^{\frac{1}{D_f-3}} \tag{3.2}$$

This relation is used later for the analysis of the permeametry experiments.

For the analysis of the percolating gel structures, as observed in microscopical images, we need the assumption that the structure is a

homogeneous fractal over a regime a_{eff} to R_{gel}. For a fractal structure one has [22]

$$c(r) \propto r^{D_f - 3} \tag{3.3}$$

where r is a distance between one pixel and the other, and $c(r)$ is the Density Auto-Correlation Function (DACF)

$$c(r) = \frac{\langle \rho(r')\rho(r'+r) \rangle_{r'}}{\langle \rho(r') \rangle_{r'}^2} \tag{3.4}$$

Here $\rho(r')$ is the casein density at the position r', and $<\ldots>_{r'}$ denotes an average over *all* positions r' in the image. The quantity $<\rho(r')>_{r'}$ is the average density. It is assumed that the density of fluorochrome is simply proportional to the density of casein. Our experimental setup distinguishes 256 gray scale units.

In a double logarithmic plot of $c(r)$ a structure as described above will give a linear regime between a_{eff} and R_{gel}, with slope D_f-3. In the correlation analysis, for the lower cut-off of the linear regime a parameter R_0 is used. A parameter P, associated with the average pore size in the gel, can also be obtained from the DACF. The procedure for obtaining these parameters is given in the Results and Discussion.

3.3.3 Permeametry

A pressure difference, ΔP, over a gel in a tube gives rise to a superficial liquid velocity v (m s^{-1}) given by Darcy [23]

$$v = \frac{Q}{O} = \frac{B\,\Delta P}{\eta\, l} \tag{3.5}$$

where Q is the volume flow of liquid per unit time, O and l are the cross-sectional area and the length of the gel in the tube, respectively. B (m^2) is the permeability coefficient and η (Pa s) is the liquid viscosity.

The *tube method* for measuring gel permeability was originally developed by van Dijk and Walstra [3]. In this method, gels are formed inside glass tubes that are open at both ends (covered with perforated parafilm). The tubes are placed vertically in a thermostatted vessel filled with whey, with the top of the gel below the whey surface. The pressure difference over the gel

will give rise to an increasing whey liquid height $h(t)$ on top of the gel (relative to the final height $h(\infty)$ that can potentially be obtained). The level of the whey on top of each gel was read at regular time intervals by means of a cathetometer. The liquid velocity can be calculated from experimental data, using

$$v = \frac{\Delta(h(t_\infty) - h(t))}{\Delta t} \tag{3.6}$$

where t is the time. The pressure difference ΔP is

$$\Delta P = -\rho_l \, g(h(t_\infty) - h(t)) \tag{3.7}$$

where ρ_l is the liquid density. The permeability B can be obtained by inserting equations (3.6) and (3.7) in (3.5) (Δt, g, ρ_l, η and l are known and $\Delta(h(t_\infty) - h(t))$ is experimentally accessible), assuming B to be constant during Δt.

If O_p is the average cross-sectional area of a single pore and D is its diameter: $O_p \propto D^2$, $Q \propto D^4$ (assuming Poiseuille flow), $D \propto R_{gel}$; assuming equation (3.2) to hold, equation (3.5) can be rewritten as

$$B = KD^2 = K(a_{\text{eff}})^2 \varphi^{\frac{2}{D_f - 3}} \tag{3.8}$$

where K is a prefactor that can be associated with the reciprocal of the apparent tortuosity factor in the Kozeńy-Carman equation [24,25]. It should be noted, however, that K is not only determined by the tortuosity of the percolating pore, but also by the distribution of the pore sizes and their connections, etc. By performing experiments over a sufficiently wide range of volume fractions, D_f can be calculated using equation (3.8). Moreover, it is possible to determine the apparent tortuosity, assuming that $D = P$ (as determined in the confocal microscopy experiments). For a proper scaling analysis, a_{eff} should be independent of φ.

3.4 Materials and Methods

3.4.1 Skim milk preparation

Standard reconstituted skim milk was made by dissolving 12 g low heat skim milk powder (Krause, Heino; 100 g powder contains 0.6 g fat and 33.8 g casein) in 100 g demineralized water. To retard bacterial and enzymatic degradation, 200 μl of 10 wt% thiomersal (BDH Chemicals Ltd.) and 27 μl of a solution of 3.7 mg ml^{-1} (~0.9 TIU/100 ml) aprotinin (Sigma, A-1153, Lot # 46H7145) were added. To allow equilibration, the dispersion was stirred for about 10 (pH = 6.65), 16 (pH = 6.0) or 24 (pH = 5.3) hours at 25°C. After this, the pH was corrected again (usually necessary at low pH). Cold storage can influence gel properties like the elastic modulus [26].

The desired pH was reached by adding appropriate amounts of a 0.5 molar HCl solution. To assure a constant ionic strength and casein volume fraction, appropriate amounts of a 1 molar NaCl solution and demineralized water were added. The total volume of solution added was always 21 ml. Assuming a voluminosity of 3 ml g^{-1} [27] and a milk density of 1.036 kg l^{-1}, the casein micelle volume fraction, φ, equals about 0.089.

For the microscopic experiments we added about one droplet per 100 ml of a solution of 4 mg ml^{-1} Lissamine Rhodamine B (Molecular Probes, L-20), giving a slightly pink color to the skim milk.

Commercial calf rennet (10.800 SU, Leeuwarder Kaasstremsel) was added to the milk. The additions in the milk were 0.02 (pH = 6.65), 0.004 (pH = 6.0) and 0.002 (pH = 5.3) vol%, to obtain an approximately constant time lapse between rennet addition and gelation of 4-5 ks. It should be noted that all results are presented as a function of *time after rennet addition* and not as a function of time after gelation. The gelation time, which is used in the calculation of the fractal parameters from the permeametry, is defined as the moment at which G' surpasses G''. [28]

For the permeability experiments the milk was diluted. This was done by adding appropriate amounts of whey, obtained by gelation of skim milk and subsequent cutting and filtering off of the curd. Standard skim milk dispersions studied had volume fractions (φ) of casein of 0.054, 0.063, 0.076 and 0.089.

3.4.2 Confocal microscopy

The microscope used was a Biorad MRC 600 with an ILT Argon/Krypton laser as a light source. At the detector side a Biorad YHS filter block was used. A Nikon Plan-Apo 60× 1.4 N.A. oil-immersion objective was used for imaging.

In a confocal microscopy experiment, laser light is focused in a given plane. A focal point scans the whole plane as 512 × 512 pixels, which takes (in 'slow' mode) about a second per plane. Each plane was scanned 16 times. The resulting image is an average of these 16. Next, the sample is moved downwards over a distance of 100 nm and another image is taken. This is repeated until a stack of 16 raw images is obtained.

The whole stack of planes is used for the deconvolution. The deconvolution involves incorporation of the following standard parameters: λ_{ex} = 755 nm, λ_{em} = 831 nm, N.A. = 1.4, z = 90 nm (value corrected for the refractive index difference between solvent and immersion oil) and κ = 1. Note that the wavelengths are those obtained in water; not in air. Also incorporated are the pixel size p and the threshold gray scale ρ_t, which varied from image to image. All calculations of fractal parameters were made on deconvolved data. There are systematic changes of the fractal parameters with changes in all input parameters. However, apart from the influence of ρ_t, the effects are very small. For instance; a tenfold increase of κ or a 30% decrease of λ_{ex} and λ_{em} did change the fractal parameters at most by one percent. The effect of ρ_t will be discussed later.

The preparation of the samples was as follows: After addition of the rennet to a larger amount of milk, a small amount was placed in a hollow object glass. Next, a cover slide was placed over it and it was sealed to the objective glass by using nail polish to assure no contact of the gel with air. Samples were stored at the appropriate temperature, T (20, 25 or 30°C), and taken out for measuring at 25°C as briefly as possible (maximally 10 minutes). Several samples were prepared to ensure that each one was not taken out of the thermostatted environment more than three times during an experiment.

Sometimes syneresis effects were observed: the gel showed very large pores or had lost contact with the glass surface. If this happened, the images were discarded.

In the (fractal) analysis, use is made of gray scale images where white indicates the highest casein concentrations. However, for visual inspection the black and white confocal micrographs are tranformed to color images (white/blue/red).

3.4.3 Permeametry

For a full description of the technique, see ref. [3]. Gels were made in glass tubes, that were open at both ends (inner diameter 3.7 mm, length 25 cm). After gelation, the tubes were placed in a thermostatted vat filled with the appropriate whey liquid. The level of the percolating liquid was then measured in time, relative to the level in an empty glass tube. For flow through casein gel pores, the Reynolds number is maximally 10^{-5}, which is small enough to ensure laminar flow [4]. Occasionally, insufficient adhesion of the gel to the glass tube or 'syneresis' was observed. These results were discarded. The same samples (at the same conditions) were used for permeametry and microscopy.

3.5. Results and Discussion

3.5.1 Visual characteristics from micrographs

Figures 3.1a-c, 3.2a-c and 3.3a-c give a number of confocal micrographs, considered representative for some important time stages, temperatures and pH values studied. In table 3.1 the values of the storage modulus G' at the corresponding conditions, taken from refs.[29,28] are shown. All times are in ks after rennet addition.

Figure	t (ks)*	G' (Pa)*	pH	T (°C)
3.1a	10	70	6.65	25
3.1b	20	100	6.65	25
3.1c	80	150	6.65	25
3.2a	10	80	6.65	30
3.2b	20	100	6.65	30
3.2c	80	100	6.65	30
3.3a	10	45	5.3	25
3.3b	20	50	5.3	25
3.3c	60	50	5.3	25

Table 3.1. Conditions of the gels presented in figure 2.1-3. Storage moduli G' taken from refs.[29,28]. *Approximate values.

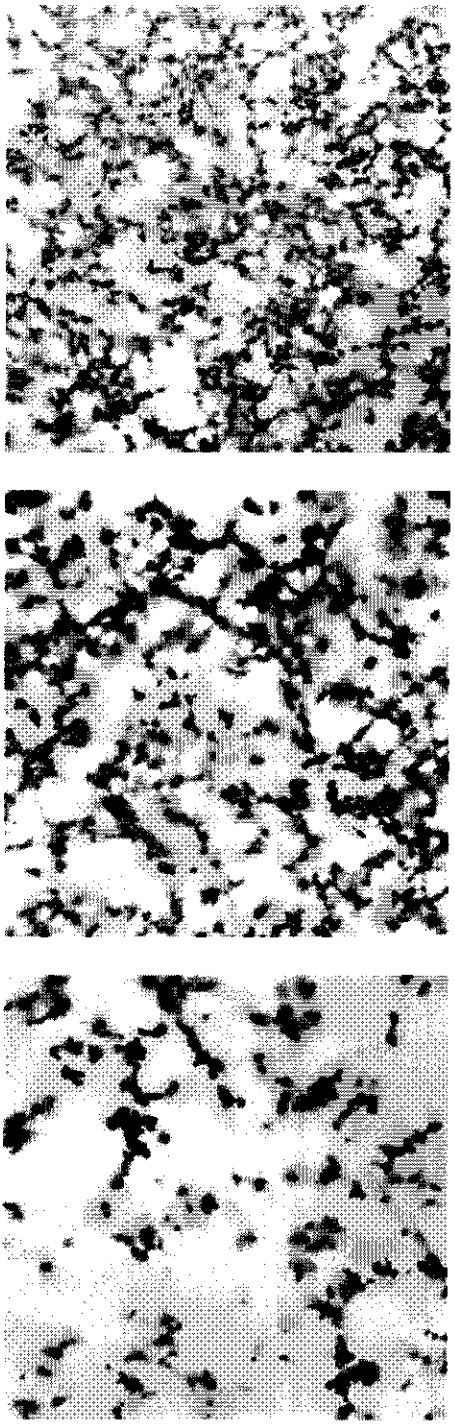

Figure 3.1: Confocal micrographs of rennet-induced casein gels at various times after rennet addition.

pH = 6.6, T = 25°C

t ~ 10 **(a)**, 18 **(b)** and 80 **(c)** ks, respectively. Each image is taken at a different place in the sample.

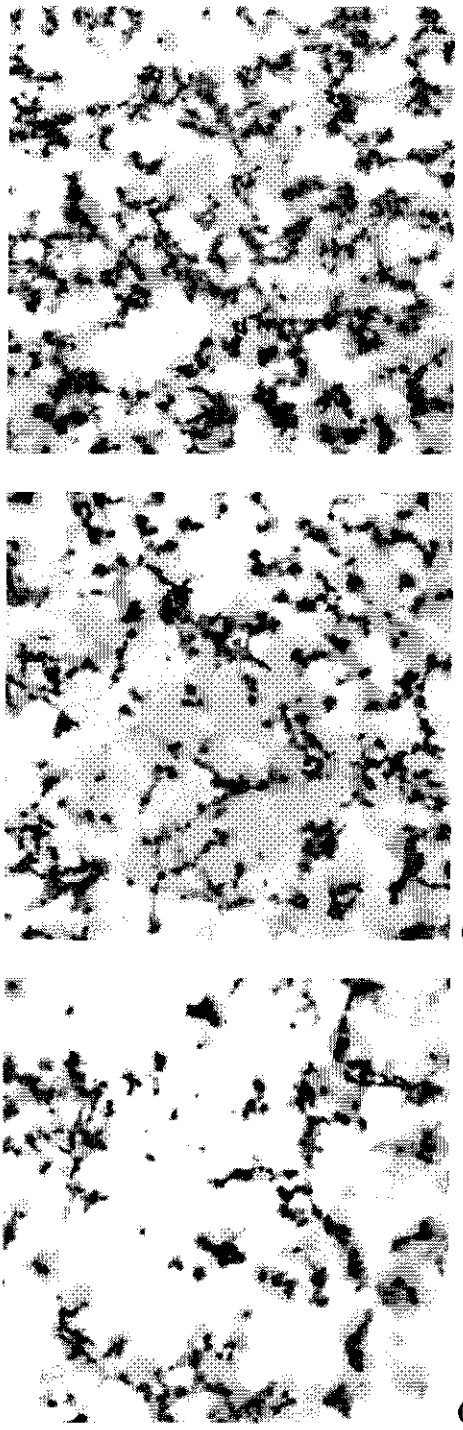

Figure 3.2: Confocal micrographs of rennet-induced casein gels at various times after rennet addition.

pH = 6.6, T = 30°C

t ~ 10 **(a)**, 18 **(b)** and 80 **(c)** ks, respectively. Each image is taken at a different place in the sample.

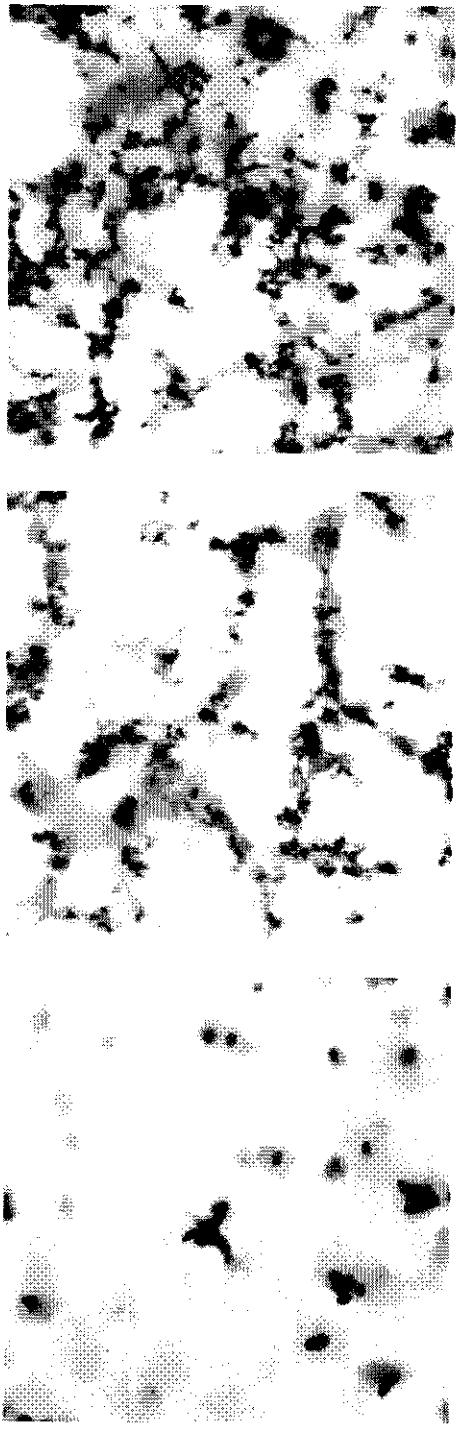

Figure 3.3: Confocal micrographs of rennet-induced casein gels at various times after rennet addition.

pH = 5.3, T = 25°C

t ~ 10 **(a)**, 16 **(b)** and 60 **(c)** ks, respectively. Each image is taken at a different place in the sample.

In the microscopic images, black indicates the highest, gray intermediate levels of rhodamine (i.e. casein) present. The image represents a 'slice' of maximally 90 nm thickness, rather than a projection of a 3D network. A 'cloudy' network of material is observed, very similar to images of simulated aggregates [30]. The picture frames are ~90 × 90 μm, corresponding to pixel sizes p of approximately 180 nm. Fractal parameters were also calculated from micrographs with $p \sim 80$ nm, but this did not give systematic differences.

From the images it is clear that gel aging is accompanied by a gradual formation of larger gel pores, 'smooth' and compact gel matrix or clusters, and thin, straight strands. According to a nice series of confocal images by Auty *et al.* [11], very similar processes take place during acid casein gelation. The strands are randomly distributed through the matrix and the chance to find the length of a thin, straight strand fully in a focal plane is not very large. Presumably, the gels contain a much greater concentration of these strands than seen in the images. Straight strands are mainly present in fresh gels (pH = 5.3) and older gels (pH = 6.0 and 6.65). This is supported by the analysis of rheological data [29,28]. Formation of straight strands can also be observed for acid-induced casein gels [13,11]. However, for GDL-induced (acid) gelation changes in structure due to aging cannot be separated from those due to the decrease in pH.

Broadly speaking; lowering pH or increasing temperature speeds up the gel aging or rearrangement process. Especially in figure 3.3c (high age, low pH) the rearrangements have reached a very advanced stage, because the matrix has 'collapsed' to thick strands connecting compact aggregates, which cannot be considered fractal. At this point the system has a very short (rheological) linearity and is about to show extensive syneresis [28]. The effect of pH and temperature on the aging of the structure is further discussed in the next section.

3.5.2 Fractal characteristics from micrographs

In figure 3.4 two examples are presented of the density (or gray scale) autocorrelation function (i.e. $\log(c)$ as a function of $\log(r)$), corresponding to the images of figures 3.2c and 3.3a. Both curves show a relaxation of the DACF at intermediate length scales (to which a linear fit is applied to obtain fractal parameters).

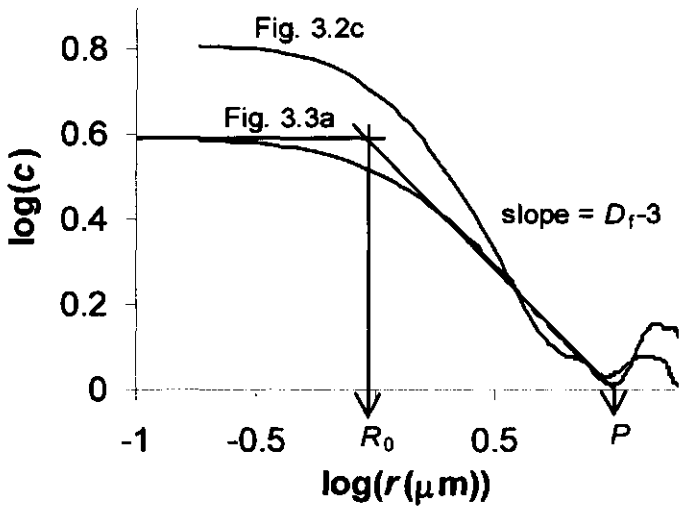

Figure 3.4. Density correlation functions for the images of figures 3.2c and 3.3a. Dashed lines are given to indicate the procedure to derive fractal parameters.

The parameter R_0 is the length scale at which the extrapolation of the fractal regime crosses the extrapolation of the 'horizontal' regime at small length scales. In our experience, variations in the procedure of fitting the DACF curves by eye, lead to minor variations in D_f (~5 %) and R_0 (~5 %), but to larger variations in P (~15 %).

The parameter P is the intercept of the linear fit with $c = 1$, or (if the curve crossed the x-axis near this intercept) the intersection value was taken, i.e. the intercept of the DACF curve with $c = 1$ was taken. In the former case, P would be a true fractal parameter, i.e. the correlation length ξ [30,29]. In the latter case (~25% of the images), P is merely a characteristic of the 'outer tail' of the DACF. The presence of such a tail to the DACF may be due to rearrangements at large length scales, although we did not find a relation between age of the gel, pH or temperature and the presence of a tail.

In figures 3.5, 3.6 and 3.7 the full time evolution of the parameters D_f, R_0 and P^2 is presented, at the temperatures and pH values given in the legend. All results are plotted as a function of time after rennet addition. Especially at low pH and high T, the data series stop at an earlier time than at high pH and low T, due to syneresis occurring. If macrosyneresis (i.e. contraction of the matrix and expulsion of whey) occurs, very compact aggregates are formed and the system cannot be considered fractal anymore.

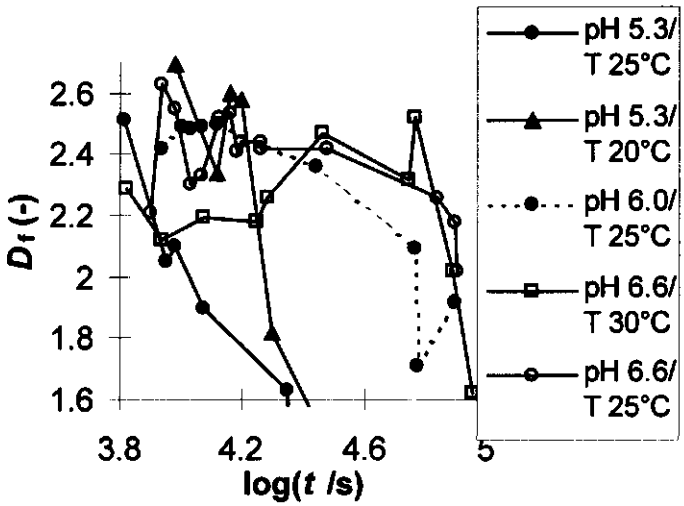

Figure 3.5. Fractal dimensionality, D_f, as a function of time after rennet addition. Calculated from confocal microscopical data.

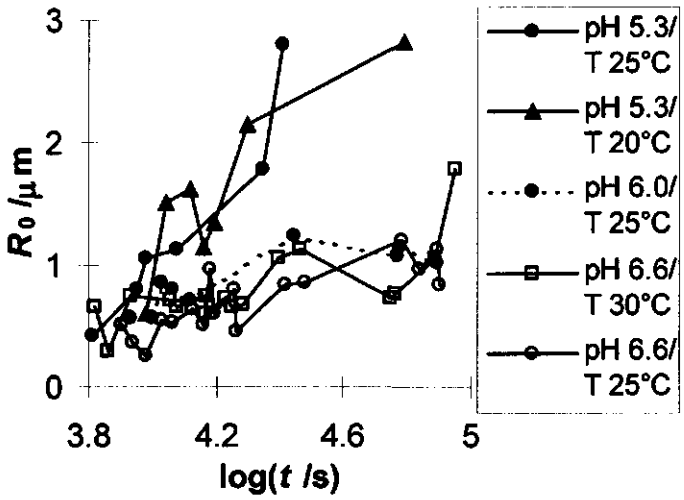

Figure 3.6. Lower cut-off length, R_0, as a function of time after rennet addition. Calculated from confocal microscopical data.

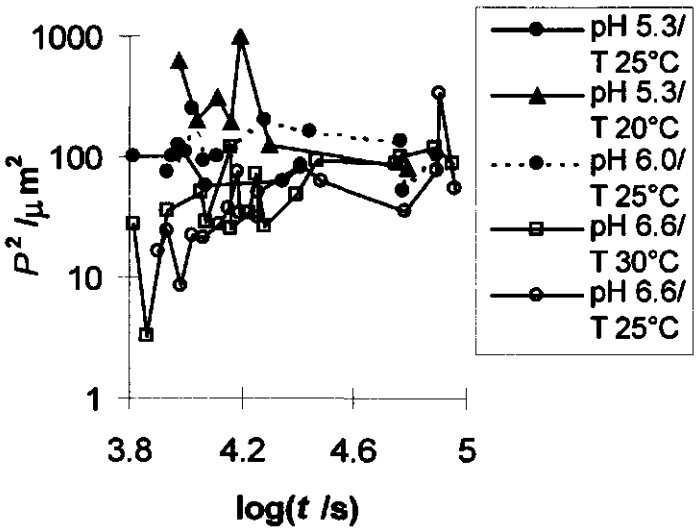

Figure 3.7. Squared pore size, P^2, as a function of time after rennet addition. Calculated from confocal microscopical data.

For a large number of images the value of D_f is the same, whereas the structures are notably different. This indicates that the value of D_f is insufficient to characterize gel structures.

Figure 3.5 shows that D_f equals about 2.5 for all gels for short aging times. This is in accordance with values for D_f obtained from computer simulations for irreversible and delayed aggregation due to a repulsive barrier (i.e. high Fuchs ratio [30]). Light scattering experiments on polystyrene particles have also shown that the value of D_f is higher if aggregation takes place in the presence of surfactant molecules that constitute a repulsive barrier [31]. Considering the typically high value of D_f from the confocal microscopy (this study), is reproduced at the latest time stages in the simulations, there is probably an overlap in time stage between the end of the simulations, and the beginning of casein gel aging. Possibly, at high T (30 °C), D_f is somewhat smaller. Rearrangements during the aggregation stage decrease the size of the aggregates already formed, hence the size of the fractal regime. With R_0 constant or even increasing, this leads to an increase in D_f during aggregation. Upon gel aging, D_f decreases, especially at low pH. In general, rearrangements of the gel matrix after the gel is formed, appear to go along with a decrease in D_f. This can be understood from the DACF. Local compactification during gel aging will lead to an increase of $c(0)$, an increase of R_0 and (on a log-scale) only minor systematic changes in ξ. This would result in a decrease in D_f.

The overall value of the fractal dimensionality (2.4-2.5) is higher than the values calculated from the micrographs of acid casein gels: 2.35 [21] and 2.2 [17]. As discussed below, the permeability data give $D_f \sim 2.2$-2.3. So our values of D_f calculated from the microscopical data may be (systematically) too high. This problem is discussed in the next section.

The average size of the compact building blocks of the gel matrix, R_0, gradually increases in time and becomes especially high at low pH. This can be seen in figure 3.6. During the whole aging process, the value of R_0 seems to be in the right order of magnitude to be a measure of the radius of the most compact parts of the gel matrix (see figures 3.1-3.3). The value of R_0 at gelation (taking place at approximately $\log(t) = 3.7$), is already a few times the average casein micelle radius, confirming that some rearrangement does take place before gelation [5,9]. Before gelation, trimers of particles can, for instance, rearrange into triangles. After gelation, formation of more bonds per junction (a junction comprises all bonds between two particles), will slow down this process [17]. Because figure 3.6 shows that R_0 keeps increasing, this is likely due to particle fusion or breakage of strands.

In figure 3.7 it is shown that P^2 increases with time at high pH; it is also clear that the uncertainty in P is considerable. This is related to the arbitrariness in determining this parameter.

The reason why P^2 and not P is plotted, is to facilitate comparison with the permeametry results. The parameter P can be interpreted as the length scale at which the density correlations have become zero, i.e. the structures at larger length scales are 'homogeneous'. The values of P appear of the same order of magnitude as the radii of the gel pores at an early stage (see figures 3.1-3.3). In the later stages of gel aging (especially at low pH), P is too small to be a measure of the visual pore size and the apparent value derived from permeametry, because the parameter is a combined measure of the size of the pores *and* the clusters. In addition, the permeability is affected by the tortuosity, which would change upon aging. For instance, there may be a change in (effective) tortuosity due to straightening of strands.

The values of P (and R_0) calculated from the confocal microscopic data are much larger than those obtained from computer simulations [30], presumably because the simulations do not allow such extensive rearrangements as occur in the casein gels. The correlation length ξ can be two-third times P (not shown). In addition, ξ^2 decreases after $t \approx 30$ ks, whereas P^2 stays constant or keeps increasing. Note that the error in large length scale parameters like ξ and P is considerable. The correlation length ξ steeply depends on D_f. Hence, if D_f is slightly wrong, ξ may be off by an order of magnitude.

Summarizing: during aging, R_0 increases, D_f decreases and P increases (slightly), especially at low pH (5.3) and high T (30 °C). The visual

appearance is affected accordingly (larger compact clusters and pores). During aging, strands connecting the clusters are stretched, become very thin and eventually break. This is especially true for rennet-induced casein gels at pH = 5.3.

3.5.3 Effect of gray scale threshold on D_f

An important observation from figure 3.5 is that values for D_f are relatively high. Even though this may be expected for delayed aggregation [30], the values are too high as compared to those obtained from the permeability measurements (see next section). The cause of this discrepancy may be as follows. An important factor determining the estimate of D_f, is the choice of the gray scale threshold value ρ_t. If a higher value of ρ_t was chosen (i.e. lesser pixels taken into the analysis), the value for D_f was smaller. This observation is probably due to part of the rhodamine not being associated with the casein network (i.e. remaining in solution or being attached to whey protein), resulting in a background fluorescence. It is known by the manufacturers [32] that Lissamine rhodamine B can have a low reaction yield. To remove the background, for each image an appropriate threshold gray value had to be chosen. This was done before the DACF analysis was performed. Its choice is explained in figure 3.8.

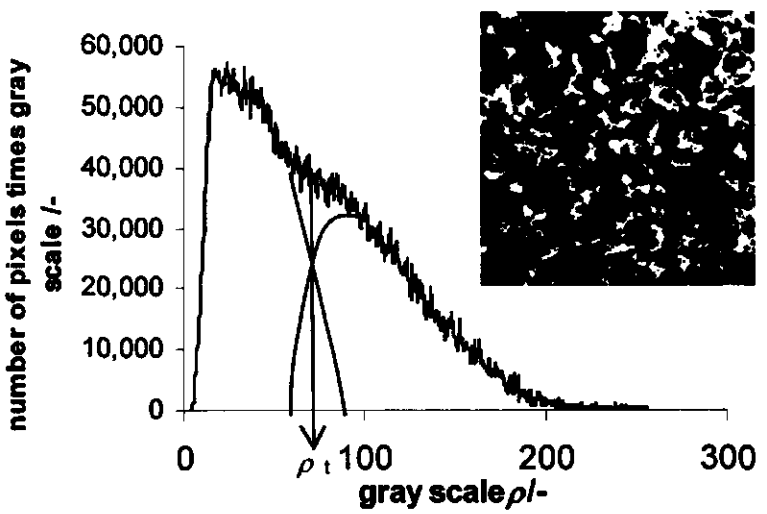

Figure 3.8. Example of an intensity-weighted histogram (pH = 6.0, T = 30°C) of a confocal micrograph of a rennet-induced casein gel. Add-in is the corresponding micrograph, thresholded at ρ_t.

In figure 3.8 a typical example of a density-weighted histogram (number of pixels × intensity) is plotted. A large fraction of the total intensity stems from the lower intensity voxels. However, at the right-hand side there is a 'shoulder', which we assume to be due to a second peak in the signal associated with the casein network [17]. The threshold value ρ_t was chosen here to be 1.1×10^{12}, and any slightly higher choice on the basis of this procedure, would lead to a decrease in D_f by almost 0.1. If only 10% of the brightest pixels were taken into account, D_f approximately decreased an additional 0.4, leading to irrealistic values for D_f (not shown).

In figure 3.9 the values of D_f resulting from the DACF analysis, are plotted as a function of the threshold value choice for three randomly selected images. The values for D_f are systematically larger if smaller threshold values are chosen. These results are in accordance with a confocal microscopy study on fractal aggregates of latex particles [19].

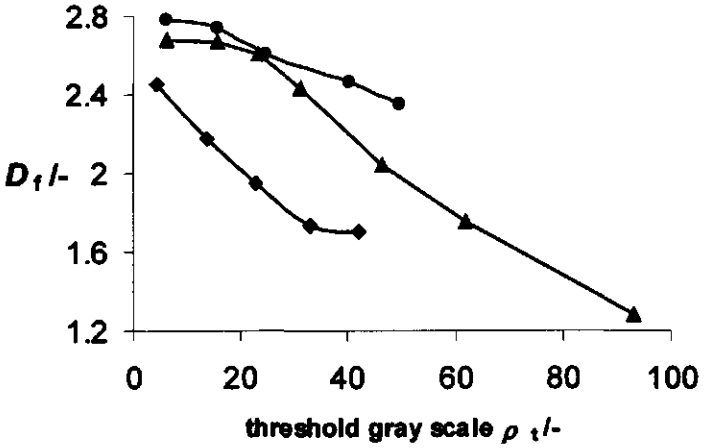

Figure 3.9. Fractal dimensionality D_f obtained from correlation analysis, as a function of threshold intensity ρ_t, for three randomly chosen microscopical images.

So the choice of ρ_t is crucial, due to its effect on D_f. To at least keep the correct trends in D_f, it is essential that the same threshold value should be selected for all of the images. The parameters R_0 and P are also influenced by the choice of ρ_t, though much less than D_f. Both parameters are only slightly smaller at lower ρ_t (results not shown).

The technique used by Hassan *et al.*[33] differs from the one used here. Their approach involves reflectance confocal microscopy on unstained samples. In principle, this allows less arbitrary gray scale threshold selection.

3.5.4 Permeametry

The permeability is plotted as a function of time in figure 3.10 for the same conditions (T , pH) as in figures 3.5, 3.6 and 3.7. An increase of the permeability is generally observed, which is indicative for rearrangements taking place in the gels, that cause gel pores to become larger. The increase in pore size may be due to local compactification of casein into larger clusters and, in later stages, due to breaking strands. For a lower pH and for a higher T the B values are much larger at all gel ages, confirming that rearrangements proceed at a faster rate under these circumstances. In the range of pH and T values studied, the effect of the pH is larger.

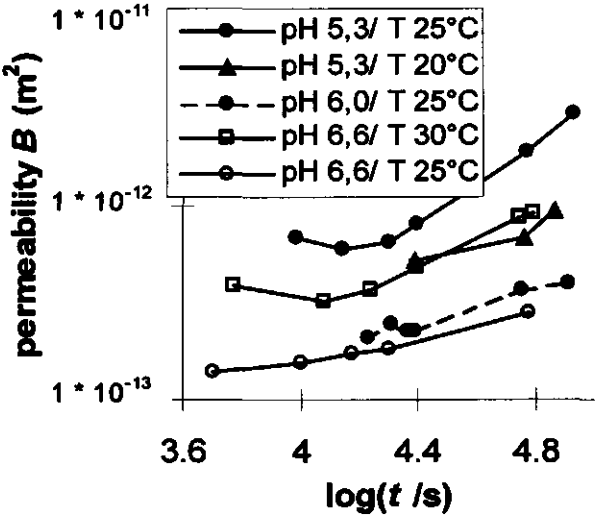

Figure 3.10. Permeability, B, as a function of time, t, at 8.9 vol% casein. Conditions (pH and T) as indicated in the legend.

Using equation (3.8), the order of magnitude of K and a_{eff} can roughly be estimated for the system showing the least rearrangement (i.e. pH = 6.65, T = 25 °C, 6 ks). The parameters corresponding to this system are $D^2 \approx P^2 \approx 2.0 \times 10^{-11}$ m^2 (figure 3.7), $B \approx 1.4 \times 10^{-13}$ m^2 (figure 3.10), $D_f \approx 2.45$ (figure 3.5) and $\varphi \approx 0.089$. This leads to $K \approx 0.007$ and $a_{eff} \approx 55$ nm. The apparent pore tortuosity would then equal about 140, and the effective particle size be similar to the size of a para-casein micelle (but smaller than R_0). For the system at pH = 5.3, T = 30 °C and 20 ks, the same calculations can be performed incorporating $P^2 \approx 8.0 \times 10^{-11}$ m^2, $B \approx 6 \times 10^{-13}$ m^2, $D_f \approx 1.7$ and $\varphi \approx 0.089$. This would lead to $K \approx 0.0075$ and $a_{eff} \approx 1.5$ μm. So the apparent

tortuosity would be the same (~130) and a_{eff} is much larger, and very similar to R_0, namely ≈ 1.4 μm. Note that for polystyrene latex gels Bremer [13] found $K \approx 0.01$.

A linear fit to the experimental data of B as a function of time (linear scales), is used to obtain B as a function of time after rennet addition (t). In this way, at each timescale a fractal analysis can be performed. In figure 3.11, log$B$ determined by interpolation at a certain t, is plotted as a function of logφ for a random selection of gel conditions (pH, T and t given in the legend). A linear fit to this data works reasonably well, which does corroborate fractal behavior. At low pH, the error in the linear fits was largest. From the slope of the lines a fractal dimensionality D_f is derived using equation (3.8). Not all the raw data used to calculate D_f are presented. For each set of pH and T, we performed at least five measurements of B as a function of time, at four different volume fractions.

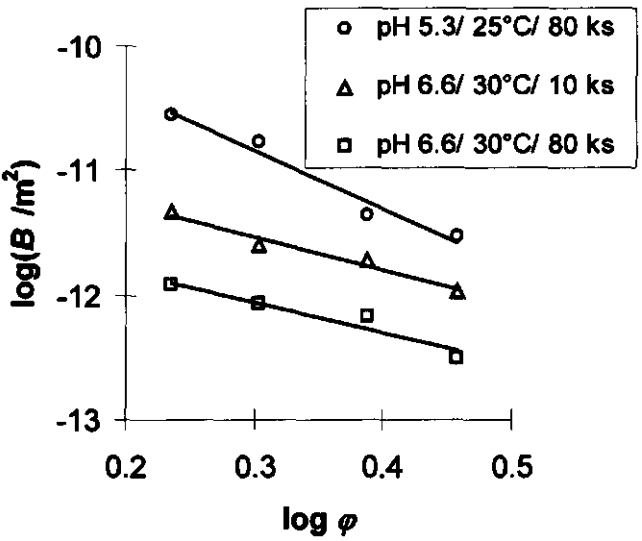

Figure 3.11. Permeability, B, as a function of volume fraction, φ. Shown are some typical results indicating the procedure to derive the fractal dimensionality. Conditions (time, pH and T) as indicated in the legend.

The values of D_f calculated from the permeability data are given in table 3.2. Most of the values are in the range 2.2-2.3 and they did not change much in time. The trends of the results from the permeability experiments are similar to those from confocal microscopy; e.g. D_f is fairly constant in time with a tendency to decrease with gel aging, more strongly so at low pH.

pH	T	microscopy (~6 ks)	(~40 ks)	permeametry (~6 ks)	(~40 ks)
6.65	25	2.5	2.4	2.4	2.3
6.65	30	2.2	2.4	2.2	2.3
6.0	25	2.5	2.2	2.1	2.0
5.3	20	2.6	2.0*	2.3	2.0*
5.3	25	2.5	1.8*	2.3	2.2*

Table 3.2. Fractal dimensionalities D_f of gels at given temperature and pH. Data calculated from microscopy and permeametry data. *Up to the maximum age at which the structure still appears to be fractal, i.e. 13-20 ks.

3.5.5 Effect of pH and temperature on micelles

The strong effects of pH and T can be explained in terms of the properties of the micelles (see *e.g.* refs. [6,7,12,1,29,28] and references therein). The first aspect is the interactions between the micelles. At low pH the para-casein micelles are less repulsive because the system is approaching the average pI of the casein proteins. At low T, more of the β-casein will reside in the hairy layer, which has a stabilizing effect.

The second aspect is the 'viscous behavior' (tendency to be deformed permanently) of the micelles or the lifetime of protein-protein bonds in the micelles [34]. Evidence for the effect of increased viscous particle behavior is mainly obtained from electron microscopy (particle fusion), and the correlation between the loss tangent (tan δ) obtained in dynamic measurements of the complex modulus, and the rate of gel aging. This is especially true for rennet-induced casein gels at low pH (5.3) and high T (30 °C) probably because near-absence of the hairy layer and dissolution of the colloidal calcium phosphate (CCP) from the micelles, renders them more subject to fusion. CCP is essential in keeping the casein proteins in the micelles together.

At high T in general, tan δ is higher. This may be because the mobility of all entities is higher at high T. Therefore, the rate of rearrangements like particle fusion would be slightly enhanced. However, at high T also, internal hydrophobic interactions are stronger and the micelles are smaller. The increased hydrophobic interactions could be a driving force for rearrangements. However, the decreased voluminosity would make the micelles less deformable and decrease the tendency to exhibit particle fusion. These counteracting effects may explain why the effect of T on the rearrangement rate is not very strong. Even though rheological properties [28]

are affected, the fractal structure seems not affected by changing T in this range, apart from an unexpected increase in D_f at intermediate timestages.

Using electron microscopy and at a different range of temperatures (26-40°C), some minor structural differences of rennet-induced casein gels were observed by others [35]. Especially particle fusion seems to be enhanced at temperatures like 40°C.

The breakdown of the matrix, or coarsening of the gel, can be seen as an early stage of (macro)syneresis. Syneresis is known to be promoted by a low pH and a high T [34,12].

An additional point of interest is the continued activity of rennet [4,36]. Continued rennet action is partly responsible for the softening of cheese texture. Detailed information on the hydrolysis has been established in solutions of various caseins at physiological pH. It is observed that rennet does not only activate hydrolysis of the Phe-Met bond in κ-casein, but that it can also hydrolyse several types of casein molecules at several places, the more so at a lower pH. In the timescales of this study, non-specific rennet activity may possibly contribute to the instability of the micelles; thereby enhancing rearrangement. However, this field is largely unexplored.

The effect of rearrangements on structure and rheology (in relation to the effect of pH and T on the properties of (para-)casein micelles) will be discussed in more detail in ref.[28] and [29].

3.6 Conclusions

Confocal micrographs can be used to probe the coarsening of rennet-induced casein gels in time. The gel pores become larger, the clusters become more compact (i.e. non-fractal) and thin straight strands between clusters are formed (at low pH within ~20 ks; at high pH from ~20 ks onwards).

This is also expressed in the fractal parameters calculated from the (deconvolved) micrograph images: P, and especially R_0 increase in time and D_f decreases in time. The scaling analysis of both microscopic and permeability data shows that the fractal dimensionality, D_f, is high (~2.2-2.6), which would indicate slow aggregation and rearrangements during aggregation. The parameter R_0 is a suitable measure of the size of the compact building blocks. Especially at low pH, the parameter P is too small to be a measure of the size of the gel pores in the late stages of gel aging. It can be concluded that sole knowledge of the value of D_f is not sufficient to characterize gel structure.

All aging effects proceed faster at higher T and lower pH (down to 5.3) and are probably due to gel matrix rearrangements, like particle fusion.

The fractal parameters obtained from the micrographs are highly dependent on the gray scale threshold value chosen.

The fractal scaling relations for the permeability work surprisingly well for the prediction of the apparent tortuosity and compact building block sizes.

3.7 References

[1] Horne, D. S., *Int Dairy J* **8**, 171, (1998)
[2] van Hooydonk, A. C. M.; Walstra, P., *Neth Milk Dairy J* **41**, 19, (1987)
[3] van Dijk, H. J. M.; Walstra, P., *Neth Milk Dairy J* **40**, 3, (1986)
[4] Roefs, S. P. F. M.; van Vliet, T.; van den Bijgaart, H. J. C. M.; de Groot-Mostert, A. E. A.; Walstra, P., *Neth Milk Dairy J* **44**, 159, (1990)
[5] Bauer, R.; Hansen, M.; Hansen, S.; Ogendal, L.; Lomholt, S.; Qvist, K.; Horne, D., *J Chem Phys* **103**, 2725, (1995)
[6] Knoop, A.-M.; Peters, K.-H., *Kieler Milchwirtschaftliche Forschungsberichte* **27**, 315, (1975)
[7] Zoon, N.; van Vliet, T.; Walstra, P., *Neth Milk Dairy J* **42**, 249-312 and 43:17-52, (1988 and 1989)
[8] Lucey, J. A.; van Vliet, T.; Grolle, K.; Geurts, T.; Walstra, P., *Int Dairy J* **7**, 381 and 389, (1997)
[9] van Vliet, T.; Lucey, J. A.; Grolle, K.; Walstra, P. In *Food Colloids; Proteins, Lipids and Polysaccharides*; Dickinson, E., Bergenståhl, B., Eds.; Royal Society of Chemistry: Cambridge, 1997.
[10] Lucey, J. A.; Tet Teo, C.; Munro, P. A.; Singh, H., *Food Hydrocoll* **12**, 159, (1998)
[11] Auty, M. A. E.; Fenelon, M. A.; Guinee, T. P.; Mullins, C.; Mulvihill, D. M., *Scanning* **21**, 299, (1999)
[12] Walstra, P. In *Cheese: Chemistry, Physics and Microbiology 1*; Fox, P. F., Ed.; Chapman & Hall: London, 1993.
[13] Bremer, L. G. B. , PhD Thesis, Wageningen Agricultural University, 1992.
[14] Barrett, A. H.; Peleg, M., *Lebensm-Wiss Tech* **28**, 553, (1995)
[15] Blonk, J. C. G.; van Aalst, H., *Food Res Int* **26**, 297, (1993)
[16] Chesnutt, M. H., *Current Opinion Coll Interf Sci* **2**, 158, (1997)
[17] Bos, M. T. A. , PhD Thesis, Wageningen Agricultural University, 1997.
[18] Bos, M. T. A.; van Opheusden, J. H. J. *Royal Society-Unilever INDO-UK Forum - Fifth Meeting: Supramolecular and Colloidal Structures in Biomaterials and Biosubstrates*; CFTRI, Mysore, India, 2000
[19] Thill, A.; Veerapaneni, S.; Simon, B.; Weisner, M.; Bottero, J. Y.; Snidaro, D., *J Coll Interf Sci* **204**, 357, (1998)

[20] Witten, T. A.; Sander, L. M., *Phys Rev Lett* **47**, 1400, (1981)
[21] Bremer, L. G. B.; Bijsterbosch, B. H.; Walstra, P.; van Vliet, T., *Adv Coll Interf Sci* **46**, 117, (1993)
[22] Viscek, T. *Fractal growth phenomena*; 2 ed.; World Scientific: Singapore, 1992.
[23] Darcy, H. P. G. *Les fontaines publiques de la ville de Dijon*; Victor Dalmont: Paris, 1856.
[24] Scheidegger, A. *Physics of flow through porous media, 3rd ed.*; University of Toronto Press, 1974.
[25] Bremer, L. G. B.; van Vliet, T.; Walstra, P., *J Chem Soc Faraday Trans 1* **85**, 3359, (1989)
[26] Renner-Nantz, J. J.; Shoemaker, C. F., *J Food Sci* **64**, 86, (1999)
[27] Walstra, P., *J Dairy Res* **46**, 317, (1979)
[28] this thesis, chapter 5
[29] this thesis, chapter 4
[30] this thesis, chapter 2
[31] Tirado-Miranda, M.; Schmitt, A.; Callajas-Fernández, J.; Fernández-Barbero, A., *Langmuir* **15**, 3437, (1999)
[32] Molecular Probes *Handbook of Fluorescent Probes and Research Chemicals, 7th edition*, 1999.
[33] Hassan, A. N.; Frank, J. F.; Farmer, M. A.; Schmidt, K. A.; Shalabi, S. I., *J Dairy Sci* **78**, 2629, (1995)
[34] van Vliet, T.; van Dijk, H. J. M.; Zoon, P.; Walstra, P., *Coll Polym Sci* **269**, 620, (1991)
[35] Lagoueyte, N.; Lablee, J.; Lagaude, A.; Tarado de la Fuente, B., *J Food Sci* **59**, 956, (1994)
[36] Fox, P. F.; Law, J.; McSweeney, P. L. H.; Wallace, J. In *Cheese: chemistry, physics and microbiology*; Fox, P. F., Ed.; Chapman & Hall:, 1993.

Chapter 4

Categorization of rheological scaling models for particle gels applied to casein gels*

4.1 Summary

Rennet-induced casein gels made from skim milk have been studied rheologically. A scaling model constituting a framework for describing the rheological behavior of gels is discussed and used for classification of the structure of the casein gels. There are two main parameters in the model, describing the number of deformable links in a strand and the link bendability. In the model at least five types of gel structure can be distinguished.

Application of the model to experimental data on rennet-induced casein gels at pH 6.0-6.65 and 25°C, shows that these contain straight strands with a high number of deformable links. Analysis of experimental data of the storage modulus, maximum linear strain and yield stress as a function of volume fraction, results in the same information about the gel structure.

*article submitted

4.2. Introduction

In literature various models describing rheological properties of gels formed by fractal aggregation can be found. In this paper a scaling model is described, that reproduces the main models. The model is used to analyze the scaling of small- and large-deformation rheological parameters with the volume fraction, of rennet(-induced) skim milk gels. These types of casein gels are intermediate products in cheese production and therefore of industrial importance.

The elastic behavior of a particle gel can in principle be related to that of the elements that build up the structure and their mutual interactions. The effect of the suspending fluid can usually be neglected. The problem is that neither the precise structure, nor the detailed microelastic behavior of the elements is known for the specific sample under consideration. Here we present scaling laws, in terms of the volume fraction of particles, for the elastic behavior of certain generic types of structures, based on a simple microelastic model. The scaling exponent appears to depend rather sensitively on the type of structure assumed, allowing direct assessment of gel structure through rheological experiments.

In the classical model by Flory [1], a gel is described as a collection of cross-linked macromolecular chains. Only entropic contributions to the resistance against deformation are taken into account, which makes the model inapplicable to particle gels like casein(ate) gels. One of the first gel network models relating colloidal interactions and gel structure to rheology of particle gels was developed by van den Tempel [2]. This early model was based on an equal contribution of the particles in the gel to its stiffness, and could not describe the experimentally observed scaling of the moduli of particle gels with the volume fraction. The stress-carrying strands were assumed to be straight. Kantor and Webman [3] were the first to develop a model, in which the stress-carrying strands take the form of a random walk. This model was combined with percolation theories. Soon after, making use of the fractal concept developed by Mandelbrot (see *e.g.* [4]), models were developed where the strands have a chemical dimensionality. The fractal character of the aggregation preceding the gelation, was shown [5] to result in a systematic relation between the storage modulus and the volume fraction of particles. At about the same time, it was shown [6] that fractal structures can be found in computer simulations of particle gels formed by fractal cluster-cluster

aggregation. Later, Shih *et al.* [7] showed that the existing 'fractal strand' or 'strong link' model could be extended to a so called 'weak link' category and could successfully be used to analyze experimental results. Recent applications or extensions in the spirit of Kantor and Webman and Shih *et al.*, are refs. [8-13].

Bremer *et al.* [14-16] independently developed a model that resulted in two additional categories of gel models; the so called 'straight strands' and 'hinged strands' models. These models were based on a very useful but more intuitive perception of the gel structure (see [17]). The outcome of these models was shown to correlate better with experimental data obtained for casein particle gels, than existing models based on the Kantor and Webman approach. According to Vreeker *et al.* [18], for heat-induced whey protein gels both approaches could be applicable.

In this paper it is shown that the straight and hinged strand models by Bremer can also be derived using the framework of Kantor and Webman. For this purpose, the Kantor and Webman model is generalized by introducing a scaling parameter δ (as a measure of the number of deformable links in a strand) and a parameter ε (as a measure of the link bendability). The results of the generalized model effectively categorize gel structure into five types. The model constitutes a tool for engineers for relating gel structure to rheology for a widely varying range of particle gels.

The model is applied to rennet-induced casein gels. The model requires knowledge of the fractal dimensionality D_f. We have obtained this by confocal microscopy and permeametry [19]. Rennet-induced casein gels are soft and visco-elastic materials, produced in the early stages of cheese making by adding rennet enzyme to (skimmed) milk. The rennet enzyme cuts off the outer hairy layer of the casein particles, or casein micelles. This induces aggregation of the micelles into tenuous clusters that will finally form a space-spanning network. For an overview on casein micelles and related subjects see *e.g.* [20] and references therein.

4.3. Models and theory

4.3.1 The fractal aggregation model

Fractal models predict a power law behavior of the volume fraction of particles in a cluster, φ_c, with the cluster radius R_c, according to (see *e.g.* [14])

$$\varphi_c \propto \left(\frac{R_c}{a_{eff}}\right)^{D_f - d}, \qquad (4.1)$$

where D_f is the fractal dimensionality (generally a non-integer number ≤ 3), a_{eff} is a characteristic size of the compact building blocks of the aggregate and d is the Euclidean dimensionality (= 3). At the gel-point the average particle volume fraction in the clusters equals the overall bulk volume fraction, *i.e.* $\varphi_c = \varphi$. Combined with relation (4.1), this yields

$$R_c \propto a_{eff} \varphi^{\frac{1}{D_f - 3}}. \qquad (4.2)$$

We assume that at the gel point a gel can be described as a close packing of fractal clusters. According to *e.g.* ref. [4], their cluster size R_c can be identified with the blob size or correlation length ξ of a percolating network. We may rewrite relation (4.2) as

$$\xi = a_{eff} \varphi^{\frac{1}{D_f - 3}}. \qquad (4.3)$$

4.3.2 The microelastic model

The model described in this paper assumes that the particles form a homogeneous network with a hierarchy of structural elements, each at a different length scale. Figure 4.1 shows the framework of the model concerning the gel structure. Four length scales of structure are considered: *particles*, (rigid) strand *segments*, *clusters* and the *whole gel*. This figure illustrates that the primary particles (*e.g.* para-casein micelles or caseinate particles) may build up mechanically stiff structures called rigid segments. The rigid segments are identified with the compact building blocks of size a_{eff} mentioned in the previous section. These segments build up the stress-carrying strands within a (fractal) cluster, and a close packed stacking of clusters finally builds up the macroscopic gel. A cluster can be seen as consisting of more or less tortuous strands, of which only a few are stress-carrying upon deformation. The clusters are linked by the stress-carrying strands crossing the periphery of the clusters. The number of stress-carrying strands per cluster is independent of cluster size, which is a consequence of the assumed scale invariance of the structure of the clusters [14]. Each consecutive level has a length scale associated with it, indicated to the right in figure 4.1, and these levels increase, $a \leq D \leq \xi \leq g$.

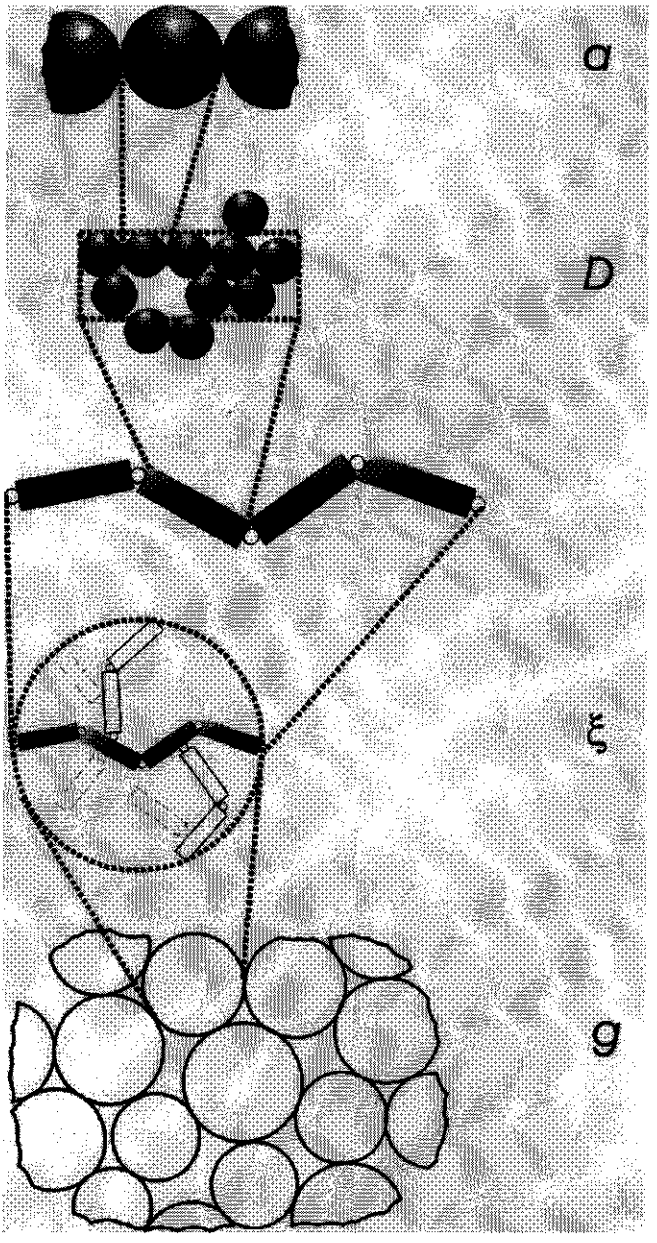

Figure 4.1. Schematic representation of the various structural levels in a particle gel, as used in the scaling model. Only a selection of clusters is drawn to represent the gel. In the modeling, the deforming link has no actual size. The exact structure and shape of the rigid segments is chosen arbitrarily.

In the modeling, the elastic constant of each level is linked to the one below, using the proper scaling relation. The scaling relations are based upon the way a deformation at one level translates into that of the next level. Thus, a macroscopic deformation is related to a microscopic deformation. For each length scale P an elastic (scalar) constant K_P can be defined. It relates the force involved to the pertaining change in length ΔP of the structure considered along the force F_P. We assume linearity between the displacement and the associated force (Hookean spring)

$$F_P = K_P \, \Delta P . \tag{4.4}$$

The appropriate length scale P can be any of a, D, ξ or g.

Not all relations are of the form of equation 4.4 (stretching of a spring). Depending on the type of structure of the stress-carrying strand (straight/curved), the deformation at the interlinks between the smallest structural level, may also be bending: suppose we consider both the individual particles at level a and the segments at level D as rigid objects ($K_D = \infty$, $K_a = \infty$), but the interlinks or junctions between them may be deformed. We distinguish two types of deformations at this lowest level, with elastic constants K_e and K_ρ. These deformations form our microelastic model. The parameter K_ρ represents an elastic constant of bending (N m). The parameter K_e represents an elastic constant of extension or stretching (N m^{-1}).

$$K_\rho = \frac{M}{\Delta\rho}, \qquad \text{bending} \tag{4.5a}$$

and

$$K_e = \frac{F_e}{\Delta e}, \qquad \text{stretching} \tag{4.5b}$$

where $\Delta\rho$ is the (very small) change in angle as a result of bending, M is the torque, F_e is the force (component) of stretching and Δe is the resulting (small) displacement. If the network can deform without stretching of the individual links, bending will be the dominant mode. If the network is (*i*) inter-multiply connected and (*ii*) the strands are straight, stretching of the links becomes necessary for deformation, and this will be the dominant mode.

Figure 4.2 shows a situation of a rod attached to a wall. This can be used to represent a segment of particles connected to the gel matrix. With the help of this figure, we will write the appropriate scaling relations for an

apparent elastic constant for bending (K_b) and an apparent elastic constant for stretching (K_s).

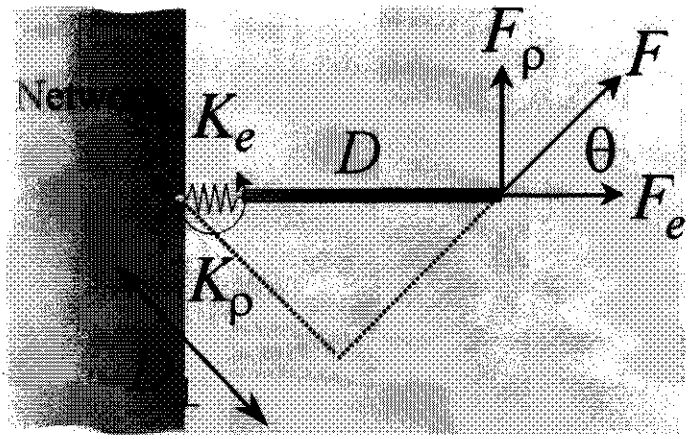

Figure 4.2. Explanation of the effect of forces acting on a strand or strand segment, resulting in (a) bending, (b) stretching. Parameters are explained in the text.

In figure 4.2 a force F is applied at the end of a rigid segment. Note that the sizes of the springs are highly exaggerated. The theoretical (very small) bending deformation as a result of the transversal component of the force (F_ρ) is $\Delta b = D\,\Delta\rho$, the torque $M = D_\perp \cdot F$, and the lever $D_\perp = D \cdot \sin\theta$, where the angle between the direction of the segment and the direction of displacement is θ. We can write

$$\Delta b = \frac{F D^2 \sin\theta}{K_\rho} \qquad \text{bending} \qquad (4.6a)$$

The same structure of figure 4.2 can also be considered in an experiment dominated by stretch. The lateral component of the force (F_e) stretches the end of the segment over a (very small) distance Δe according to

$$\Delta e = \frac{F \cos\theta}{K_e} \qquad \text{stretching} \qquad (4.6b)$$

Suppose the rheology of the system is only determined by the effective elastic constant of bending (K_b). No stretching is assumed to take

place. Using equations (4.6a) and (4.6b), we can write the energy of the system. To find the case of bending only, we can conveniently write

$$U = \frac{\frac{1}{2}F^2 \cos^2\theta}{K_e} + \frac{\frac{1}{2}F^2 D^2 \sin^2\theta}{K_\rho} \qquad (4.7)$$

which is identical to equation (4.6) in the paper by Kantor and Webman [3], for one segment. Next we let $K_e \rightarrow \infty$. If we then use $U = \frac{1}{2} F^2 / K_b$, the apparent elastic stretch constant of the displacement resulting from the bending, K_b (N m^{-1}), is as follows

$$K_b = \frac{K_\rho}{D^2 \sin^2\theta} = \frac{K_\rho}{D_\perp^{\,2}}. \qquad \text{bending} \qquad (4.8)$$

Alternatively, the rheology of the system may be only determined by the effective elastic constant of stretching (K_s). The energy of the system can conveniently be written as follows

$$U = \frac{1}{2}\Delta s^2 K_e \cos^2\theta + \frac{\frac{1}{2}\Delta s^2 K_\rho \sin^2\theta}{D^2} \qquad (4.9)$$

where Δs is the displacement of the end of the segment ($\Delta s = \Delta e/\cos\theta = \Delta b/\sin\theta$). In the case of stretch only, the bending energy is assumed to be zero and we take $K_\rho \rightarrow 0$. If we next use $U = \frac{1}{2}\Delta s^2 K_s$, the effective or apparent elastic constant during stretch (K_s) equals:

$$K_s = K_e \cos^2\theta, \qquad \text{stretching} \qquad (4.10)$$

An important assumption in our model is that the macroscopic characteristics are supposed to be determined by K_s and K_b, depending on the type of microscopic deformation (respectively stretching or bending). The corresponding microscopic deformations are considered small (*i.e.* Δb, $\Delta e << D$).

Extensive reorganization or rearrangement within the segments, may include particle fusion or similar processes of the individual particles ([21,22]), which rigidifies the originally inter-multiple connected network of springs. This on the one hand leads to an increase of K_D, which was already assumed infinite, but more importantly can lead to an increase of D, the size of the rigid segments.

4.3.3 The model of Kantor and Webman

In this section the relationship between the elastic constants of the structural levels is determined. As discussed above, the smallest relevant structural level are the rigid segments (size D), because these are the largest rigid entities (i.e. the elastic constant K_D is infinite). At the level of the links between these segments, deformation is allowed to take place. The relevant elastic constants for bending and stretch at this level, are respectively K_e and K_ρ.

The next level is that of the cluster size or correlation length ξ. Within the clusters of size ξ, the rigid segments form a cluster spanning strand of contour length L. Giving the size of the segments (D), there are $N = L/D$ segments per strand. A deformation of the strand will be distributed over all links between the rigid segments. Upon stretching of a straight strand of size ξ, the stretch energy is distributed equally over the links between the segments. The elastic constant of the strand is

$$K_\xi = \frac{K_e \cos^2\theta}{N}. \qquad \text{stretching} \qquad (4.11a)$$

Because the strands are straight, the factor $\cos^2\theta$ is the same for all segments and can be left out of the equation (according to equation 4.10).

Upon deformation of a curved strand of (end-to-end) size ξ, the dominant effect is that the links between the segments are bent. Each bending junction will give a contribution according to equation (4.7), with the provision that now the lever effect differs between segments. It appears [3], that one may treat all junctions independently. Instead of D one should take the lever of a specific junction to be the vector between that junction and the end of the strand, the application point of the force. The combined effect is given by the r.m.s. average $L_\perp$ of the projected lengths of all these vectors, one for each of the N segments. Concluding: during bending there is a combined effect of N and $L_\perp$ [3]

$$K_\xi = \frac{K_\rho}{N(L_\perp)^2}. \qquad \text{bending} \qquad (4.11b)$$

Furthermore, Kantor and Webman mentioned that particularly if N is large and if the strand is in a curved configuration, bending will dominate stretching effects.

4.3.4 Scaling of the storage modulus

In this section we present a scaling law for the storage modulus. The derivation is given for clusters with size ξ. The largest length scale is the whole gel with size g. The gel with size g is dealt with as a collection of clusters with size ξ. We assume affine deformation at length scales beyond ξ. This means that the structure of length ξ is deformed just as the whole sample is, but below ξ this is not necessarily the case. We assume the storage modulus, G', is given by (using equation (4.4))

$$G' = \frac{\sigma}{\gamma} = \frac{F}{A\gamma} = \frac{K_\xi \Delta\xi}{A\gamma}. \tag{4.12}$$

where A is the surface area to which the shear force F is applied. The parameter γ is the resulting macroscopic deformation. It can be written in terms of the deformation at the level of ξ (assuming affine deformation at the level of ξ)

$$\gamma = \frac{\Delta\xi}{\xi}, \tag{4.13}$$

while

$$A \propto \xi^2. \tag{4.14}$$

The scaling of the storage modulus, G', becomes [7]

$$G' \propto \frac{K_\xi}{\xi}, \tag{4.15}$$

In the appendix it is shown that a prefactor for the scaling relation (4.15) can be calculated, based on theory starting with a stress tensor expression [23]. Incorporated in this prefactor is the 'structural connectivity' of the clusters. From the prefactor follows that if we use equation (4.15), we effectively assume a constant 'connectivity' per cluster. This connectivity is also an important determinant for the type of network. Straight strands and *high* connectivity results in an inter-multiply connected network with stretching as the dominant deformation. Straight strands and *low* connectivity allows the network to relax without stretching (just as for bending strands).

4.3.5 Scaling at large deformations

In this section the scaling relations between the elastic constant of the clusters, K_ξ, and the rheological parameters at large deformations will be presented.

First, we will deal with the maximum linear strain (*i.e.* strain at the limit of linearity), γ_0. At the maximum linear strain we assume there is still affine deformation down to cluster level. Rewriting equation (4.13) and incorporating equation (4.4) gives respectively

$$\gamma_0 = \frac{\Delta\xi_0}{\xi} = \frac{F_{\xi,0}}{K_\xi \xi}. \qquad (4.16a,b)$$

Next we assume the critical force in the cluster at the (macroscopic) maximum linear strain ($F_{\xi 0}$), to be independent of the size of that cluster (ξ). This is justified by the fact that only one 'weak junction' has to start behaving non-linearly (*e.g.* fracture) due to the stress concentration at that spot. Incorporating this assumption into equation (4.16b) gives [8]

$$\gamma_0 \propto \frac{1}{\xi K_\xi}. \qquad (4.17)$$

Of course the scaling of the elastic constant itself is given by equation (4.11b) for bending and (4.11a) for stretching.

Next, we deal with yielding. The yield stress is somewhat more complicated, because we cannot use the scaling relations above. These were derived under the assumption that the microelastic constants K_ρ and K_e would not change, and the system behaves linearly, but at yielding deformations this cannot be maintained. It appears we do not need them. Again affine deformation assumes the stress at the cluster level is the same as at sample level

$$\sigma_y \propto \frac{F_y}{\xi^2} \qquad (4.18)$$

where F_y is the tension force within the strand at the fracture point, which is a constant independent of the size of ξ or g. At this tension force the weakest spot in the chain will give way, because it is stretched beyond the limit where it will relax reversibly. Also, this tension force will be independent of the

cluster size. So it appears that the detailed structure of the clusters is unimportant for the scaling of the yield stress with cluster size

$$\sigma_y \propto \frac{1}{\xi^2} \tag{4.19}$$

Note that the value of the yield stress at a given cluster size, may depend upon the cluster structure. However, in view of the microscopic character of F_y, we do not expect this to be the case either.

Following different arguments the scaling of σ_y may become more complicated. One may for instance assume that microscopic fracture during yielding results from microscopic bending, instead of stretching [8]. In such cases the parameters ε or δ (see next section) may enter scaling relation (4.19), leading to different predictions of the scaling behavior for some categories of gel structures.

4.3.6 Definition of structural scaling exponents

In the previous sections it was stressed that several parameters are independent of the cluster size, ξ, and hence the volume fraction, φ. We now discuss the scaling of two remaining parameters: N (in equations (4.11a, b)) and $L_\perp$ (in equation (4.11b)).

Others [24,8] have introduced an exponent ε to describe the scaling of $L_\perp$ with the cluster size:

$$L_\perp \propto \xi^\varepsilon, \tag{4.20}$$

where $0 \leq \varepsilon \leq 1$. For bending the lever ($L_\perp$) plays a role and for stretching $L_\perp$ plays no role, which can formally be identified with ε being equal to, respectively, 1 and 0. Important to note is that one cannot interpret ε as a parameter that can vary between 0 and 1, depending on the degree of strand curvature. Actually, $\varepsilon = 1$ and $\varepsilon = 0$ only means that the dominating microscopic deformation is, respectively, bending and stretching. We will keep the exponent in our model as a criterion for making this distinction.

Next, we will deal with N. A scaling exponent δ is introduced as follows

$$N \propto \xi^\delta, \tag{4.21}$$

where $0 \leq \delta \leq 2$. Three situations are distinguished: $\delta = 0$, 1 and 2. One case is N = constant (*i.e.* independent of ξ) and $\delta = 0$. This can occur if the originally fractal clusters have rearranged such, that $D = \xi$. This means that the strand is rigid. Another case is $\delta = 1$. Then the number of rigid segments $N \propto \xi$ and the strand can be considered elastic or 'flexible'. A separate case mentioned in the literature [6,25] is the case of $1.0 < \delta < 1.3$. The δ then equals the chemical dimensionality of the stress-carrying strand in the cluster. In the case of a random walk, $\delta = 2$. Since this implies ideal chains, this situation is not very realistic. The excluded volume effects cannot be neglected, like in some polymer gels.

To further simplify matters, K_ε and K_ρ are assumed to be independent of φ and therefore of ξ. There is no obvious rationale to assume that the junction forces between two segments are volume-fraction or strand size dependent. Also, the exact interactions are usually unknown in practice. Thus, these elastic constants are considered constant, and hence can be omitted from scaling equations (4.15) and (4.17) and (4.19).

Summarizing, the elastic constant for different configurations can be written in terms of equation (4.11b), incorporating relations (4.20) and (4.21)

$$K_\xi \propto \frac{1}{\xi^\delta \xi^{2\varepsilon}} \tag{4.22}$$

Incorporating relation (4.22) into (4.15) for G' and (4.17) for γ_0 gives

$$G' \propto \xi^{-(1+2\varepsilon+\delta)}, \tag{4.23}$$

$$\gamma_0 \propto \xi^{2\varepsilon+\delta-1}, \tag{4.24}$$

$$\sigma_y \propto \xi^{-2}. \tag{4.25}$$

Relations 4.23-25 are applicable to any kind of particle gel. For particle gels formed by fractal aggregation, one may use relation (4.3) between ξ and the volume fraction, φ, which parameter can readily be varied in an experiment.

4.3.7 Definition of five categories of gel types

In this section, five categories of gels with specific strand types (specific values of ε and δ) are named and summarized. Figure 4.3 can be used in the explanation of the five categories, following next.

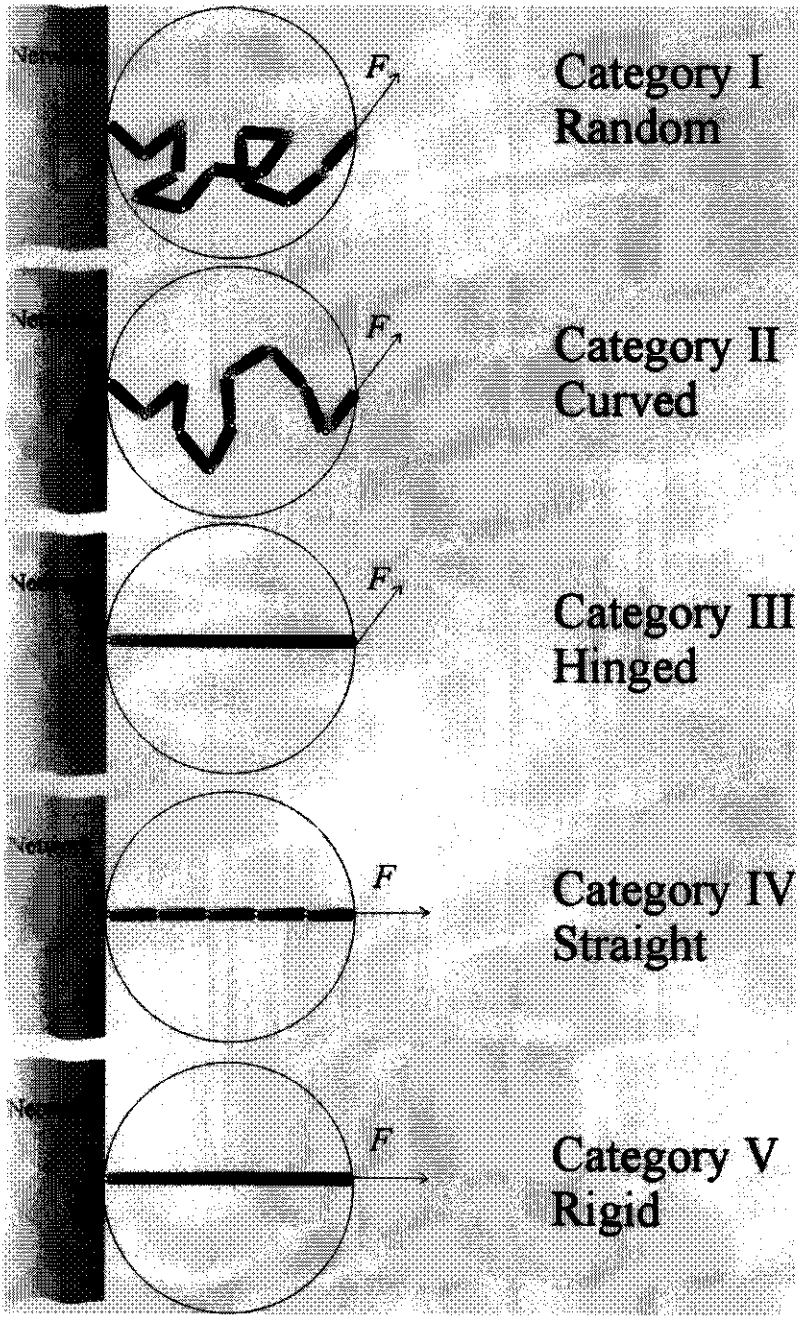

Figure 4.3. Schematic representation of the five categories of gel structures that are distinguished in the scaling model.

The first category of gels contains '**random**-walk strands'. A random walk behavior corresponds to $\delta = 2$. In addition, a random walk is very curved and bending dominates, so $\varepsilon = 1$. This model was described by ref. [3].

The second category contains '**curved** strands'. Again, bending is the dominant deformation at the microscopic level (especially for large N), so $\varepsilon = 1$. In addition, the structure is such that the number of segments in a stress-carrying strand increases linearly with the cluster size, which means $\delta = 1$. This category may describe very large and tenuous clusters formed at relatively low volume fractions. Shih *et al.* [7] consider the internal structure of such clusters to be weak, relative to the links between the clusters. This is why they refer to this category as 'strong-link'. A refinement of this category for 'fractal strands' involves the chemical dimension x [6]. In this case $\delta = x$, where $1.0 < x < 1.3$.

The third category contains '**hinged** strands'. This category assumes $\varepsilon = 1$ and $\delta = 0$. This category of gels may be formed as a result of rigidifying of curved strands, *e.g.* due to rearrangements. Furthermore we assume that the clusters are still so loosely interconnected that bending will dominate. For bending $L_\perp$ reduces to $D_\perp$. Since we will always deal with a collection of strands with different angles between the force and the strand, the effective elastic constant is in the case of bending: $K_b = K_\rho \langle 1/D_\perp^2 \rangle$, and for stretch: $K_s = K_e \langle \cos^2\theta \rangle$. The brackets indicate the average of the collection. Since $D_\perp \propto \xi$ for bending, $\varepsilon = 1$ for the collection. The scaling corresponding to this category was first calculated by Bremer *et al.* [15] using a different model.

The fourth category contains '**straight** strands' where a series of segments of constant size are linked to each other in a perfectly straight line, or the stress-carrying structures are highly interconnected. Stretch is the dominating deformation. This means $\varepsilon = 0$ and $\delta = 1$. Bremer *et al.* [14] were the first to acknowledge the scaling corresponding to this category, calculated using a somewhat intuitive model. Later [16], they explained the mathematics of this category more thoroughly.

The fifth and last category contains '**rigid** strands'. Like in category III, there is one weak link in a rigid strand, *i.e.* $\delta = 0$. Stretch will dominate the microscopic deformation, so $\varepsilon = 0$. This type of gel is most likely formed at relatively high volume fractions in combination with extensive crosslinking in the clusters. In this case, the clusters are more rigid. Multiple connections between the nodes may also lead to more rigid structures, and multiple connections in combination with straight strands will lead to a deformation dominated by stretch. The scaling of the rheological parameters that follows from this category is the same as predicted by the weak-link category [7].

Finally, some minor remarks on assumptions of the categories III, IV and V remain. In principle, for the given structure of category III also stretching can occur (*e.g.* if the clusters are highly interconnected). In this

case $<\cos^2\theta>$ is a constant determined by the distribution of θ and is considered independent of ξ, thus $\varepsilon = 0$. This situation is then equivalent to category V.

4.3.8 Application to particle gels formed by fractal aggregation

In this section, the link between the cluster size ξ and the volume fraction of particles, φ, is given using fractal theory. This allows us to write the relations as a function of a parameter that is directly experimentally accessible. The applicability of fractal theory is clear for categories I and II. Rearrangements, both before and after gelation, may lead to locally more rigid or straight structures generic for categories III-V. The scaling between fractal cluster size and volume fraction should be preserved during later rearrangements. This is the case if the strands become mechanically more rigid (*e.g.* due to partial particle fusion), while the overall structure remains fractal. It is sufficient if the rearrangements occur below ξ, inside the clusters. Clusters may then lose their fractal structure, but the scaling between ξ and φ remains.

For particle gels formed by fractal aggregation, the scaling of the storage modulus, the maximum linear strain and the yield stress with the volume fraction can be derived, by incorporating equation (4.3) into relations (4.23-25)

$$G' \propto (a_{\text{eff}})^{-\alpha} \varphi^{\frac{\alpha}{3-D_f}}, \text{ where } \alpha = 2\varepsilon + \delta + 1 \qquad (4.26)$$

$$\gamma_0 \propto (a_{\text{eff}})^{-\beta} \varphi^{\frac{\beta}{3-D_f}}, \text{ where } \beta = -2\varepsilon - \delta + 1 \qquad (4.27)$$

$$\sigma_y \propto (a_{\text{eff}})^{-\nu} \varphi^{\frac{\nu}{3-D_f}}, \text{ where } \nu = 2. \qquad (4.28)$$

We assume that the parameter a_{eff}, the size of the compact building blocks, is independent of the volume fraction. Such a dependence would prevent a direct calculation of the scaling exponents α, β and ν from experiment.

Finally, we incorporate the definitions of the five categories into the scaling laws of the storage modulus (relation 4.26), the maximum linear strain (relation 4.27) and the yield stress (relation 4.28). The five categories of gels each have their specific values for the exponents α, β and ν, associated with

the scaling behavior of the particular rheological parameter with the volume fraction. The results are summarized in table 4.1.

Category	Type of strand	Deformation	α	β	ν
I. Random	randomly curved; flexible	Bending	5	-3	2
II. Curved	curved; flexible	Bending	4	-2	2
III. Hinged	rigid	Bending	3	-1	2
IV. Straight	straight; flexible	Stretch	2	0	2
V. Rigid	rigid	Stretch	1	1	2

Table 4.1. Values of α, β and ν resulting from the choice of ε and δ for the five categories of gel types. For explanation of symbols see main text.

Note that the exponent ν is determined by the value of ε that applies to the structure *at* yield. This means that the outcome after application of the model may be that $\varepsilon = 0$ (no bending $\rightarrow$ straight strands), even though the structure at rest contained curved strands. In this special case, the strands have straightened as a result of the deformation.

The added value of the model is that, if the values of D_f are known, *e.g.* from microscopy and permeability [19] or computer simulations [26], α, β and ν can be calculated from experimental data (if D_f is not known, knowledge of the relation between ξ and φ suffices). After gel formation, the gel structure may change due to rearrangements (see *e.g.* [21]). These rearrangements may cause a change in gel category with time. In addition, information about a_{eff} and $\tilde{n}$ (for the latter parameter, see Appendix) could contribute to an exact calculation of the elastic constants.

Finally: the exact relation between G' and a_{eff} may actually be more complicated, because the interactions (written as elastic constants K_ρ and K_ε or by an energy factor d^2F / dx^2 by e.g. [14]) between the particles (which also contribute to G') can in principle also depend on the size a_{eff}. There are scopes for further refinement of the model at this point.

4.4 Materials and methods

4.4.1 Skim milk preparation

Standard reconstituted skim milk was prepared by dissolving 12 g skim milk powder (Krause, Heino; 100 g powder contains 0.6 g fat and 33.8 g casein protein) in 100 g demineralised water. To retard bacterial and enzymatic degradation, 200 µl of 10 wt% thiomersal (BDH Chemicals Ltd.) and 27 µl of a solution of 3.7 mg ml^{-1} (~0.9 TIU/100 ml) aprotinin (Sigma, A-1153, Lot #46H7145) were added. We also added 7 ml of a 0.5 molar NaCl solution (pH = 6.65) or 3.27 ml 0.5 molar HCl and 3.73 ml 0.5 molar NaCl solution (pH = 6.0). To reach equilibrium the dispersion was stirred for at least 16 hours at 25°C. In this way, reproducible results could be obtained from this milk for at least 4 days.

Whey was added to the milk to make skim milk with a lower mass or volume fraction of casein. This whey was prepared by allowing milk to gel (by adding doubled concentrations of rennet) and subsequently cutting and filtering it. Next, thiomersal was added and the whey was kept a few days at room temperature prior to using it, to allow the rennet action in the whey to become negligible. It should be noted that milk was diluted with whey made from milk of the same composition. Standard casein mass fractions studied were approximately 0.054, 0.063, 0.076 and 0.089 (assuming a voluminosity of 3 ml g^{-1} [27], and a milk density of 1.036 kg l^{-1}).

Commercial calf rennet (10.800 SU, Leeuwarder kaasstremsel) was added to the milk, to reach a final concentration in the milk of 0.02 (pH = 6.65) or 0.004 (pH = 6.0) vol%.

4.4.2 Rheometry

During gel aging, dynamic moduli were measured in a strain-controlled (VOR) rheometer (Bohlin Rheology, UK). A concentric stainless steel cylinder geometry (C14) was used, with an inner and outer cylinder radius of 14.0 and 15.4 mm, respectively, and a content of 2 ml. A 3.60 gf × cm torsion bar was used. A sinusoidal oscillating low amplitude strain (0.01), was applied. For the strain sweeps a strain from 0.0002 up to (maximally) 0.1 was applied. The deformation frequency was 0.1 Hz.

The yield stresses were measured using a stress-controlled (CVO) rheometer (Bohlin Rheology, UK). A concentric stainless steel cylinder geometry (C25) was used. The yield stress σ_y (Pa) is defined as the stress at which the apparent viscosity $\eta_{app} = \sigma / \dot{\gamma}$, where $\dot{\gamma}$ is the shear rate) passes through a maximum. The stress was increased (gradually; no steps) from 1 to

50 Pa in 300 sec. Every 6 seconds the stress and the strain rate were determined and the apparent viscosity calculated.

Directly after rennet addition, the milk was brought into the gap of the concentric cylinder; gels were thus formed in the apparatus itself, at 25 °C. To prevent evaporation gels were covered with oil during aging.

4.5 Results and discussion

Below, the results of the rheological experiments with rennet(-induced) casein gels are presented. In addition, the scaling model is applied to the data obtained.

After having added the rennet, the storage modulus or shear modulus, G', became systematically higher than G'' in approximately 3 to 5 ks. This time was taken as the gel time, t_{gel}. At t_{gel}, $t = 0$, *i.e.* all results are plotted as a function of gel age (time after t_{gel}).

In figure 4.4 four typical curves of G' as a function of time, t, are shown. The parameter G' gradually increases in time and is lower for lower volume fractions. Figure 4.5 gives four examples of G' as a function of the applied strain. Dashed lines are plotted to guide the eye in determining the linear (*i.e.* horizontal) regime and thereby γ_0. Three examples of curves of η_{app} versus shear stress are shown in figure 4.6. The stress corresponding to the maximum in the viscosity, was taken as the yield stress σ_y.

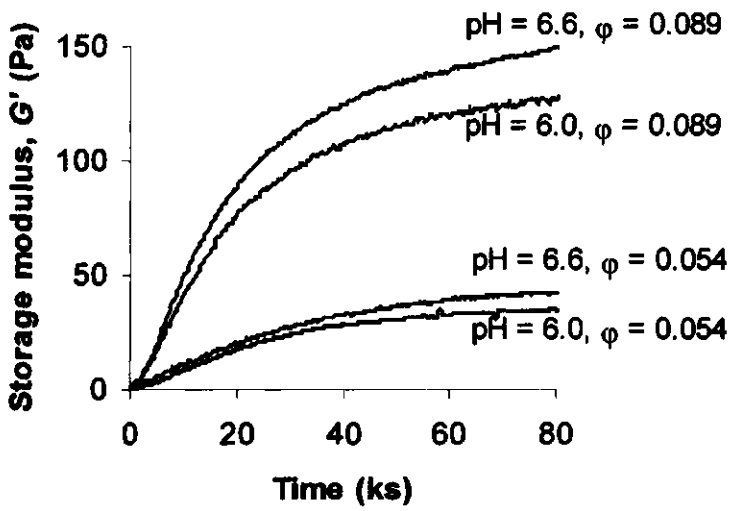

Figure 4.4. Typical examples of storage moduli, G', of rennet-induced casein gels as a function of time. Volume fractions and pH as indicated.

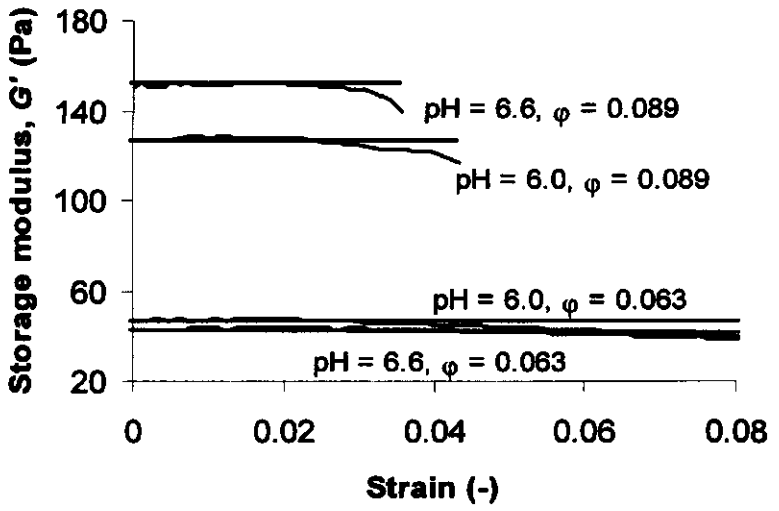

Figure 4.5. Typical examples of strain sweeps of rennet-induced casein gels at volume fractions and pH values as indicated. At the point at which the curves deviate from the dashed lines, the maximum linear strain, γ_0, is determined.

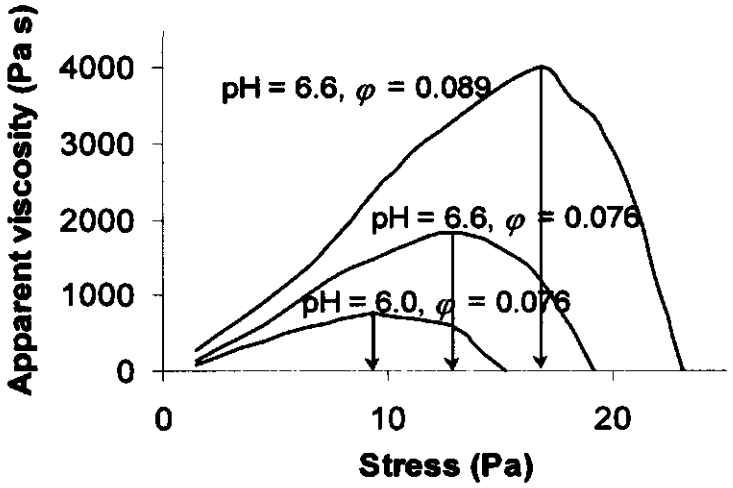

Figure 4.6. Typical examples of η_{app} versus shear stress curves calculated from successive 'creep' measurements on rennet-induced casein gels at volume fractions and pH values indicated. At the point at which the curve reaches a maximum, the yield stress σ_y is determined.

The values of G', γ_0, and σ_y as a function of volume fraction are compared at a fixed time after gelation, t. These values are plotted in figures 4.7, 4.8 and 4.9, respectively. From these figures, the scaling exponents according to relations (4.26-28) are calculated.

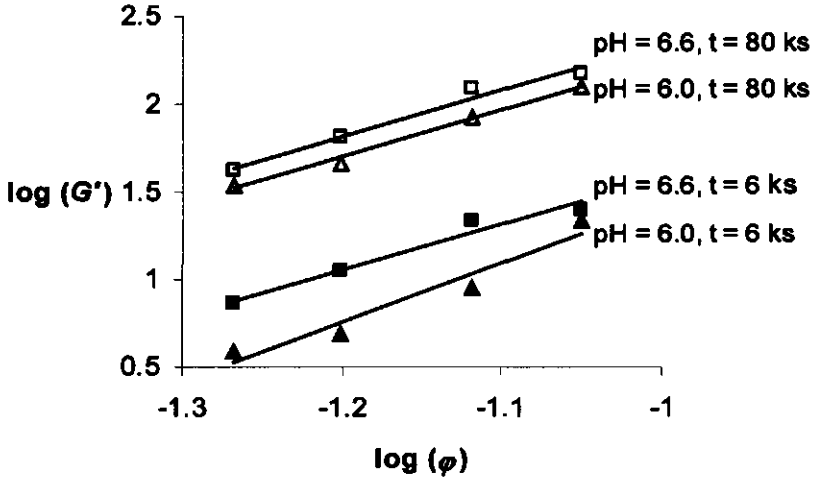

Figure 4.7. Four examples of (linear) log(G')-log(φ) relations for rennet-induced casein gels, at the gel aging times and pH indicated.

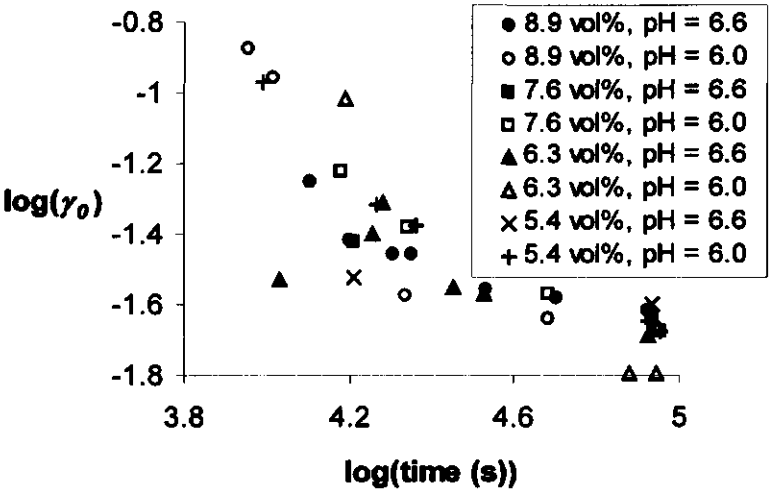

Figure 4.8. The maximum linear strain, γ_0, as a function of time for rennet-induced casein gels. Volume fraction and pH as indicated.

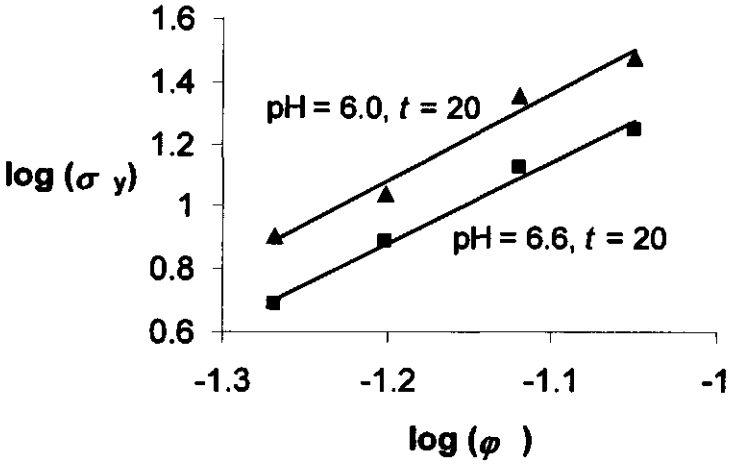

Figure 4.9. Two typical examples of the yield stress, σ_y, as a function of φ for rennet-induced casein gels. Gel aging times (t, ks) and pH as indicated.

Figures 4.7 and 4.9 show that reasonable linear fits of the parameters are obtained as a function of volume fraction. This is in accordance with the predicted scaling behavior, and values for α and ν can be determined with acceptable accuracy. This corroborates the (silent) assumption that no 'critical' φ [7] is crossed, in the range of φ studied. To calculate α and ν from the slopes of the linear fits in figure 4.7 and 4.9, we use the fractal dimensionality D_f obtained from confocal and permeability data [19]. According to the experimental results, the values of D_f probably slightly decrease in time. In this study, we used a single constant value of 2.3 for all data.

From figure 4.8, we conclude that for all pH values and gel ages γ_0 is approximately the same, so independent of φ. This means that (relation 4.27) $\beta \sim 0$. The reproducibility of the results does not allow a more detailed analysis. The error in determining γ_0 is especially high at low G' (see figure 4.5).

In table 4.2 we present the final results: the resulting average values of α, β and ν at pH = 6.65 and 6.0 are given. Not all data used to calculate α and ν in table 4.2 are presented in figures 4.7 or 4.9. Actually, G' was determined for four volume fractions and several different ageing times at each pH value studied. For the yield stress data we only determined the scaling of systems aged for 20 ks.

pH	α	β	ν
6.65	1.9	~0	1.8
6.0	2.0	~0	1.9

Table 4.2. Scaling parameters α, β and ν calculated from experimental data, making use of relations (4.26-28), with $D_f = 2.3$ ([19]). Temperature = 25 °C

All scaling exponents presented, indicate that the relevant scaling category for casein gels at or around physiological pH and room temperature is of category IV ('straight strands'). The fact that all different types of measurements point in this direction, validates the applicability of the model and corroborates that there is fractal aggregation. The presence of straight strands, especially at long aging times, has been confirmed by confocal microscopy experiments [28,19].

In addition, this study shows that it is impossible to determine a fractal dimensionality of a particle gel directly from rheological measurements without any knowledge about the structure of the strands.

Our results are similar to the findings of Bremer [28], who identified acid casein gels by rheometry, confocal microscopy and permeability as a category in between III and IV and consequently found $D_f \sim 2.3$ from combined measurements of the storage modulus, permeability and confocal images. Others have also presented studies that combine results on D_f and scaling of rheological parameters with the volume fraction. As an example, we will try to identify the type of gel from the results by Verheul *et al.* [29], who studied whey protein gels. They determined $D_f = 2.4$ (from measurements of permeability) and a scaling exponent $\alpha / (3 - D_f) = 5$ from measurements of the storage modulus. This gives $\alpha = 3$, which corresponds to category III ('hinged strands').

At lower pH (5.3) and higher temperatures (30 °C) application of the model is more complicated [30]. This is due to a higher rate of gel matrix rearrangements and a subsequently strong increase of a_{eff} during aging under these circumstances. In this paper, we have assumed D_f and a_{eff} to be constant during gel aging, which is not correct at low pH.

4.6 Conclusions

A categorization of types of gels is presented, based on two main parameters (the number of deformable links in a strand and the dominant type of microscopic deformation). The scaling of at least three rheological parameters, for a wide range of gel types, can be described using the model.

The model leads to similar conclusions regarding the structure of rennet-induced casein or skim milk gels based on data for the storage modulus, the yield stress and the maximum linear strain as a function of volume fraction: Casein gels at pH = 6.0-6.65 and T = 25 °C, are particle gels formed by fractal aggregation and consist of straight and elastic strands. Interestingly, clusters may then lose their fractal structure, but the scaling between ξ and φ remains.

4.7 Appendix I: List of symbols

a	radius of primary particle
a_{eff}	radius of compact building block
A	surface area on which the applied macroscopic force acts
D	length of rigid segment in a strand
$D_{\perp}$	length of lever with respect to the direction of the force acting on the end of a rigid segment
D_{f}	fractal dimensionality
Δb	displacement as a result of bending
Δe	displacement as a result of stretch
Δs	displacement as a result of a deformation dominated by stretch
F	force
F_P	force acting on a structure of length P (which can be any of a, D, ξ, or g)
$F_{\xi 0}$	force on a cluster at maximum linear strain
F_{y}	force at macroscopic yield
g	size of gel system
G'	storage modulus
K_P	elastic constant at length P (which can be any of a, D, ξ or g)
L	length of a strand of segments
$L_{\perp}$	projection radius of gyration of all links in the strand with respect to the direction of the force acting on the end of the strand (measure of lever effect in a cluster)
M	torque during microscopic bending
N	(= L / D) number of segments per strand
R_{c}	aggregate radius
x	chemical dimensionality of a strand
α	scaling exponent in relation between G' and φ
β	scaling exponent in relation between γ_0 and φ
δ	scaling exponent in relation between N and ξ; measure of strand flexibility

ε	scaling exponent indicating (microscopic) bending versus stretching
γ	macroscopic strain
γ_0	maximum linear strain; limit of linearity
φ	volume fraction of particles in whole system
φ_c	(local) volume fraction of particles in aggegate
ν	scaling exponent in relation between σ_y and φ
θ	angle between force (acting on end of segm. or strand) and segment or strand
$\Delta\rho$	change in angle of strand as a result of bending
σ	macroscopic stress
σ_y	macroscopic yield stress
ξ	average cluster radius; radius of average aggregate at gel-point

4.8 Appendix II: Calculation of prefactor

This section briefly deals with the calculation of the prefactor to relation (4.15). Van der Vorst [23] gave an expression for the static shear modulus of a closely packed crystal of latex spheres, assuming that only nearest-neighbor interactions are important:

$$G_0 = \frac{\varphi_{cp}\tilde{n}}{5\pi r}\left(U'' + \frac{4U'}{r}\right), \qquad (4.A1)$$

where φ_{cp} is a characteristic volume fraction at close packing, r is the distance between the latex particles in close packing, $\tilde{n}$ is the 'connectivity' or coordination number at the level of the particles and $U(r)$ is the interaction potential between the spheres (U' and U'' are derivatives with respect to r). The nature of the interactions is not specified so the electrostatic pair interaction energy between the latex particles in the crystal can readily be replaced by the deformation energy between clusters. Therefore r and $U(r)$ are replaced with ξ and $U(\xi)$, and $G_0 = G'$:

$$G' = \frac{\varphi_{cp}\tilde{n}}{5\pi\xi}\left(U'' + \frac{4U'}{\xi}\right). \qquad (4.A2)$$

Next, from equation (4.4) the deformation energy $U(\xi) = 0.5\, K_\xi(\Delta\xi)^2$, the first ($K_\xi\, \Delta\xi$) and second ($K_\xi$) order derivatives can be calculated. Incorporating these in equation (4.A2) and assuming $\Delta\xi$ is very small compared to ξ, gives:

$$G' = \frac{\varphi_{cp}\tilde{n}}{5\pi}\frac{K_\xi}{\xi}. \qquad (4.A3)$$

4.9 Appendix III: The model of Bremer *et al.*

The model presented in this paper is similar to the model presented by Bremer [14,15,16,28]. The framework of their model is given by the following equation:

$$G' = N_i C\left(\frac{\mathrm{d}^2 E}{\mathrm{d}e^2}\right) \qquad (4.A4)$$

where N_i is the number of stress carrying strands per unit area in a cross-section perpendicular to e, dE is the change in Gibbs energy when the particles in the strands are moved apart over a distance e and C is a characteristic length, determined by the geometry of the network, which relates the distance over which a bond between two particles is extended or compressed to the macroscopic shear strain.

Note that N and N_i have different meanings. The parameter N_i always scales with $1/A$, and therefore with ξ^2. The parameter C scales with $\Delta\xi / (N\gamma)$. For stretch, the term d^2E/de^2 is equal to K_s. For bending, d^2G / de^2 is equal to $K_\rho / (L_\perp)^2$. This eventually results in the same scaling relation for G' as given in relation (4.26).

4.10 References

[1] Flory, P. J. *Principles of Polymer Chemistry*; Cornell University Press: Ithaca, 1953.
[2] van den Tempel, M., *J Coll Sci* **16**, 284, (1961)
[3] Kantor, Y.; Webman, I., *Phys Rev Lett* **52**, 1891, (1984)
[4] Gefen, Y.; Aharony, A.; Mandelbrot, B. B.; Kirkpatrick, S., *Phys Rev Lett* **47**, 1771, (1981)
[5] Sonntag, R. C.; Russel, W. B., *J Coll Interf Sci* **116**, 485, (1987)
[6] Brown, W. D. , PhD Thesis, University of Cambridge, 1986.
[7] Shih, W. H.; Shih, W. Y.; Kim, S. I.; Lui, J.; Aksay, I. A., *Phys Rev A* **42**, 4772, (1990)
[8] de Rooij, R.; van den Ende, D.; Duits, M. H. G.; Mellema, J., *Phys Rev E* **49**, 3038, (1994)

[9] Potanin, A. A.; de Rooij, R.; van den Ende, D.; Mellema, J., *J Chem Phys* **102**, 5845, (1995)
[10] Wolthers, W.; van den Ende, D.; Breedveld, V.; Duits, M. H. G.; Potanin, A. A.; Wientjes, R. H. W.; Mellema, J., *Phys Rev E* **56**, 5726, (1997)
[11] Gisler, T.; Ball, R. C.; Weitz, D. A., *Phys Rev Lett* **82**, 1064, (1999)
[12] Ikeda, S.; Foegeding, E. A.; Hagiwara, T., *Langmuir* **15**, 8584, (1999)
[13] Narine, S. S.; Marangoni, A. G., *Phys Rev E* **60**, 6991, (1999)
[14] Bremer, L. G. B.; van Vliet, T.; Walstra, P., *J Chem Soc Faraday Trans 1* **85**, 3359, (1989)
[15] Bremer, L. G. B.; Bijsterbosch, B. H.; Schrijvers, R.; van Vliet, T.; Walstra, P., *Coll Surf* **51**, 159, (1990)
[16] Bremer, L. G. B.; van Vliet, T., *Rheol Acta* **30**, 98, (1991)
[17] van Vliet, T.; Walstra, P., *Neth Milk Dairy J* **39**, 115, (1985)
[18] Vreeker, R.; Hoekstra, L. L.; den Boer, D. C.; Agterof, W. G. M., *Food Hydrocoll* **6**, 423, (1992)
[19] this thesis, chapter 3
[20] Horne, D. S., *Int Dairy J* **8**, 171, (1998)
[21] van Vliet, T.; Lucey, J. A.; Grolle, K.; Walstra, P. In *Food Colloids; Proteins, Lipids and Polysaccharides*; Dickinson, E., Bergenståhl, B., Eds.; Royal Society of Chemistry: Cambridge, 1997.
[22] Walstra, P., *Int Dairy J* **9**, 189, (1999)
[23] van der Vorst, B.; van den Ende, D.; Mellema, J., *J Rheol* **39**, 1183, (1995)
[24] Potanin, A. A., *J Coll Interf Sci* **145**, 140, (1991)
[25] Buscall, R.; Mills, P. D. A.; Goodwin, J. W.; Lawson, D. W., *J Chem Soc Faraday Trans 1* **84**, 4249, (1988)
[26] this thesis, chapter 2
[27] Walstra, P., *J Dairy Res* **46**, 317, (1979)
[28] Bremer, L. G. B. , PhD Thesis, Wageningen Agricultural University, 1992.
[29] Verheul, M.; Roefs, S. P. F. M.; Mellema, J.; de Kruif, C. G., *Langmuir* **14**, 2263, (1998)
[30] this thesis, chapter 5

Chapter 5

Effects of structural rearrangements on the rheology of rennet-induced casein particle gels*

5.1 Summary

During ageing of casein gels or skim milk gels, structural changes take place that affect gel parameters like pore size and storage modulus. These changes can be explained in terms of rearrangements of the gel network at various length scales.

In this chapter, rheological experiments on rennet-induced casein gels, and a general model on rearrangement are presented. The results of the experiments, the model, and recent literature on casein gels and other types of particle gels (*e.g.* computer simulations, microscopy and permeametry) are compared to each other.

Experiments presented include measurements of storage and loss moduli and maximum linear strain of the casein gels. Parameters varied include pH (5.3 and 6.65) and temperature (25 and 30 °C). In addition, the casein volume fraction (5-9 vol%) was varied, which enables application of fractal scaling models.

For rennet-induced casein gels, it is demonstrated that at the lower pH, all types of rearrangements proceed significantly faster. The rearrangements include: the increase in the size of compact building blocks (and subsequent disappearance of fractal structure) and the formation of (straightened) strands which eventually tend to break. These rearrangements are most likely a consequence of particle fusion.

*article in preparation

5.2 Introduction

The finite lifetime of bonds in particle gels can cause such bonds to fluctuate, relax and reform during the observation time. These phenomena result in viscoelastic behaviour, which is often found for gels. However, it is less realized that the dynamic character of the bonds may also lead to gradual changes in the structure that, in turn, change the rheological properties. This 'ageing' can be found in particle gels in *e.g.* foods, paints and soils, and it is spontaneous in the sense that it does not result from mechanical disturbance (i.e. shear-induced bond breaking). The ageing may involve a gradual coarsening of the structure and a change in firmness. The specific structural 'rearrangements' that occur are found at various length and/or time scales. Identification and description of these rearrangements can enhance the general understanding of particle gels and can be of practical importance, *e.g.* to control rheological properties.

In this study, we discuss what types of rearrangements occur in rennet-induced skim milk or casein gels that affect the rheology of the system. By analyzing results of rheological measurements as a function of pH and temperature, we determine what specific types of rearrangements occur, and are affected by these parameters. Use is made of a scaling model and a categorization of types of rearrangements, that are expected to be applicable to a wide range of particle gels. In casein gels, an ultimate effect of structural rearrangement is syneresis (expulsion of liquid). Syneresis can be either desired (manufacture of cheese) or not (manufacture of yogurt) [1].

Casein gels can be made by adding rennet enzyme (first stage in the manufacture of cheese) or lactic acid bacteria (manufacture of yogurt). In both cases the stability of the dispersion of casein particles ('casein micelles', radius ~25-125 nm) is lost. As a result, aggregation takes place, eventually leading to the formation of a space-spanning structure. The particles in rennet-induced casein gels are para-casein micelles. Para-casein micelles are casein micelles that have been submitted to rennet action. A casein micelle is a roughly spherical particle formed by association of casein molecules, possibly with one structural level called sub-micelles between them. The main casein proteins are α_{s1}-, α_{s2}-, β- and κ-casein. At the surface of casein micelles, a hairy layer of the hydrophilic parts of κ-casein accounts for a (predominantly) steric stabilization of the casein dispersion. The main active component in rennet (chymosin) induces aggregation, and consequently gelation, by cutting this hairy layer. For recent overviews on casein micelles see refs. [2-4] and references therein.

The interest in rearrangements in particle gels has been stimulated by the results of computer simulations. In simulations, structural rearrangements were especially reported for gels formed by reversible aggregation [5,6].

Rearrangement in gels formed by reversible aggregation or being subject to bond-breaking shear, leads to a finite lifetime of the gels, which are therefore called 'transient' gels [7,8]. In other simulation models, rearrangements can take place in gels formed by irreversible aggregation by allowing bond flexibility without bond breakage [9-12].

Most experimental results in the studies on rearrangements have been obtained for casein gels, mostly making use of rheometry, permeability and microscopy. The occurrence of rearrangements is literally mentioned in experimental studies on acid casein gels [13] and rennet-induced casein gels [14,15,16] made from skim milk.

There are several papers that have focused on rearrangements like those occurring in casein gels. Here we mention papers on syneresis [17] and sintering [18] of silica particle gels.

There are a number of models available to describe aggregation and gel formation, *e.g.* adhesive sphere, percolation, and fractal scaling models. Not all of these are suitable to study rearrangements. The adhesive sphere model is useful to study the very early stages of aggregation. Theories for transient gels are usually based on percolation or on thermodynamic considerations and assume reversible aggregation. In principle no structural information can be obtained. Gels formed by irreversible aggregation and not disturbed by bond-breaking shear strains, appear to be best described by fractal models. In addition, the fractal model is the only model that can describe the geometric structure of the particle network. In this study, we use a fractal scaling model [19] in the study of rearrangements in rennet-induced casein gels.

Apart from measurements of the storage modulus (G'), to which we will apply the fractal scaling model, also results will be presented of rheological measurements of the maximum linear strain (γ_0) and tan δ (G''/G'), as a function of pH and temperature. These rheological parameters are useful to the food industry. According to van Vliet *et al.* [16], the magnitude of tan δ is a measure of the 'liquid'-like behaviour of the casein gel, and is thereby related to the rate of rearrangements and eventually syneresis. Arshad *et al.* [20] argued that the parameter γ_0 and the permeability coefficient [21] are useful parameters in describing the tendency of a gel structure to break down during processing. Finally, a decrease in G' may be an indication of spontaneous breakdown of the gel (i.e. syneresis).

5.3 Models and theory

5.3.1 Scaling behaviour

During fractal aggregation, the clusters formed are self-similar: the volume fraction of particles (φ) inside the clusters decreases with increasing cluster radius (R) according to

$$\varphi = \left(\frac{R}{a_{\text{eff}}} \right)^{D_f - 3} \tag{5.1}$$

where a_{eff} is the (effective) particle radius and D_f is the fractal dimensionality. The process of fractal aggregation causes that the clusters formed become sufficiently tenuous for the packing of such clusters to result in a space-spanning network. The structure of the network can be approximated as fractal over a range of length scales from the compact building blocks a_{eff} (lower cut-off length) to the correlation length or blob size ξ (upper cut-off length).

Several experimental studies have specifically considered the effect of rearrangements in the context of a fractal description of aggregate or gel structure. These include microscopical [21] and rheological [22] studies on casein gels, an X-ray study on silica particle gels [18], and optical studies on aggregated polystyrene spheres [23], aerosols [24,25], and bovine serum albumin (BSA) particles [26].

In fractal aggregation theory, the three main fractal parameters are the fractal dimensionality (D_f) and the upper and lower cut-off lengths of the fractal regime. In casein gels [22,21] and BSA aggregates [26], typically a relatively high value of D_f (~2.3-2.4) is reported shortly after gelation. There are two main mechanisms that can lead to a high value of D_f: rearrangements during aggregation [9,10] and irreversible aggregation being delayed by a considerable repulsive barrier [12]. Various other simulation and experimental studies have considered the behaviour of D_f of particle gels or aggregates during ageing. In these studies, both increase [24,25] and decrease [27,6,21] of D_f have been reported. In rennet-induced casein gels, the apparent D_f value becomes very small (<1.7) after long ageing times, which suggests that the structure has lost its fractal character [22,21]. In some types of gels, D_f is affected by particle fusion. Depending on the extent of particle fusion, this can result in a decrease (silica particle gels [18]), an increase (aerosol particle aggregates [24,25]) or no substantial change (simulated aggregates [28]) in D_f. In the case of aerosol particles, particle fusion leads to coalescence. This may result in the observed increase of D_f. In conclusion: the effect of

rearrangements on the value of D_f, is complicated because it is highly dependent on the time- and length scales at which the rearrangements occur. Also: information on changes in D_f alone is usually not sufficient to describe the (dynamic) relation between structure and rheology. For instance, in ref. [19] (see next section) it is argued that the relation between structure and rheology also depends on other (fractal) scaling parameters and on the properties of the stress-carrying strands.

Besides D_f, another fractal parameter of importance is the lower cut-off length of the fractal regime. The lower cut-off length is comparable to the size of the compact building blocks. Recent confocal microscopy and permeability studies of casein gels (Chapter 3, ref. [21]) have given evidence that ageing is accompanied by an increase in lower cut-off length of the fractal regime. Such an increase is also observed in other particle aggregates and gels [9,18,6,24].

5.3.2 Incorporation of casein after gelation

In this study, a discussion is included on the initial increase in G' during gel ageing. This can result from rearrangements, but can also result from ongoing incorporation of extra casein material into the gel matrix [29]. This has been done experimentally (using a 'free casein detection method', see Materials and Methods) and by applying a 'time scaling' model for gel dynamics by Horne [29]. This model assumes that all bonds formed are of equal strength and that no internal reorganisation of the gel takes place. Consequently, the type of structure of the gel would not change with time. It can only change by addition of new particles and small clusters of particles. Within the model, G' increases with the number of particles incorporated in the gel matrix during gel ageing. The equation used is as follows

$$G' = G'_{\infty} f\left(t/t_{gel}\right) \qquad (5.2)$$

where G'_{∞} is the storage modulus at maximum incorporation of casein in the gel matrix and f describes the dynamics of gel growth in terms of a dimensionless time. The scale factor or 'gel time' t_{gel} is the time at which $G' \geq G''$. As aggregation is the only relevant physical process, the function f is assumed to be universal. This then implies that if G'/G''_{∞} is plotted as a function of t/t_{gel} for *e.g.* different volume fractions of milk, all curves should coincide to one mastercurve.

Finally, a minor aspect of the relation between structure and rheology of casein gels is considered: it is investigated whether the decrease of G' after

some ageing can be due to continued rennet activity (*i.e.* enzymatic break-down of the casein) [30].

5.3.3 Scaling modelling and categorization of structures

In this study we use a fractal scaling model as a tool in studying rearrangements in rennet-induced casein gels. The mathematics of the scaling model is described elsewhere (Chapter 4, ref. [19]) and makes use of (and effectively combines) refs. [31] and [22]. The model constitutes a useful tool for relating gel structure to rheology for a widely varying range of particle gels.

In the model four levels of structure are considered, which in the next section are also used to define the types of structural rearrangements:

(A) The elementary building blocks. These are the individual particles (*i.e.* paracasein micelles in the present case)
(B) The rigid segments or secondary, compact, building blocks, often containing several elementary building blocks.
(C) The fractal clusters containing (stress-carrying) strands of rigid segments.
(D) The macroscopic gel; a close packed stacking of the fractal clusters.

The length scale increases with each consecutive structural level. Note that a_{eff} from equation (5.1) is associated with structural level B, the size of the compact building blocks. The clusters of size ξ are linked at the stress-carrying strands crossing the periphery of the clusters. The average number of these strands per cluster is independent of the cluster size, which is a direct consequence of the scale invariant (i.e. fractal) structure of the clusters [32].

In the scaling model, two different scaling exponents describe the strand structure as a function of cluster size. One is related to the number of 'junctions' (or 'links') per strand (δ), the second depends on the dominant type of microscopic deformation: bending or stretching (ε). The types of gels that result from the model vary with respect to these parameters.

Finally, fractal aggregation theory is applied. Incorporation of equation (5.1) into the scaling relation for the storage modulus G', leads to

$$G' \propto (a_{\text{eff}})^{-\alpha} \varphi^{\frac{\alpha}{3-D_f}}, \qquad (5.3)$$

where $\alpha = 2\varepsilon + \delta + 1$, and ε and δ are the exponents mentioned above. Similar expressions can be derived for the maximum linear strain and the yield stress.

Incorporating the definitions of the four types of gels (based on limiting values of the parameters incorporated) into the scaling relation, leads to specific predictions for the four categories of the parameter α. The results of this categorization are summarized in table 1. We have not included a fifth category (category I, $\alpha = 5$), because this is the so-called 'random walk' category, which assumes that excluded volume effects can be neglected. This is very unlikely for particle gels. We will use the scaling relation for G' together with information on the volume fraction and estimates for the fractal dimensionality D_f obtained by confocal microscopy and permeametry [21], to yield information about the type of stress-carrying strands and the size of compact building blocks of the gel, within the context of that model. Consequently, we can quantify the coarsening of the gel structure and the stretching of strands as a result of the rearrangements during gel ageing.

Category	Type of strands	Micr. deformation	α
II	Curved, flexible	bending	4
III	Hinged, rigid	bending	3
IV	Straight, flexible	stretching	2
V	Rigid	stretching	1

Table 5.1. Model types of gels. Exponent α for the various types of gel structures that are distinguished by the fractal scaling model given by the scaling relation (5.3). Taken from ref. [19].

5.3.4 Categorization of rearrangements

In this section we categorize the main types of rearrangements affecting the structure and hence the rheology of particle gels formed through fractal aggregation. Bos [33] distinguished two types of processes affecting the (fractal) structure of a particle gel: (*i*) local compactification: *i.e.* reorganisation of a connected network leading to transport of particles to structures of a length scale below a_{eff} (and hence to a decrease in fractal dimensionality and increase of a_{eff}) and (*ii*) global compactification: *i.e.* aggregation, cluster overlap or connection of long sidechains to the gel backbone, leading to transport of particles from the long-range homogeneous regime to the fractal regime; a length scale between a_{eff} and ξ. This leads to an increase in fractal dimensionality and an increase of ξ.

In the categorization of rearrangements given here, processes of type (*i*) are included because this is the main process during ageing. Of type (*ii*), only the process of dangling side chains connecting to the gel backbone will be considered. The other processes (aggregation, cluster interpenetration) are

expected to take place mainly during formation of the gel. In addition, we have included some forms of particle fusion.

In a simplified approach of the ageing process, rearrangements occur at four length scales. This is shown schematically in figure 5.1 and table 5.2. In terms of these length scales, four main types of rearrangements are distinguished. In this model approach, 'junction' is defined as an ensemble or collective of bonds that constitute a connection between two particles [4].

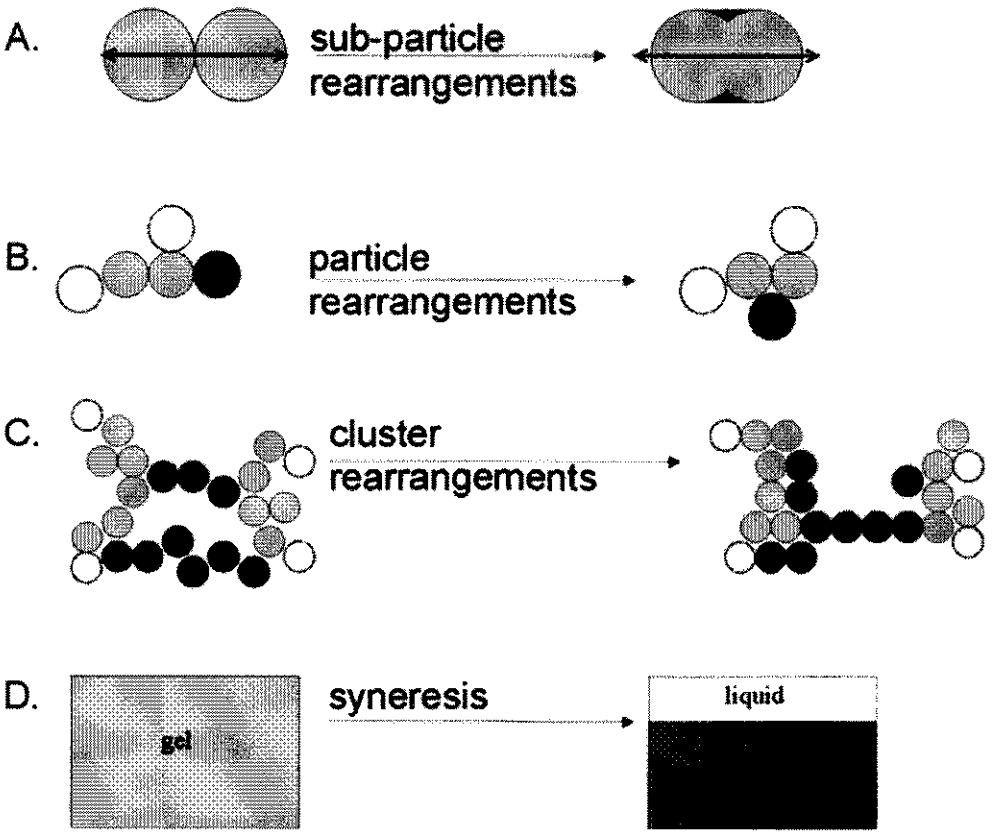

Figure 5.1. Four types of rearrangements that can be distinguished at various levels: (A) the molecules or 'sub-particles', (B) the particles and (C) the strands of particles and (D) the whole gel.

Type	A	B	C	D
Name	Intraparticle rearrangement	Interparticle rearrangement	Intercluster rearrangement	Syneresis
Other names	Particle fusion	Reorganisation	Coarsening/ microsyneresis	Shrinkage
Length-scale	Sub-particle	Particles to small clusters	Clusters /strands/pores	Gel
Time-scale	Mainly during gel ageing	Mainly during aggregation	Only during gel ageing	After some gel ageing
Probed by (e.g.)	-electron microscopy -tan δ at low frequency	-computer simulations -light scattering -confocal microscopy	-confocal microscopy -permeametry -large-deformation rheometry	-Eye and other (semi-) empirical methods

Table 5.2. Model types of rearrangements. Summary of the characteristics of the four main types of rearrangements given in figure 5.1. Size level: (A) molecules or sub-particles, (B) particles, (C) strands and (D) the whole gel.

(A) Subparticle or **intraparticle** rearrangements (size level in casein gels < approx. 0.2 μm). At this level, the particle contact area or number of bonds per particle-particle junction can be increased by particle fusion. Particle fusion of primary particles can occur, for instance, by sintering of fat crystal particles. (Partial) particle fusion as a result of the viscous or liquid-like behaviour of the primary particles, is a well-known phenomenon in rennet-induced casein gels. The latter can be observed by electron microscopy (for a recent example, see ref. [14]).

Walstra [4] has presented evidence, also deduced from electron microscopy [34,35,14], that micellar fusion in casein gels is not a result of mobility of molecules, but of casein 'sub-'micelles. Note that in another equally accepted model [36], sub-micelles are not incorporated and fusion can only take place if rearrangements occur at the level of the molecules.

In principle, there are two subtypes: fusion due to particle deformation and due to diffusion of parts of the micelles. The former occurs due to slow liquid-like flow processes inside the micelles. The latter can only occur if sub-micelles or molecules go into solution, and re-enter in the casein matrix at the junctions between the micelles. In the case of mobility at the molecular level, we are dealing with a kind of Ostwald ripening. In our approach, we can not really distinguish between subtypes; the effect is always particle fusion.

(B) Interparticle rearrangements (size level in casein gels ~0.2 - 1 μm). Rearrangements at this level involve changes in the mutual positions of the particles. These can occur due to rolling of the particles over each other. The density of aggregates is increased because the number of particle-particle junctions is increased. After gelation, it will virtually be limited to particles in dangling ends of strands.

Again, two main subtypes can be distinguished: rearrangements due to reversibility of bonds and of junctions. This distinction only makes sense if one junction consists of more than one bond, which is generally true for casein gels. Interparticle rearrangements due to reversibility of bonds probably occurs in casein gels (see *e.g.* ref. [13]). Rearrangements of the latter type account for the collapse of so-called 'transient gels', and have been investigated in various computer simulation studies (see above) and by light scattering of various systems [26,23].

It is hard to distinguish between the rearrangement types A and B, both in analyzing experimental data (*e.g.* microscopy) and in terms of the model (if complete particle fusion occurs, the length scale of the compact building blocks shifts from level A to B). There is a parameter that can be used to predict the rate of both: tan δ. Van Vliet *et al.* [16], showed an empirical positive correlation between tan δ (at small strain and low frequency, *e.g.* 10^{-3} Hz) and the rate of rearrangements of type D. This correlation is most likely due to the relation between tan δ and the rate of rearrangements of type A, B (and C) that *induce* rearrangements of type D. The parameter tan δ is a measure of the proportion of bonds with a relaxation time about equal to the reciprocal of the applied frequency, and thereby a measure of the dynamics of the system at length scales from molecules to particles

(C) Rearrangements taking place at the level of the size of the **clusters, gel pores** or **strands** (in casein gels ~1 – 40 μm). During the whole ageing process particle rearrangements will lead to denser aggregates and larger pores. This process, together with particle fusion, can lead to tensile stresses nearby in strands. Thereby, strands will be stretched and may become thinner [16,21]. Especially at long ageing times, this can cause strands to break.

The above process can be seen as microsyneresis, because liquid is forced out of parts of the gel that become more dense and moves to growing pores. In the case of casein gels, this liquid is whey. It is often a prelude to rearrangement of type D, because extensive strand breakage in the system will induce syneresis. It can therefore be argued that a distinction between rearrangements of type C and D can not really be made in the present case. Also, rearrangements at level C should be extended to sub-subtypes such as

stretching of strands, breaking of strands and growth of the average pores size in the gel (leading to increased permeability).

(D) Syneresis at the level of the **gel** (*i.e.* macrosyneresis). If many strands break or if macroscopic compactification or contraction sets in due to detachment of the gel matrix from the vessel, liquid is forced out of the (shrinking) gel. This process is called syneresis. The type of syneresis we deal with is due to endogenous forces. The strand breakage is caused by contractional forces inside the gel. At a stage before endogenous syneresis, the gel may have become so sensitive that external forces can readily induce syneresis.

Already in the 1920's it was observed that an increase in the apparent particle size in CeO_2 gels is accompanied by syneresis [37]. Moreover, it was recognized that syneresis is promoted by all conditions that promote aggregation. Even though this is generally true, the relation is more complex for casein micelles, because the rheological properties of the particles themselves also change with changes in these conditions. Moreover, the rate of syneresis is related to the size of the gel pores. Pores should be sufficiently large for flow of liquid out of the gel network to occur during syneresis. So syneresis is determined by the stress that acts on the gel *and* the permeability of the network. It thereby indirectly depends on rearangements of type B and C, that increase permeability. As a *result* of the syneresis, the average pore size, and hence the permeability eventually decreases (for a recent example, see ref. [17]).

Because of the generalized character of the categorization of types of rearrangements presented above, it is expected to apply to a wide range of particle gels (especially those formed through fractal aggregation).

5.4 Materials and methods

5.4.1 Skim milk Preparation

Standard reconstituted skim milk was made by dissolving 12 g skim milk powder (Krause, Heino; 100 g powder contains 0.6 g fat and 33.8 g casein protein) in 100 g demineralised water. To retard bacterial and enzymatic degradation, 200 µl of 10 wt% thiomersal (BDH Chemicals Ltd.) and 27 µl of a solution of 3.7 mg ml^{-1} (~0.9 TIU/100 ml) aprotinin (Sigma, A-1153, Lot #46H7145) were added. An amount of 7 ml of a 0.5 molar NaCl solution (pH = 6.65) or 7 ml 0.5 molar HCl (pH = 5.3) was also added, to reach the same ionic strength. To reach equilibrium the dispersion was stirred for at least 10 (pH = 6.65) or 24 (pH = 5.3) hours at 25°C. From trial

experiments we found that poor reproducibility is obtained if we stirred for shorter times. Small amounts of HCl were added during equilibration at pH = 5.3, to keep the correct pH. Reproducible results could be obtained from this milk for at least 3 (pH = 6.65) or 5 (pH = 5.3) days.

Commercial calf rennet (10.800 SU, Leeuwarder kaasstremsel) was added to the milk, to reach a final concentration in the milk of 0.02 (pH = 6.65) or 0.002 (pH = 5.3) vol%. Rennet was always freshly diluted (×100 at pH = 5.3, ×50 at pH = 6.65) prior to addition, to prevent loss of rennet activity after dilution. Important to note is that the amount of rennet added was less at low pH. The amounts were chosen such that t_{gel} was reached in approximately the same time (~ 4 ks).

Skim milk with a lower concentration of casein was prepared by whey addition to maintain standard solvent conditions for the casein micelles. The whey was prepared by allowing skim milk to gel at a high rennet concentration, and subsequent cutting and filtering. Then, thiomersal was added and the whey was kept a few days prior to using it, to allow the rennet action in the whey to become negligible. Skim milk was diluted with whey made from skim milk of the same composition. Standard casein volume fractions φ were approximately 0.054, 0.063, 0.076 and 0.089, assuming a voluminosity of 3 ml g^{-1} [38] and a skim milk density of 1036 kg m^{-3}.

5.4.2 Rheometry

To determine the rheological properties of the gel, the skim milk was brought in the gap of a concentric cylinder, directly after rennet addition. The gel was thus formed in the apparatus, at the appropriate temperature (25 or 30°C). The device used was a VOR rheometer (Bohlin Rheology, UK). The storage modulus (G') and the loss modulus (G'') were determined in a dynamic low amplitude oscillatory mode. A sinusoidally oscillating strain was applied at a frequency (ω) of 0.1 Hz, and the resulting stress (σ) was continuously measured as a function of time. The maximum value of the strain (γ_m) was kept constant at 0.01, except during a strain sweep (see below). The ratio of the maximum stress (σ_m) over the maximum strain gives the absolute shear modulus $|G| = \sigma_m / \gamma_m$. Using the phase shift δ between the stress and the strain, G' and G'' can be calculated. The ratio G''/G', equals $\tan \delta$.

A concentric stainless steel cylinder geometry (C14) was used, with inner and outer cylinder radii of 14.0 and 15.4 mm, respectively, and a volume of 2 ml. A 3.60 gf cm torsion bar was used. In the strain sweeps a strain from 0.0002 up to (maximally) 0.1 was applied. The range of

frequencies probed during a frequency sweep was 0.001-10 Hz. To prevent drying out of the gel it was covered with soy oil during ageing.

In a separate set of experiments, renneting was performed at 5°C to study the effect of continued rennet activity at pH = 6.65. Renneting took place for 16 hours at 5°C, after which no significant formation of caseinomacropeptide by rennet action is expected anymore [39, 40]. Next, the milk was put into the VOR rheometer at 25°C, after which rapid gelation took place and the storage modulus was measured in time.

5.4.3 Detection of free casein

The presence of free micelles in the whey during in the gel during ageing was checked by analyzing permeated whey, using gel electrophoresis. For this purpose, permeated whey was extracted using a tube method as described elsewhere [41,21]. This implies that the gel should be fairly stiff (G' about 10 Pa), to prevent damaging its structure. In a vessel, 0.5 ml of this whey, 0.25 ml water and 0.25 ml of an electrophoresis solution (10% SDS and 0.04% bromidephenolblue dissolved in water) were mixed and heated for 10 minutes at 100°C. Next, separation was performed making use of an SDS homogeneous 20 gel and SDS buffer strips (Pharmacia). Thereafter, the gel was developed (*i.e.* the caseins were stained) making use of a Silverkit from Pharmacia LKB Biotechnology. This method will be referred to as free casein detection method 1 (FCD1).

Another experiment with the same purpose involved the following steps: Gels of various age were gently stirred, centrifuged (1 min at 12.000 × *g*) and the whey obtained was put through a nanofilter (cutoff 400 nm, Schleicher & Schuell). The absorbance of the whey samples was measured at 610 nm, in a Biochrom 4060 spectrometer (Pharmacia) in plastic cuvettes (1 × 1 × 4.5 cm). To be able to quantify the amount of micellar casein corresponding to the absorbancy, reference measurements were performed on skim milk samples diluted with whey to a known casein density. In addition, we measured G' of a system made with milk that had passed the nanofilter. Making use of relation (5.3), which would allow estimating the volume fraction from the value of G', the loss of casein through this step was estimated as at most 40%. The results were corrected accordingly (*i.e.* % of free micellar casein were multiplied by 1.6). This method will be referred to as free casein detection method 2 (FCD2).

5.4.4 Cryo-SEM

Gels prepared for scanning electron microscopy (SEM) were aged in small aluminium sample holders that were held together by a pair of tweezers. The tweezers were immersed in the gelling milk at the appropriate temperature. This setup protects the gel from exhibiting syneresis and prevents air getting into the sample. After various times, samples were pulled out of the gel and immediately after this, high pressure freezing was performed using a Leica EM-HPF #7225-01. Samples were stored in liquid nitrogen.

The scanning electron microscope used was a JSM-6300F(JEOL Japan). Samples were placed in a dedicated cryo-preparation chamber (CT 1500HF Oxford Instruments England) and subsequently fractured at -90°C and freeze dried for 10 minutes in high vacuum. The samples were sputter coated with 5 nm platinum and analysed in the SEM at -160°C. Micrographs were digitally recorded.

5.5 Results and discussion

5.5.1 Effect of rearrangements on rheology

In figure 5.2, the storage modulus, G' (a) and the maximum linear strain, γ_0 (b), are given as a function of time after rennet addition. First curves (1) and (2) in figure 5.2a will be compared, which were both taken at pH = 6.65 and T = 25 °C. Curve (2) is different from all other curves, because renneting took place at 5 °C (where κ-casein is being split, but the para-casein micelles formed do not aggregate), and gelation was induced by heating to 25 °C at t = 0. In all other cases, rennet was added at t = 0 at the gelation temperature (25 or 30 °C).

For curve (2) in figure 5.2a, renneting took place at 5 °C for 16 hours, which should be a sufficient amount of time to achieve complete cutting of the κ-casein [30]. From a comparison of (1) and (2) it follows that the main characteristics of the ageing curves are the same: the high rate of increase and the levelling off of G'. The asymptotic (maximum) values of G' were even precisely the same. It was shown before [15] that the rate of increase of G' is not fully determined by the reaction rate of the rennet. Presumably, the typical behaviour of G' is also determined by the rates of various structural rearrangements.

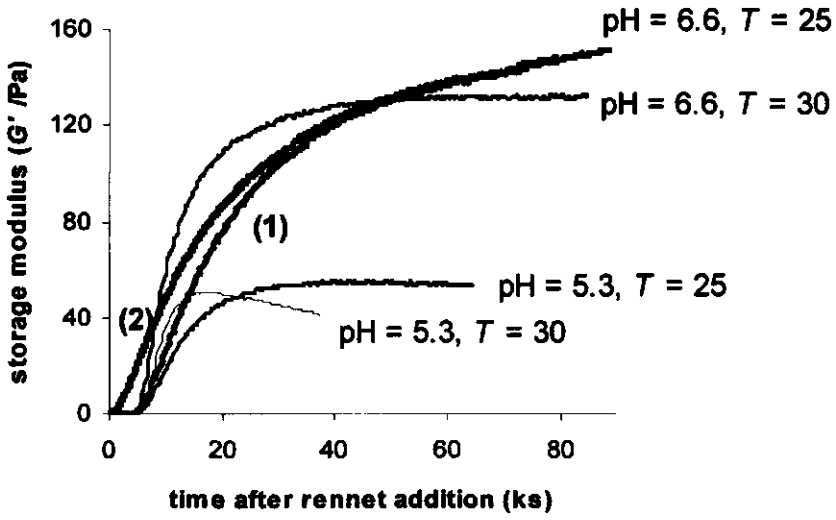

Figure 5.2a. Storage modulus, G', of rennet-induced casein gels as a function of time after rennet addition. pH and T are indicated. The gel corresponding to curve (2) was first renneted in the cold, after which (at $t = 0$) it was brought at 25°C.

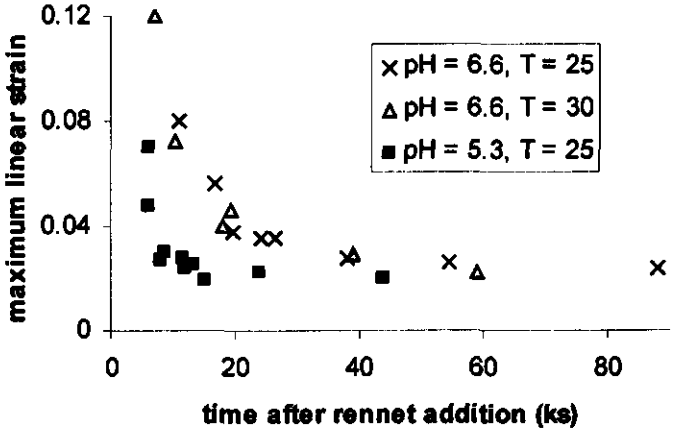

Figure 5.2b. maximum linear strain, γ_0, of rennet-induced casein gels as a function of time after rennet addition. pH and T are indicated.

In figure 5.2a, at T = 30 °C and pH = 5.3, the curve ends at the moment at which a steep decrease in G' was observed, indicating wall slip in the rheometer.

It is clear from figures 5.2a and 5.2b that gel ageing is accompanied by large changes in rheology, and that the rates of change depend on pH and T (the effects of pH and T are discussed later). The rate of ageing can be characterized by the initial rate of increase of G', the rate of decrease of γ_0 and the time at which there is a maximum in G'. These three ageing effects are discussed below, with reference to table 5.2 and figure 5.1.

The increase in G' in fresh gels can be due to an increased contact area between the micelles by particle fusion (A) and interparticle rearrangements (B) due to bond reversibility, which result in more bonds per junction (A) and in more junctions (A,B). This leads to an increase in the total 'junction energy' (especially bending energy) of the system, hence increases the storage modulus. Particle fusion occurs, probably due to viscous or liquid-like behaviour of the particles. For interparticle rearrangements (B) to occur, there should be sufficient freedom for the micelles to move around. This may be the case in the early stages of gel formation, but some time after gelation most of the junctions are probably fairly stiff if particle fusion has occurred.

Rearrangements of type A and B probably cause stretching of strands (C). This is also expected to cause an increase of G', because stretching forces are generally stronger than bending forces.

The maximum linear strain γ_0 decreased with time for all conditions. Note that at each given condition, the value of γ_0 seems to be related to the value of G' (γ_0 is lower at higher G'). The decrease of γ_0 can be understood by the formation of straightened strands and large pores; a smaller deformation would suffice to cause fracture of at least some of the straight strands. Strand fracture is an important mechanism leading to non-linearity. The increase of pore size is clear from the observed accompanying increase of the permeability [21].

The value of G' going through a maximum may be the most striking result of the temporary existence of rennet-induced casein gels at low pH. It is a final consequence of the high affinity of the micelles for each other, which will at short time scales lead to an increase in stiffness (*i.e.* higher G'), but -in our view- at longer time scales to opposite behaviour. For G' to decrease with time, either the number of stress-carrying strands must decrease or the strands themselves become less stiff. In view of particle fusion and straightening of the strands, the latter explanation can only be true if the straight strands become thinner. This supposed thinning and fracturing of strands (rearrangements of type C) is supported by results from confocal microscopy, permeametry [21], and electron microscopy [14] of rennet-induced casein

gels. At even longer ageing times (where G' decreases) fewer thin and straight strands are present and the permeability continues to increase.

Interestingly, a re-inspection of the data from ref. [21] (Chapter 3) suggests that at the time of first decrease in G', called t_c, there are constant values of the compact building blocks of the gel, $R_0 \sim 1.5$ μm, of $D_f \sim 1.8$, and of the permeability coefficient, $B \approx 1 \times 10^{-12}$ m^2 (independent of pH or T). Some time after this, syneresis (D) becomes the dominant process, which greatly changes the rate of ongoing rearrangements at the other levels.

5.5.2 Incorporation of casein after gelation

Besides rearrangements, incorporation of casein may be responsible for the observed increase of G' after a gel is formed. This was checked by performing a time scaling analysis [29] to the data that proceeds from the assumption of further incorporation of casein. Supposing a constant category of gels (α = constant, see later), it follows from the decrease in D_f [21] that the quantity $\alpha / (3 - D_f)$ changes during gel ageing at low pH, but does hardly so at physiological pH. If the (universal) time scaling would apply, this parameter should be constant. This suggests that at low pH, further incorporation of casein can not be the sole mechanism, but it still may be at physiological pH. At low pH aggregation takes place at a lower extent of hair cutting because of the formation of 'bare patches' on the micelles (see figure 5.3a and b, taken from ref. [40]). This also suggests that continued or delayed aggregation does not occur at low pH.

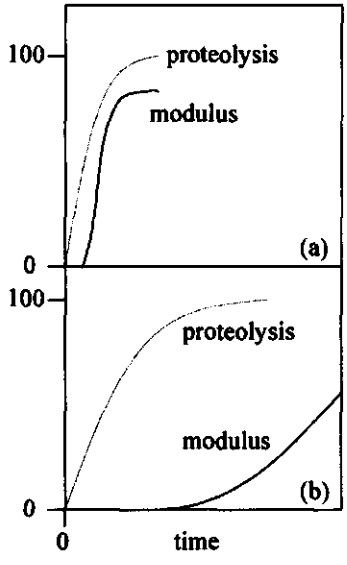

Figure 5.3: The renneting process at **(a)** pH = 5.62 and **(b)** pH = 6.74 as a function of time. 'Proteolysis' = degree of κ-casein cut. 'Modulus' = storage modulus of the gel (arbitrary scale). Rennet concentration 0.01%, temperature 30°C. Arbitrary scale readings. Taken from ref. [40].

To investigate the incorporation of casein at physiological pH (6.65), FCD1 (see Materials and Methods section) has been applied to this system, at several times during gel ageing. In all cases casein could not be detected in the SDS gels, except for a small band corresponding to the caseino-macropeptide (which are the 'hairs' that have been cut off). This implies that in gels with $G' >\sim 10$ N m^{-2}, no single micelles or small aggregates of micelles are present that can contribute to the increase in G' at longer ageing times.

To determine the amount of free casein in a gel with $G' <$ appr. 10 N m^{-2}, FCD2 was applied. The results are presented in table 3. In this table it is shown that about one percent of the total amount of casein appears to be present as single micelles at $G' \approx 10$ N m^{-2}. If large aggregates of particles, which we cannot detect using this method, would incorporate into the matrix during gel ageing, this would lead to an early loss of fractal character of the gels (and this is not the case at physiological pH). We can conclude that for the major part of the ageing curve (approx. 10-100 Pa), rearrangements must be responsible for the increase in G'.

Time t (ks) after rennet addition	**corres-ponding G' (Pa)**	**visual aspects**	**Absor-bancy ε**	**free casein ***
0	0	milky white	>>1	100%
7.2	2.5	slightly turbid	0.476	5%
8.1	5	very slightly turbid	0.15	2%
9.3	10	very slightly turbid	0.097	1%
11.7	20	as clear as whey	0.076	0%
86.4	120	as clear as whey	0.077	0%

Table 5.3. Results of FCD2. Absorbancy of whey, extracted using the FM method at various gel ages (corresponding values of G' given). Also shown are the corresponding fractions of casein present in the whey solutions, relative to the amount in milk. Condition: pH = 6.65; T = 30°C (*estimated from ε at t > 0 and assuming casein loss in the filter = 40%).

The results of table 5.3 can be compared to Brownian dynamics simulations of particle gel formation [12]. Note, however, that the particles are already 'sticky' at the start of the simulations which is not the case for rennet-induced agggregation. These simulations show that at the moment of gel formation, the amount of single particles would be only a few percent. The small amount of single or free particles follows from the cluster-cluster type of irreversible aggregation in the simulations.

One last comment in favor of the time scaling model by Horne [29], is that rearrangements may be responsible for the incorporation of additional

particles. 'Incorporation' then means sticking of dangling ends of strands of micelles to the percolating backbone of the gel matrix (a rearrangement of type B or C). In this case, the function f in equation (5.2) would change in time, and the applicability of the model becomes very complicated. In other words, probably the gel can be considered a close-packing of clusters at t_{gel}, but not all clusters that are neighbors are already at this moment connected.

5.5.3 Application of fractal scaling model

More information on the ageing of the gels can be obtained by application of the fractal scaling model. The parameters α and a_{eff} in relation (5.3) can be calculated from the linear fits to plots of $\log G'$ versus $\log\varphi$, assuming that the characteristics of the structure given by α or a_{eff} are independent of φ. Examples of such plots are given in ref. [19]. In the analysis, one of the parameters a_{eff} or α has to be taken constant as a function of time and volume fraction. The fractal dimensionality D_f must also be known. This parameter we obtained from ref. [21], and varied between 2.6 and 1.7. The value of a_{eff} can not be exactly calculated from this equation, because relation (5.3) only indicates a proportionality. However, if other (not identified) proportionality factors are assumed to be constant, a dimensionless parameter, a_α , can be calculated. One of these factors represents the interactions between the particles [32,19]. These factors can only be constant if all the contact areas between rigid segments of any size do equal that of a single particle-particle junction with a constant number of bonds (per junction). Obviously, this is not true and we will return to this point later. However, if this argument is ignored, a_α is an interesting parameter because it scales with a_{eff}.

In figure 5.4a and 5.4b the results of such calculations based on the experimental data are presented. It can be seen from figure 5.4a that for rennet-induced casein gels at physiological pH and room temperature, α would be about 2.5. This corresponds to a structure of gels intermediate between 'hinged' and 'straight' in table 1, which would imply that the strands in the network at the level of the clusters are straight within the clusters, with some minor degree of bending. The presence of straight strands is what we expected from the results of the rheometry and from confocal and electron micrographs.

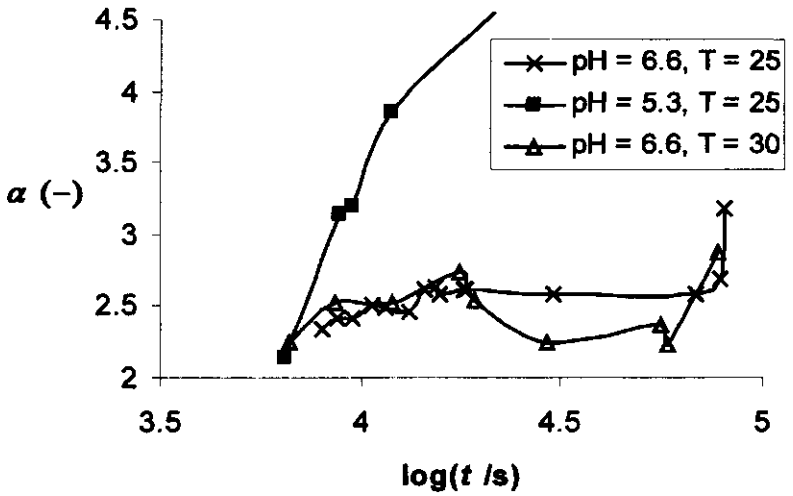

Figure 5.4a. Scaling parameter α (-), assuming a_α to be constant and calculated by using relation (5.3). Results presented as a function of time after rennet addition. Temperature and pH as given in the legend.

At pH = 5.3, α would increase with time to values beyond model discription (> 4.3). This observation suggests that the structures become *more* flexible or curved in time, which is exactly the opposite to what follows from the assumed rearrangements and is predicted by confocal microscopy [21]. Therefore, the model appears not applicable to low pH gels at these long ageing times. From this we conclude that it is more likely that a_{eff} changes in time and that α stays constant or at least does not increase. The parameter a_α is a measure of a_{eff}, the size of the compact building blocks of the gel. If α is taken constant at 2.5, the value of a_α can be calculated. These results are shown in figure 5.4b. The figure shows that a_α would increase in time at low pH. At long ageing times (about 16 ks), the compact building blocks become so large, that the structures cannot be considered fractal anymore, and the model is no longer valid. Fractal analysis of confocal micrographs [21] also showed that at these time stages the fractal length scale has greatly decreased so that the structure cannot be considered fractal anymore. Note that this time is shorter than the critical time t_c (at which *e.g.* G' is at a maximum), but approximately equal to the time at which γ_0 levels off according to figure 5.2b.

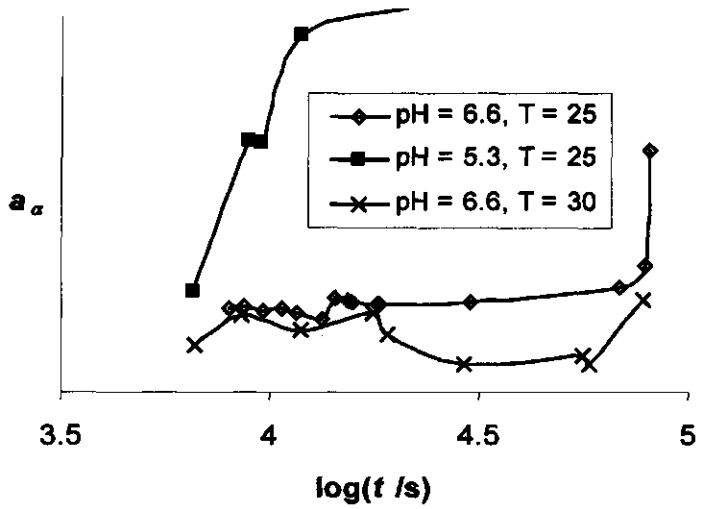

Figure 5.4b. prefactor a_α (arbitrary scale) assuming α to be constant and calculated by using relation (5.3). Results presented as a function of time after rennet addition. Temperature and pH as given in the legend.

There is no further proof that either of the assumptions made in the calculation of α (a_α is constant) or a_α (α is constant) is entirely correct. This means that in reality the increase in a_α at pH 5.3 may be less than as presented in figure 5.4b. This is probably the case, also following from the observation that the calculated increase is stronger than the increase in size of the compact building blocks as calculated from confocal micrographs, as well as from the value of the permeability coefficient as a function of volume fraction [21].

The increase in a_{eff} in time can be ascribed to particle fusion (rearrangement of type A), rolling of the particles over each other, thereby forming close packed structures (rearrangement of type B). Very important is that strand breakage (rearrangement of type C) will increase the rate of rearrangement A and thereby also influence a_{eff}. Rearrangement B occurs most likely only before gelation. Another aspect is that as a result of the occurrence of these rearrangements the total number of bonds increases. In view of this, the calculated changes in a_{eff} or α at low pH should not merely be seen as a consequence of structural changes. Part of the increase may be apparent, if due to an increase in total bond energy per junction.

As a consequence of the rapid increase in a_{eff} (or decrease in D_f) at low pH, the structures cannot be considered fractal anymore at late time stages.

Note that the value of α is very sensitive to the value of D_f used. Most of the deviations in figures 5.4a and b originate from deviations in D_f. In the

previous chapter [19] an average value of $D_f = 2.3$ was used and a_{eff} was assumed to be independent of φ, which resulted in $\alpha \approx 2.0$ at all times for pH = 6.0 and 6.65.

5.5.4 Effect of pH and temperature

In this section, the results of the rheometry as a function of pH and T will be explained in terms of the properties of the micelles.

Over the last decade, a number of papers have been published on the effects of parameters like pH and temperature on the properties of the casein micelles during and after renneting [42,40,43,44,1]. Figure 5.5 is based on the results of these studies. The figure summerizes some important aspects of the behaviour of casein gels as a function of pH and T.

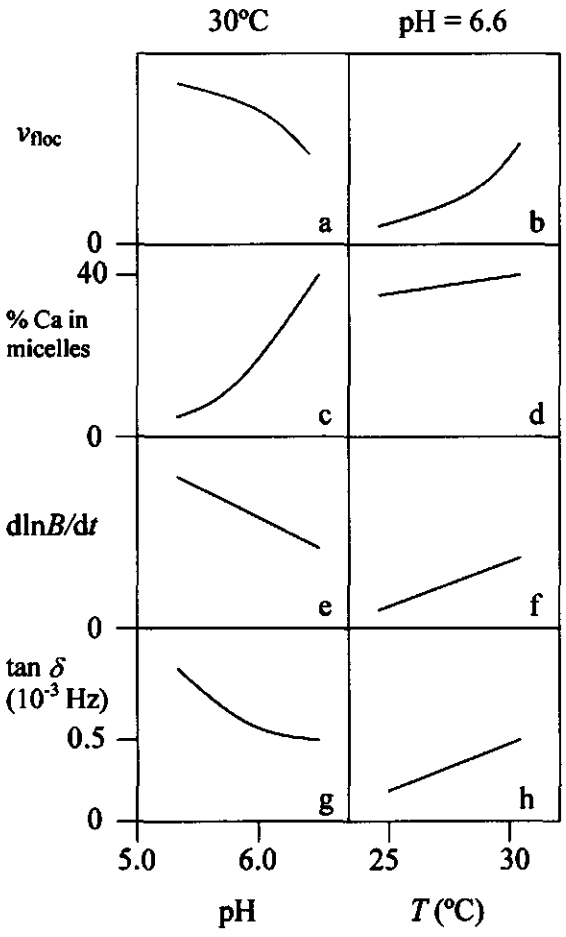

Figure 5.5: The effect of pH (left-hand side) and temperature (right-hand side) on

(a-b) the rate of flocculation of paracasein micelles,

(c-d) percentage of calcium in the micelles,

(e-f) rate of change of the permeability, and

(g-h) the loss tangent characterizing the gel (frequency = 10^{-3} Hz).

The most important link that seems to be missing is how the dynamic macroscopic gel properties are determined by the properties of the micelles. The effect of some micellar properties on the fractal structure of rennet-induced casein gels, as a function of pH and T, was briefly discussed before [21]. In that paper it was mentioned, in short, that at low pH the dissolution of CCP seems to have a large effect on the liquid-like behaviour (i.e. the value of tan δ, see figure 5.5g and 5.6), and consequently micellar fusion processes, which eventually led to an increased rate of syneresis. At high T the rate of syneresis was also increased. However, the effect was less in the range studied and the underlying mechanism seemed more complicated. At high T hydrophobic interactions are stronger, which in principle leads to a stronger driving force for particle fusion.

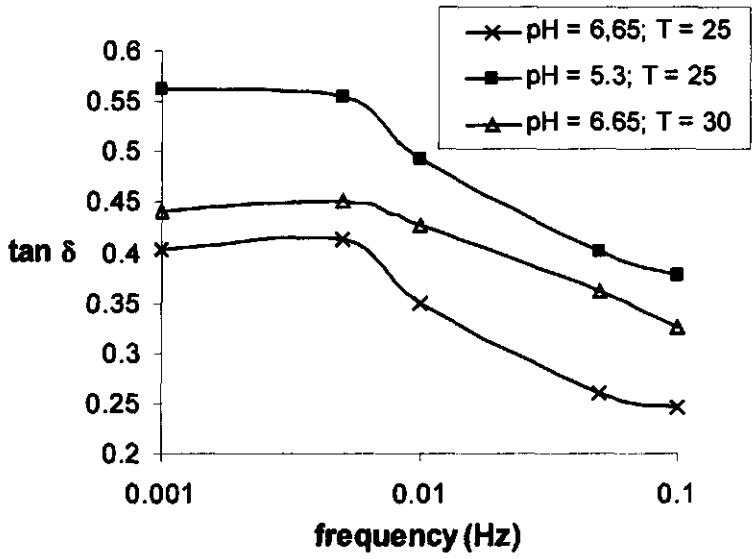

Figure 5.6: Parameter tan δ as a function of frequency for rennet-induced casein gels. Temperature and pH as given in the legend.

It can be concluded that the central aspects in the prediction of the rate of rearrangements are the (adhesion) forces in micellar junctions and, related to that, the degree of liquid behaviour of the casein. As a function of pH, the liquid behaviour of the casein depends mainly on the form and distribution of calcium.

Interestingly, tan δ is independent of the ageing time for rennet-induced casein gels at any pH or T (results not shown; this was also concluded in ref. [43]). This confirms that tan δ is determined by the structure of the casein junctions or bonds at a molecular scale, and not by rearrangements. In

figure 5.6 tan δ is presented as a function of frequency, at the conditions (pH, T) given in the legend. The figure confirms figure 5.5g [43] that in general tan δ is higher at a lower pH and a higher T. Rearrangements will probably take place at a higher rate at these conditions, because (sub-)particles have a higher mobility due to lower bond energies. Note that tan δ does not indicate change, but the conditions that promote it.

At incipient gelation ($\sim t_{gel}$) the structural characteristics (α, a_α) of the gels are very similar for all conditions (pH, T). This is in accordance with observations by confocal microscopy [21] and means that, although rearrangements can take place before gelation (esp. type B), there are no significant differences within the ranges of pH and T studied.

At a first glance, the effects of pH and T on the processes *after* gelation are as follows: from the rheological data presented above (figure 5.2) it is clear that a low pH leads to a faster rate of the ageing during the whole ageing process. The effect of a higher T is the same, but less pronounced over the range studied. There is no significant effect of T on γ_0. From the application of the scaling model (see figures 5.4a and b), it was concluded that at low pH, a large increase in the size of the compact building blocks with time occurred. At high T, there was no effect except after long times, when a significant increase of α or a decrease of a_α with T was observed.

Below, a detailed discussion of the processes ocurring after gelation is given. The effect of the pH will be discussed first. The parameter tan δ is much higher at a lower pH (figure 5.5g) because of calcium phosphate having left the micelles (figure 5.5c). Consequently, the rate of rearrangements of type A and/or B would be higher. This is particularly clear from the considerable increase of a_{eff} at low pH. It leads to a higher rate of increase of G' and can also lead to a decrease of γ_0, because of the formation of larger rigid structures. As mentioned earlier, a subsequent effect can be expected from rearrangement of type C (strand straightening and fracture, increase of pore size) resulting from these local compactifications. Straightening of strands will cause G' to increase and γ_0 to decrease. Spontaneous breaking of strands would explain the rather early occurring decrease in G' at low pH and makes the observed strong increase in a_{eff} possible. The considerable increase in pore size, and hence of permeability (ref.[21] and figure 5.5e), at low pH and late time stages is probably mainly caused by strand breaking, and allows syneresis to occur (rearrangement of type D).

Taking into account that a tenfold lower concentration of rennet was used at low pH, the effect of pH on the initial rate of increase of G' is much stronger than that of temperature (in the ranges studied). This is probably due to a higher affinity of the main active component on rennet (chymosin) for the micelles and greater affinity between the micelles, leading to a higher rate of flocculation at low pH (figure 5.5a).

We now discuss the effect of the temperature on ageing. The value of γ_0 did not vary with temperature in figure 5.2b. This means that variation in tan δ can not quantitatively explain the results for the range studied. With respect to γ_0: there is possibly a combination of factors like tan δ and the thickness of the strands [19]. With respect to G': because the building blocks of the gel will be smaller (supported by the lower value of a_α at high T, see figure 5.4b), the volume fraction of particles decreases and G' would also be smaller. However, figure 5.2a shows that as long as the gel has not fully developed (early stages of gel ageing), G' is larger at high T. This is probably caused by the stronger hydrophobic interactions at higher T [44] and therewith stronger interactions between the casein molecules, which can increase the driving force for rearrangements of type A and B.

From figure 5.5 it is clear that the effects of an increasing T are similar to decreasing pH, though less pronounced. In order to obtain measurable changes with T in terms of γ_0 or a_{eff}, it may be necessary to increase the range of temperatures studied. In the range of 32-40 °C, Lagoueyte *et al.* [14] found significant effects of temperature on the structure of rennet-induced casein gels, as determined by scanning electron microscopy. At 40 °C, the micelles fused together faster and clusters became denser, resulting in a more open structure with increased permeability.

In our data, the clearest effect of the temperature is the decrease or levelling off of G' occuring earlier at higher T. With confocal microscopy [45,21], at pH = 6.65 straight strands are mostly observed at longer ageing times, and they appear to be more frequent and thinner at a higher T.

5.5.5 Analysis of cryo-SEM images

In figures 5.7a en 5.7b electron micrographs are shown of the gel stucture. From a comparison of figure 5.7a with confocal micrographs [21] we can conclude that the largest whitish particulate material is casein. As a result of the high amount of dissolved molecules in the whey, some fine-grained network is visible in between the casein network. From the minor open areas (cracks) close to the casein network it is clear that etching (which essentially involves a drying process) leads to shrinkage of the casein.

Figure 5.7b is a small section of a compact area of the gel structure after considerable ageing. In this image provides further proof for the occurrence of partial particle fusion: even though the original positions of the separate particles may still be distinguished in some cases, the casein matrix appears very smooth. Interestingly, (especially at low pH) the particles themselves also appear very smooth. Possibly the limit of resolution is not good enough to show sub-micellar structures.

(a)

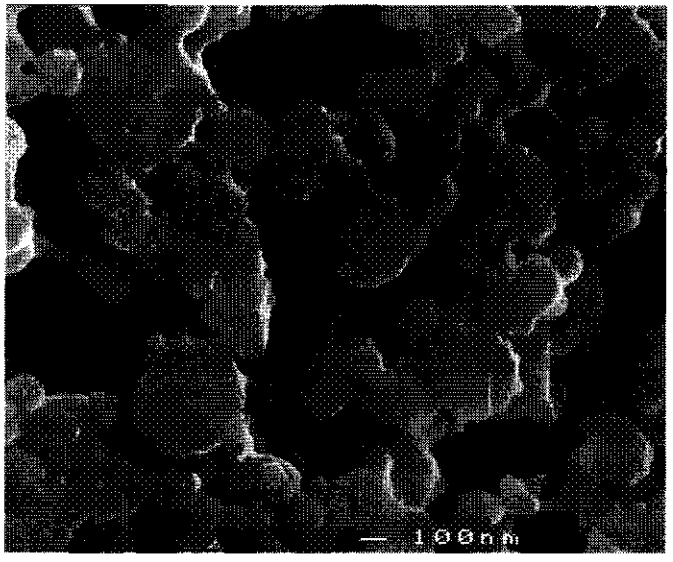

(b)

Figure 5.7: Cryo-SEM images of freeze-fractured rennet-induced casein gels at pH 5.3, after 10 min of etching. (**a**) typical overview of general gel structure, time after rennet addition = 15 ks, and (**b**) part of a compact section of the gel structure, time after rennet addition = 30 ks.

5.5.6 Tuning of rearrangements

In this paper, the relative importance of all various types of rearrangements (particularly as a function of pH) and their mutual relationship are identified. The newly gained knowledge will make it easier to find more ways to 'tune' the rate of specific types of the rearrangements by other means than by the pH.

It was shown that by enzymatic crosslinking of milk proteins [46], high pressure treatment [47], or addition of minor amounts of $CaCl_2$ [43] or ethanol [48] to skim milk, the gel strength of rennet-induced casein gels was increased and syneresis was reduced. In at least three of these cases (enzymatic crosslinking, calcium and ethanol), this can presumably be explained by an increased casein-casein affinity without increased particle fusion. High pressure treatment fragments casein micelles into smaller and more compact particles that form gels built from structures that are more cross-linked. Similar (straight-strand) structures are found in acid casein gels made from preheated milk [49,50]. As expected, these gels also have a higher G'.

5.6 Conclusions

The changes in structure and rheology of rennet-induced casein gels during ageing, can be explained in terms of specific rearrangements. Several types of rearrangements are distinguished, occurring at different time- and length scales.

Application of a (fractal) scaling analysis to rheological data confirmed earlier results from microscopy and permeability: the increase of the compact building blocks during ageing and the presence of straight strands. The short-range compactification is probably caused by two sub-types of rearrangements closely related to each other: micellar fusion and bond reversibility. In this respect, the particle fusion is greatly enhanced by breakage of strands. The partial micellar fusion effects were observed by SEM. These two types of rearrangements cause an increase of junction energy and, indirectly, some stretching of strands of micelles. In turn, this causes an increase of G'.

Rearrangements at the level of the pores and the strands can directly be observed as an increase in permeability and as the formation of straight strands in the micrographs. This latter observation also follows from the strong decrease in the value of the maximum linear strain during ageing. Syneresis is a final result of the 'transient' character of the gel structure. The prelude to perceptible syneresis is the increase in the size of the compact

building blocks and large-scale disappearance of strands. Both result in a disappearance of fractal structures and the latter also results in a decrease in storage modulus.

All types of rearrangements occur much faster at a low pH (5.3 as compared to 6.65), and slightly faster at high temperature (30 as compared to 25 °C). This can be understood from the change in the properties of the casein micelles as a function of pH and temperature. The large effect of a low pH can be explained by dissolution of colloidal calcium phosphate, a subsequent increase in liquid behaviour of the micellar material, and thereby (due to yielding/flow) to an increase of micellar fusion and to a decrease in strand thickness. As a function of pH, there appears to be a correlation between the value of tan δ and the rates of the rearrangements.

5.7 References

[1] Walstra, P. In *Cheese: Chemistry, Physics and Microbiology 1*; Fox, P. F., Ed.; Chapman & Hall: London, 1993.
[2] Dalgleish, D. G., *J Dairy Sci* **81**, 3013, (1998)
[3] Horne, D. S., *Int Dairy J* **8**, 171, (1998)
[4] Walstra, P., *Int Dairy J* **9**, 189, (1999)
[5] Shih, W. Y.; Aksay, I. A.; Kikuchi, R., *Phys Rev A* **36**, 5015, (1987)
[6] Bos, M. T. A.; van Opheusden, J. H. J., *Phys Rev E* **53**, 5044, (1996)
[7] Poon, W. C. K.; Haw, M. D., *Adv Coll Interf Sci* **73**, 71, (1997)
[8] Lodge, J. F. M.; Heyes, D. M., *J Chem Phys* **109**, 7567, (1998)
[9] Meakin, P.; Jullien, R., *J Physique* **46**, 1543, (1985)
[10] Meakin, P.; Jullien, R., *J Chem Phys* **89**, 246, (1988)
[11] van Garderen, H. F.; Dokter, W. H.; Beelen, T. P. M.; van Santen, R. A.; Pantos, E.; Michels, M. A. J.; Hilbers, P. A. J., *J Chem Phys* **102**, 480, (1995)
[12] this thesis, chapter 2
[13] van Vliet, T.; Lucey, J. A.; Grolle, K.; Walstra, P. In *Food Colloids; Proteins, Lipids and Polysaccharides*; Dickinson, E., Bergenståhl, B., Eds.; Royal Society of Chemistry: Cambridge, 1997.
[14] Lagoueyte, N.; Lablee, J.; Lagaude, A.; Tarado de la Fuente, B., *J Food Sci* **59**, 956, (1994)
[15] Lopez, M. B.; Lomholt, S. B.; Qvist, K. B., *Int Dairy J* **8**, 289, (1998)
[16] van Vliet, T.; van Dijk, H. J. M.; Zoon, P.; Walstra, P., *Coll Polym Sci* **269**, 620, (1991)
[17] Scherer, G. W., *Langmuir* **12**, 1108, (1996)
[18] van Santen, R. A.; Beelen, T. P. M.; van Garderen, H. F.; Dokter, W. H.; Pantos, E., *Nucl Instr Meth Phys Res B* **97**, 231, (1995)
[19] this thesis, chapter 4

[20] Arshad, M.; Paulsson, M.; Dejmek, P., *J Dairy Sci* **76**, 3310, (1993)
[21] this thesis, chapter 3
[22] Bremer, L. G. B. , PhD Thesis, Wageningen Agricultural University, 1992.
[23] Tirado-Miranda, M.; Schmitt, A.; Callajas-Fernández, J.; Fernández-Barbero, A., *Langmuir* **15**, 3437, (1999)
[24] Weber, A. P.; Baltensperger, U.; Gäggeler, H. W.; Schmidt-Ott, A., *J Aerosol Sci* **27**, 915, (1996)
[25] Tandon, P.; Rosner, D. E., *J Coll Interf Sci* **213**, 273, (1999)
[26] Kumagai, H.; Matsunaga, T.; Hagiwara, T., *Biosci Biotech Biochem* **63**, 223, (1999)
[27] Bijsterbosch, B. H.; Bos, M. T. A.; Dickinson, E.; van Opheusden, J. H. J.; Walstra, P., *Faraday Discuss* **101**, 51, (1995)
[28] Yang, G.; Biswas, P., *J Coll Interf Sci* **211**, 142, (1999)
[29] Horne, D. S., *J Chim Phys* **93**, 977, (1996)
[30] Fox, P. F.; Law, J.; McSweeney, P. L. H.; Wallace, J. In *Cheese: chemistry, physics and microbiology*; Fox, P. F., Ed.; Chapman & Hall:, 1993.
[31] Kantor, Y.; Webman, I., *Phys Rev Lett* **52**, 1891, (1984)
[32] Bremer, L. G. B.; van Vliet, T.; Walstra, P., *J Chem Soc Faraday Trans 1* **85**, 3359, (1989)
[33] Bos, M. T. A. , PhD Thesis, Wageningen Agricultural University, 1997.
[34] Knoop, A.-M.; Peters, K.-H., *Kieler Milchwirtschaftliche Forschungsberichte* **27**, 315, (1975)
[35] Roefs, S. P. F. M.; van Vliet, T.; van den Bijgaart, H. J. C. M.; de Groot-Mostert, A. E. A.; Walstra, P., *Neth Milk Dairy J* **44**, 159, (1990)
[36] Holt, C.; Horne, D. S., *Neth Milk Dairy J* **50**, 85, (1996)
[37] Kruyt, H. R.; van Klooster, H. S. *Colloids*; John Wiley & Sons: New York, 1927.
[38] Walstra, P., *J Dairy Res* **46**, 317, (1979)
[39] Mellema, M.; Leermakers, F. A. M.; de Kruif, C. G., *Langmuir* **15**, 6304, (1999)
[40] van Hooydonk, A. C. M. , PhD Thesis, Wageningen Agricultural University, 1987.
[41] van Dijk, H. J. M.; Walstra, P., *Neth Milk Dairy J* **40**, 3, (1986)
[42] Walstra, P.; van Vliet, T., *Neth Milk Dairy J* **40**, 241, (1986)
[43] Zoon, P.; van Vliet, T.; Walstra, P., *Neth Milk Dairy J* **42**, 249-312 and 43:17-52, (1988 and 1989)
[44] Walstra, P., *J Dairy Sci* **73**, 1965, (1990)
[45] Auty, M. A. E.; Fenelon, M. A.; Guinee, T. P.; Mullins, C.; Mulvihill, D. M., *Scanning* **21**, 299, (1999)
[46] Lorenzen, P. C.; Mautner, A.; Schlimme, E., *Kieler Milchwirtschaftliche Forschungsberichte* **51**, 89, (1999)

[47] Brooker, B. E.; Ferragut, V.; Gill, A. L.; Stenning, R. A.; Needs, E. C. In *Fresh Novel Foods by High Pressure*, 1998; Vol. 186.
[48] Renault, C.; Gastaldi, E.; Lagaude, A.; Cuq, J. L.; Tarodo de la Fuente, B., *J Food Sci* **62**, 907, (1997)
[49] van Vliet, T.; Keetels, C. J. A. M., *Neth Milk Dairy J* **49**, 27, (1995)
[50] Lucey, J. A.; Tet Teo, C.; Munro, P. A.; Singh, H., *Food Hydrocoll* **12**, 159, (1998)

Chapter 6

Summary

Most gels are elastic or viscoelastic materials that will either break or flow under large stresses. Their properties can be ascribed to their microstructure: gels are built of a continuous network (or 'matrix') of polymers (polymer gel) or particles (particle gel), interspaced with liquid. The particles are usually 'colloidal' particles, *i.e.* larger than molecules, but smaller than about 1 μm.

This thesis primarily concerns casein gels made of skim milk. Skim milk is milk without milk fat. Casein gels are built of particles called casein micelles, and an aqueous solution (whey). Casein micelles consist of casein molecules, calciumphosphate and water. It is useful to consider casein gels to be particle gels, albeit that the particles are built of casein -*i.e.* protein-molecules, and are therefore not invariable. There are several types of casein molecules, all of which are typically non-globular proteins.

The casein micelles give skim milk its white appearance. The dispersion is stabilized by the special properties of the outer part of the micelles, which is high in κ-casein. The hydrophilic parts of the κ-casein molecules protrude into solution, thereby forming a 'hairy layer'. The hairs account for the steric and electrostatic repulsion between micelles. Only if the properties of the hairs are affected, the micelles will aggregate.

The casein gels studied in this thesis have been made by adding rennet to the skim milk. Rennet contains enzymes from the stomach of a calf, of which especially chymosin is capable of cutting the κ-casein in such a way that the hydrophilic hairs are removed. At sufficient calcium ion activity, the micelles will subsequently aggregate. In other words, the chymosin 'activates' the micelles. However, the rate of aggregation that results from this activity is also influenced by e.g. pH, temperature and calcium ion activity.

Conditions like pH, temperature and calcium activity also affect the structure of the gel matrix that is formed, and thereby the long-term stability or ageing behaviour of the gels. Ageing of casein gels eventually leads to separation of the casein and the whey into separate 'phases', a process called 'syneresis'. During this process the number of micelle-micelle contacts is increased. Syneresis is an important process, because the resulting firm and compact casein-rich material (curd) is used in the manufacture of cheese.

During ageing, various types of structural changes take place at various length and time scales. These 'rearrangements' affect the rheological properties of the casein gels, and also the syneresis. Knowledge of the rheological properties of foods (*e.g.* in relation to syneresis), is of general importance for food industry in relation to processing conditions, and to stability and eating quality of the food.

Important rheological parameters are the storage modulus, loss modulus, maximum linear strain and yield stress. The former two parameters are a measure of the elastic and viscous properties of a material at small

deformation, respectively. The latter two parameters are a measure of how weak or brittle the material is (large-deformation properties).

Determination of structural properties during ageing of particle gels is not straightforward. Rearrangements of various types have to be considered. As a first approximation, a gel is a packing of tenuous aggregates. However, the particles may fuse or roll over each other, leading to formation of aggregates that are more compact. As a result, pores in the gel may grow and strands of particles connecting the aggregates may be stretched. The average pore size can directly be measured by permeability experiments. However, the presence or size of the other structural elements mentioned can only be determined indirectly. Application of a fractal approximation in simulations, or on microscopical or rheological results, then can be very useful.

Fractals are geometrical structures that are self-similar, independent of scale. That implies that they look the same when viewed at various magnifications. This property is called 'scale invariance'. Fractals can be completely regular (deterministic fractals) or unregular (stochastic fractals), as long as the scale invariance is maintained. Aggregates of colloidal particles are often fractal. This implies that the density of particles in such an aggregate is smaller for larger aggregates. In addition, the scaling relation between the particle number density of the aggregate and the aggregate radius, has a constant exponent. This exponent is called the 'fractal dimensionality', and is always smaller than the Euclidian dimensionality of three. Of course, in real life the scaling does not apply to infinitely small or large aggregates. The so-called fractal 'regime' only applies within certain length scales. This regime is bounded by a lower and upper cut-off length, called the compact building block size and the correlation length, respectively. The size of the compact building blocks can be several particle radii, and the correlation length is similar to the radius of the aggregate.

A gel matrix can also have fractal features. It was shown by Bremer in 1989 that this is true for casein gels. In a freshly formed gel, the correlation length is similar to the average radius of the aggregates that have filled the available space, *i.e.* formed a continuous network.

In the broadest sense, this thesis deals with the changes taking place in particle dispersions from the onset of aggregation, to the gel formation, to the visible signs of syneresis. Emphasis is on the structural changes between gelation and visible signs of syneresis of rennet-induced casein gels. The purpose of each chapter is to determine what interactions between colloidal particles lead to structures similar to fresh rennet-induced casein gels (chapter 2), what changes in structure and rheology of rennet-induced casein gels take place after gelation (chapters 3, 4 and 5), what specific structural properties affect the rheology of particle gels like rennet-induced casein gels (chapter 4),

and why and how the observed changes in structure and rheology are affected by pH and temperature (chapters 3 and 5).

In **chapter 2** the relation between particle interactions and gel structure is studied by computer simulations. The specific simulation technique is called 'Brownian dynamics'. Aggregation resulting from Brownian motion is called perikinetic aggregation.

A typical simulation involves the computer creating a three dimensional box with an intermediate volume fraction (3-10 vol%) of spherical particles. The description of the random movement of each particle and the interactions between the particles is given by an algorithm based on the Langevin equation for Brownian motion. After definition of specific parameters (temperature, particle interactions, volume fraction of particles *etc.*), the computer will calculate the structure of the aggregates and subsequently of the gel. This structure is given in terms of particle positions, which was analysed using fractal theory. This involved determination of the values of the fractal dimensionality and the correlation length.

The interactions incorporated in our simulation model were as follows: a weak long-range repulsion combined with a strong short-range attraction. Thus, upon encountering another particle, a particle can be repelled by the repulsive barrier, or cross the barrier and be permanently ('irreversibly') attached. The rate of particle encounters depends on the volume fraction of particles in the dispersion. The chance of bonding upon a particle encounter depends on the strength and width of the repulsive barrier. We found that the degree of stickiness can conveniently be quantified by the 'Fuchs ratio'.

Simulations performed by Meakin at the end of the 1980s, showed a systematic relation between stickiness and the value of the fractal dimensionality of the aggregates eventually formed. This observation was confirmed and the exact relation was identified. If aggregation is strongly delayed by a long-range repulsive barrier, a fractal dimensionality of 2.2-2.4 is obtained. In addition, there is a systematic relation between the Fuchs ratio and the fractal dimensionality and the correlation length (both parameters increase with a decrease in stickiness). Interestingly, the value of the fractal dimensionality was little dependent on the shape of the interaction potential curve, or on the volume fraction of particles. In general, comparison of the simulation results with experimental data shows that delayed and irreversible aggregation in the simulation model results in an accurate discription of rennet-induced aggregation in skim milk.

In **chapter 3** results are presented of the application of microscopy and permeametry to rennet-induced casein gels. The emphasis is on the determination of the fractal structure of the gel matrix as a function of time (0-25 hours), pH (5.3, 6.0 and 6.65), and temperature (20, 25 and 30°C). Gels with a lower pH value than the physiological pH (6.65), were obtained by

addition of minor amounts of HCl to the skim milk, before addition of the rennet.

The gels were studied by confocal scanning laser microscopy in a fluorescent mode. It involves labelling of the casein with a fluorescent dye, and allows to look inside the gel without destroying it. The permeametry involves formation of a gel in a tube. The rate at which whey flows ('permeates') through the tube filled with the gel (due to gravity), yields a permeability coefficient. This coefficient gives information on the size of the pores in the gel.

To the results of the microscopy and permeametry, fractal analysis was performed. This involved determination of the values of the fractal dimensionality, average size of the compact building blocks and the correlation length. We observed that these fractal parameters (calculated from confocal micrographs), greatly depended on the 'gray scale cutoff parameter'. This parameter is a measure of the degree of 'noise' removed. This noise probably stems from a background signal caused by the presence of dye that is not attached to the casein. The procedure for choosing its value is not straightforward.

The results of the measurements and the fractal analysis were as follows. Freshly made gels have an initially constant value of fractal dimensionality (about 2.4) and compact building block size (about 0.5 μm), independent of pH or temperature. However, considerable changes were observed during ageing. Especially at low pH (= 5.3), a strong coarsening of the structure was observed; within 6 hours the fractal dimensionality apparently decreased to 1.7 and the compact building block size increased to 1.5 μm. In the confocal micrographs we saw thin, straight strands of casein connecting large compact lumps of casein (pH 6.65: late time stages, pH 5.3: early time stages). A strand is a relatively thin chain of micelles. Below we will explain the importance of this observation for the rheological properties of the gels. At low pH the disappearance of these strands marks the moment at which the structure can not be considered fractal anymore, because of the irrealistically low values of D_f and a drastic decrease in the size of the fractal regime.

These observations also apply to gels with higher pH values, though the changes are much less pronounced. At high pH, rearrangements take place at a much slower rate.

The structural differences between gels aged at different temperature were much smaller (in the temperature range studied).

Chapter 4 is a mainly theoretical chapter. Fractal scaling relations are presented that can be applied to results of rheometry, leading to further information about the structure of model particle gels. Use is made of results of measurements of the storage modulus, the maximum linear strain, and the

yield stress, as a function of volume fraction of casein particles (in the range of 5-9 vol%). The pH was 6.0 or 6.65 and the temperature 25°C; hence, only minor rearrangements would take place. The scaling theory presented predicts the relation between these rheological parameters and the volume fraction. An essential feature of the model is that the gel is assumed to be built of fractal aggregates, which means there is a relation between the aggregate size (part of the scaling model) and the volume fraction (known).

The rheological experiments were performed using a concentric cylinder technique. The gels were formed in the gap between the cylinders. The outer cylinder was rotated clockwise and anticlockwise in a sinusoidal fashion. This leads to a well-controlled shear deformation ('strain') of the gel. At the same time, the resulting stress on the inner cylinder was measured. The ratio between maximum stress and maximum strain yields the absolute vale of the modulus, and the phase shift between applied strain and resulting stress yields the loss tangent; from these parameters, the storage and loss modulus can be derived. The strain was increased stepwise to see at what strain the modulus starts to decrease. This strain is the maximum linear strain. To measure the yield stress a different setup was used. Instead of a known strain, a known stress was applied to the gel. The stress applied was increased gradually. The stress corresponding to the maximum value of the apparent viscosity (= stress / strain rate), would equal the yield stress.

From our model it appears that one mathematical framework can suffice to derive the appropriate scaling behaviour of at least five different types of gel structures (categories I-V). These are the strong and weak-link types of gel structures by Shih et al. (1990), and the fractal, hinged and straight strand types of structures by Bremer (1989-1992). In our model, only two parameters are different between these types of gels. These are the parameters ε (which depends on the dominant type of deformation of a strand; stretching or bending) and δ (which is a measure of the number of deformable bonds in a strand).

Application of the scaling model shows that rennet-induced casein gels contain straight, elastic stress-carrying strands (category IV). The fact that application to results obtained on all three rheological parameters leads to the same conclusion as to the gel category, shows the validity of the application of the fractal scaling model to rennet-induced casein gels at or around physiological pH and room temperature.

Chapter 5 specifically deals with mechanisms of rearrangement in rennet-induced casein gels. Results of rheometry are presented and compared to the results by simulations (chapter 2) and microscopy (chapter 3). In addition, the scaling model of chapter 4 is applied to results on the storage modulus as a function of pH, temperature, and *time*. Moreover, a short literature review on rearrangements and fractal structures is given, and a

model for rearrangements is presented. The discussion includes a section on the effect of pH and temperature on the properties of casein micelles in relation to the observed rearrangements.

The changes in rheological properties of rennet-induced casein gels after gel formation, include (a) increase, (b) levelling off, and (c) decrease of the storage modulus. Stage (a) is accompanied by a steep decrease of the maximum linear strain. Stage (c) goes along with syneresis. Interestingly, the ratio of the storage modulus to the loss modulus (the loss tangent) remains constant during ageing. Because the nature of the primary bonds involved would not change during ageing (temperature and chemical composition remain constant), this suggests that the value of the loss tangent is determined by the structure of the system at the molecular level.

By comparing the results to the confocal micrographs (chapter 3), and by application of the scaling model (chapter 4), a general overview of the relevant structural rearrangements is given. In chronological order: (a) is initially due to an increase of the number of junctions between particles, but this soon stops. Subsequently, it is mainly a result of particle fusion, which causes a strenghtening of the junctions. Both processes can result in local compactification and thereby to an increase in compact building block size. Also, stretching of strands takes place as a result of this local compactification. Stage (b) is partly because the particle fusion process is complete or slows down. Stages (b) and (c) are (further) due to the strands getting thinner, eventually breaking.

All rearrangements proceed substantially faster at low pH (5.3 vs. 6.65). This can be understood from the value of loss tangent being considerably higher at lower pH. As mentioned, this parameter would be a measure of the molecular interactions in the casein micelles. At low pH, it is known that colloidal calcium phosphate (CCP) leaves the micelles and goes into solution. The CCP is important for the integrity of the casein micelles. Dissolution of CCP may decrease resistance of the casein micelles against slow deformation, and subsequently to a higher value of the loss tangent (*i.e.* a more 'liquid-like' behaviour of the micelles), and to an increased rate of particle fusion.

The effect of temperature (20-30°C) is less pronounced and more difficult to explain. On the basis of the changes in rheological properties, we would expect a slight increase in rate of all types of rearrangements at higher temperature. This may be due to increased hydrophobic interactions, which are stronger at high temperature, leading to more compact micelles.

In short, this thesis deals with the relation between particle interactions, structure and rheology of particle gels, with special emphasis on

rennet-induced casein gels during ageing. Some important conclusions are following.

Irreversible aggregation that is strongly delayed by a repulsive barrier yields a high value of the fractal dimensionality, about 2.4. This dimensionality is derived from simulations and it is similar to the values found for freshly formed rennet-induced casein gels. Additional simulations showed that this value is almost independent of the shape of the interaction potential curve, the aggregation rate and the volume fraction of particles.

Ageing of rennet-induced casein gels is accompanied by structal rearrangements of the gel matrix: compact areas grow larger, and become connected by thin, straights strands. The fractal dimensionality of the gels decreases and the compact building block size increases. At low pH all rearrangements have a higher rate and lead to an early disappearance of fractal structures and syneresis. Syneresis is preceded by strand breakage, and probably a final consequence particle fusion. Methods to affect the rate of syneresis may therefore be altering the conditions that determine the structure at the molecular level.

Finally, exploratory models on the scaling and on the types of structural rearrangements of particle gels were developed. They were applied to results of rheometry, to evaluate the structure of the rennet-induced casein gels during ageing. However, they also constitute frameworks to describe the relation between structure and rheology, and the ageing behaviour of particle gels in general.

Samenvatting voor niet-vakgenoten

Dit onderdeel geeft een samenvatting van dit proefschrift, getiteld: ***'Schalingsrelaties tussen structuur en reologie van verouderende caseïne-deeltjesgelen'***. Allereerst zal de achtergrond van het onderzoek gegeven worden. Vervolgens wordt in één alinea de inhoud van het proefschrift omschreven. Ten slotte worden de belangrijkste conclusies per hoofdstuk gegeven.

Gelen zijn zachte, elastische materialen. Dit betekent dat ze (met de hand) vervormd kunnen worden, maar dat ze daarna weer de neiging hebben hun oude grootte of vorm aan te nemen. Afhankelijk van het type gel doet het dit laatste niet volledig: het vloeit dan een beetje en is dus in zekere mate 'visceus'. De meeste gelen hebben beide eigenschappen, en zijn dus 'visco-elastisch'.

De hiervoor genoemde eigenschappen zijn het gevolg van de speciale 'microstructuur' in een gel. Deze microstructuur is vaak een ijl netwerk van deeltjes door een vloeistof (zie figuur 2.7 op bladzijde 25). De deeltjes zijn meestal kolloidale deeltjes. Dit soort deeltjes zijn groter dan moleculen, maar niet of nauwelijks zichtbaar onder een gewone lichtmicroscoop. Dit proefschrift gaat voornamelijk over gelen gemaakt van melk, zgn. 'caseïnegelen'. Caseïnegelen zijn opgebouwd uit een ijl netwerk van caseïnedeeltjes (micellen) door een waterige vloeistof (wei). Caseïnemicellen zijn kolloïdale deeltjes.

Caseïne is het belangrijkste melkeiwit; melk bevat ongeveer 10 volume% aan caseïnemicellen. Bovendien is het wei is rijk aan melksuiker (lactose) en wei-eiwitten. Melk is vooral om deze reden een belangrijke bron van voeding voor jonge zoogdieren.

Caseïnemicellen zijn ongeveer 1/100.000-ste centimeter groot. Caseïnemoleculen zijn nog een factor 10 à 100 kleiner. De aanwezigheid van de micellen zorgt ervoor dat magere melk (ondermelk) wit is. Een micel bestaat uit een aantal verschillende caseïnemoleculen, calciumfosfaat en water (60%). Alle types caseïnemoleculen zijn erg lange moleculen (polymeren), opgebouwd uit aminozuren. Een bepaald type molecuul (κ-caseïne) bevindt zich voornamelijk aan het oppervlak van de micellen. De κ-caseïnemoleculen steken deels in de micel, en deels in de wei. De caseïnemicellen hebben dus een harig oppervlak. Indien twee verschillende micellen elkaar naderen, zitten ze de haren elkaar in de weg. Dit heeft tot gevolg dat de micellen elkaar afstoten. Hierdoor zullen micellen niet aan elkaar plakken, hetgeen nodig is om een aaneengesloten netwerk te krijgen. Melk is dus stabiel in de zin dat ze niet spontaan een gel vormt.

Indien melk instabiel is, plakken de micellen aan elkaar. Er zijn verschillende manieren om dit te bereiken; daar komen we in de volgende alinea's op terug. Het aan elkaar plakken van de kolloïdale deeltjes in het algemeen (of het klonteren van de oplossing) noemen we 'aggregatie'. Als aggregatie lang genoeg onverstoord kan voorduren, leidt dit uiteindelijk tot gelering.

Waaróm de caseïnes in de melk na opheffen van de afstoting (dus in afwezigheid van de harige laag) aggregeren, is nog een groot raadsel. De aantrekking tussen de deeltjes heeft waarschijnlijk iets te maken met speciale aminozuurvolgorde van bepaalde caseïnemoleculen, en de aanwezigheid van calcium-fosfaat complexen die als een soort 'lijm' werken tussen die moleculen.

De caseïnegelen beschreven in dit proefschrift, zijn gemaakt door stremsel toe te voegen aan de magere melk. Stremsel wordt gewonnen uit kalvermagen en bevat een enzym dat de hiervoor genoemde haren afknipt (zie figuur 1.2 op bladzijde 4). Hierdoor zal melk waar stremsel aan toegevoegd is, na enkele minuten tot een uur een gel vormen. Caseïnemicellen in melk kunnen ook aggregeren door toevoeging van melkzuurbacteriën. Dit gebeurt bijvoorbeeld tijdens de bereiding van yoghurt. Bij de bereiding van kwark worden zowel stremsel als melkzuurbacteriën aan de melk toegevoegd.

De snelheid van de aggregatie en de structuur van het uiteindelijke gevormde netwerk, hangen sterk af van bepaalde omstandigheden, zoals de wijze van destabilisatie, de zuurtegraad (pH) en de temperatuur. Dergelijke omstandigheden beïnvloeden bovendien de uiteindelijke levensduur van een gel. Indien caseïnegelen verouderen, leidt dit uiteindelijk tot de uitstoot (synerese) van wei uit het caseïnenetwerk, waardoor een stevige klont (wrongel) overblijft, rijk aan caseïne. Synerese is een belangrijk proces voor de zuivelindustrie, omdat de wrongel gebruikt wordt voor het maken van kaas. Als gevolg van de synerese gaan de paracaseïnemicellen (zo heten de caseïnemicellen na verwijdering van hun harige laag) zeer dicht tegen elkaar aan liggen (compactificatie).

Gedurende de veroudering vinden allerlei veranderingen in de structuur van het netwerk van caseïnemicellen ('gel-matrix') plaats. De snelheid van dergelijke 'herrangschikkingen' bepaalt de levensduur van het gel. De herrangschikkingen bepalen echter ook de visco-elastische eigenschappen van het gel. Alle eigenschappen die iets zeggen iets over het vervormings- en vloeigedrag (zoals visco-elasticiteit), noemen we reologische eigenschappen. Reologie is van groot belang voor de industrie. De reologische eigenschappen van levensmiddelen bepalen voor een groot deel de eigenschappen tijdens het maken, bewaren en eten van levensmiddelen.

Ruwweg twee types reologische eigenschappen kunnen onderscheiden worden: kleine- en grote vervormingseigenschappen. Voorbeelden van de eerste zijn de eerdergenoemde elasticiteit (maat voor

stevigheid bij kleine vervorming) en viscositeit (maat voor stroperigheid). Voorbeelden van de laatste zijn de maximale lineaire vervorming (maat voor brokkeligheid) en de zwichtspanning (maat voor sterkte bij grote vervorming).

Voor dit proefschrift is bij het meten van de reologische eigenschappen gebruik gemaakt van enkele 'reometers'. Een reometer bestaat doorgaans uit twee metalen cylinders die verschillen van grootte, waarbij de kleine *in* de grote hangt. In de ruimte tussen de twee cylinders wordt de melk gegoten waaraan stremsel is toegevoegd; de gelering vindt aldus plaats in deze ruimte. Tijdens de meting wordt de buitenste cylinder langzaam een beetje heen en weer gedraaid. Hierdoor komt op de binnenste cylinder een spanning te staan. Uit de relatie tussen de opgelegde draaiing van de buitenste cylinder en de gemeten spanning aan de buitenste cylinder, kunnen de reologische parameters berekend worden. Bijvoorbeeld: indien de gemeten spanning vrij groot is, is het gel stevig. Ander voorbeeld: indien de opgelegde draaiing langzaam opgevoerd wordt, kan gekeken worden wanneer de gemeten spanning minder toeneemt dan verwacht. Dit kan bijvoorbeeld doordat één streng van micellen in de matrix is gebroken. De mate van opgelegde draaiing die deze breuk teweeg brengt, heet de 'maximale lineaire vervorming'.

De veranderingen van de reologische eigenschappen tijdens de veroudering kunnen direct gemeten worden, maar het determineren van de daarmee gepaard gaande structurele herrangschikkingen is lastiger. Er zijn namelijk veel verschillende types herrangschikkingen. Sommige komen tot uiting in de reologische eigenschappen, sommige kunnen zichtbaar gemaakt worden met geavanceerde miscroscopie, sommige hebben geen direct meetbaar effect. Een belangrijke vraag voor het onderzoek beschreven in dit proefschrift was: 'welke herrangschikkingen zijn van belang voor de reologische eigenschappen en de snelheid van de synerese?'.

Een gel is vlak na vorming bij benadering een opeenstapeling van ijle aggregaten van deeltjes. Gedurende de veroudering kunnen (op kleine schaal) deeltjes over elkaar gaan rollen of samenvloeien. Op grote schaal heeft dit tot gevolg dat de matrix op bepaalde plaatsen compacter wordt (compacte bouwstenen groeien), en op andere plaatsen ijler (gaten groeien). Zolang de matrix nog een aaneengesloten netwerk is, heeft het compacter worden van de bouwstenen ook tot gevolg dat op de verbindingsstukken van compacte delen, strengen of ketens van deeltjes dunner en gestrekt worden. Het groeien van de gaten is direct meetbaar met behulp van 'permeametrie'. De aanwezigheid of de grootte van de andere types structuren (compacte bouwstenen, rechte strengen) kan slechts indirect bepaald worden. In dit proefschrift is het belangrijkste 'gereedschap' voor een dergelijke indirecte bepaling de 'fractale schalingstheorie'. Hierbij wordt het gehele caseïnenetwerk beschouwd als ware het opgebouwd uit fractalen.

Fractalen zijn vormen die er hetzelfde uit blijven zien, als ze vergroot of verkleind wordt. Dit heet 'schaal-invariantie'. De term 'fractaal' werd geïntroduceerd door de wiskundige Mandelbrot rond 1980. Fractalen kunnen zeer mooi regelmatig zijn, maar ook onregelmatig. Dit laatste type fractalen kan gevormd worden door chaotische processen zoals aggregatie van deeltjes. De dichtheid aan deeltjes in een fractaal aggregaat neemt af met de grootte van het aggregaat. Deze afname kan beschreven worden met een schalingsvergelijking, waarin de 'fractale dimensionaliteit' staat. Deze variabele kan gebruikt worden om een fractaal te karakteriseren.

Een perfecte fractaal bestaat alleen in theorie. De fractale schaling gaat niet op voor heel kleine of heel grote aggregaten, maar alleen binnen een bepaalde range ('regime') aan groottes. In een echt gel wordt het regime waarbinnen fractale schaling toegepast begrensd door een onder- en bovengrens. Alle structuren in het deeltjesnetwerk die qua grootte tussen deze twee lengteschalen invallen worden als fractaal beschouwd. De 'fractale dimensionaliteit' is een parameter die iets zegt over hoe de dichtheid aan deeltjes binnen dit regime schaalt met de afstand. Zowel de fractale dimensionaliteit als de grenzen van het fractale regime kunnen verschillen per gel.

De fractale theorie is wiskundig vrij ingewikkeld, en het gaat te ver om deze hier volledig te behandelen. Voor caseïnegelen is een van de belangrijkste aspecten van de theorie dat de onder- en de bovengrens van hiervoor genoemde lengteregime ongeveer zijn gelijk aan de grootte van, respectievelijk, de compacte bouwstenen en de gaten in het gel. Bovendien; een handig (verbeterd) aspect aan de fractale theorie zoals beschreven in dit proefschrift, is de incorporatie van parameters die iets zeggen over de mate gestrektheid en flexibiliteit van de strengen.

Dit proefschrift gaat met name over hoe en waarom bepaalde omstandigheden de structuur en reologie van kolloïdale deeltjesgelen beïnvloeden. Voor de bepaling hiervan, zijn zowel experimentele (microscopie, permeametrie en reometrie) als theoretische (computersimulaties en schalingstheorieën) onderzoeksmethoden ontwikkeld en/of toegepast. De beschreven resultaten kunnen vooral gebruikt worden bij het ontwikkelen van methodes om de verouderingseffecten van kolloïdale deeltjesgelen onder controle te krijgen. Opgemerkt moet worden dat vanwege de keuze voor het gebruik van caseïnegelen voor de experimenten, de meeste conclusies specifiek gelden voor deze gelen.

Hoofdstuk 1 is een algemene inleiding, en hoeft hier als zodanig niet besproken te worden.

In hoofdstuk 2 van het proefschrift is gebruik gemaakt van computersimulaties waarbij virtuele deeltjes in een virtuele omgeving

willekeurig bewegen. De simulatietechniek wordt 'Brownse dynamica' genoemd, omdat de deeltjes elkaar middels Brownse beweging ontmoeten alvorens ze aggregeren en uiteindelijk een gel vormen. Brownse beweging is de spontane, willekeurige beweging van (kolloïdale) deeltjes in een vloeistof of gas, doordat vloeistof of gasmoleculen tegen deze deeltjes aanbotsen. Het fenomeen is genoemd naar de plantenkundige Brown (†1858), die de beweging van pollen observeerde onder een microscoop. Wij hebben (gedeeltelijk zelf ontwikkelde) Brownse dynamica simulaties gebruikt om erachter te komen welke krachten ('interacties') nodig zijn tussen de deeltjes, om een bepaalde fractale structuur van het gel te verkrijgen. Indien de interacties of krachten sterk attractief zijn, worden de deeltjes heel 'plakkerig' genoemd en zullen ze snel aggregeren. Als ze repulsief, zijn ze dus niet plakkering. Er blijkt een systematisch verband te zijn tussen de mate van plakkerigheid en de fractale structuur van de uiteindelijk gevormde gelmatrix. Uit de resultaten van de simulaties kon afgeleid worden dat de 'echte' gelen (de melkgelen) waarschijnlijk gevormd zijn door aggregatie waarbij de de deeltjes elkaar meestal afstoten door de aanwezigheid van een repulsieve barrière. Met andere woorden: de micellen plakken na een ontmoeting maar zelden aan elkaar, maar áls ze plakken blijven ze ook definitief vastzitten. Het duurt dan wat langer voordat het gel gevormd wordt, maar het is wel vrij stabiel.

In hoofdstuk 3 is gebruik gemaakt van een modern soort lichtmicroscopie (confocale laser scanning microscopie), en permeametrie (waarbij de doorstroombaarheid van het gel met wei bepaald wordt). Met deze technieken kon de structuur van de melkgelen bepaald worden, zonder dat ze kapot gemaakt werden. Het blijkt dat de gelmatrix een fractale dimensionaliteit heeft van ongeveer 2.3, onafhankelijk van pH en temperatuur. De structuur van het gel verandert vooral bij lage pH sterk in de tijd over een periode van 24 uur na stremseltoevoeging. Dit blijkt ook te gelden voor de fractale eigenschappen van de gelstructuur. In de tijd worden de gaten in het netwerk groter en de caseïne hoopt zich locaal op. De compacte bouwstenen zijn vooral bij lage pH na 6 uur al zo groot (groter dan 1.5 μm), dat het fractale regime zo klein geworden is, dat de matrix nog nauwelijks als fractaal beschouwd kan worden. Een andere interessante observatie, die vooral van belang zal blijken te zijn in hoofdstuk 4, is de aanwezigheid van dunne, rechte strengen in de matrix tijdens veroudering.

In hoofdstuk 4 wordt voornamelijk theorie gepresenteerd. Door enkele bestaande modellen van wetenschappers uit de jaren tachtig te combineren in een nieuw overkoepelend model, is een eenduidig beeld verkregen van alle mogelijke structuren die deeltjesgelen kunnen hebben. Bij dit model wordt opnieuw uitgegaan van een structuur die gevormd is door fractale aggregatie. Door het model toe te passen op reologische metingen op

gestremde caseïnegelen, blijkt dat deze opgebouwd zijn uit rechte, maar flexibele strengen. Hiermee wordt duidelijk dat slechts een deel van de structuur (nl. die van de strengen, ook genoemd in hoofdstuk 3) de reologie van het systeem bepaalt. Toepassing van het model op verschillende types reologische metingen op dezelfde caseïnegelen, leidt tot dezelfde conclusies over de structuur, hetgeen de toepasbaarheid van het schalingmodel ondersteunt.

In hoofdstuk 5 wordt opnieuw de theorie uit hoofdstuk 4 toegepast, maar nu op reologische metingen als functie van de tijd. Bovendien wordt een nieuw, exploratief model gepresenteerd over herrangschikkingen in deeltjesgelen, gevormd door fractale aggregatie. We onderscheiden in het model vier basistypes herrangschikkingen: deeltjesfusie, rollen van deeltjes over elkaar, recht trekken van strengen (en groeien van gaten) en synerese (zie figuur 5.1 op bladzijde 98). De modelvorming is geïnspireerd op eigen metingen, maar ook op bestaande literatuur over vergelijkbare systemen. Door toepassing van het schalingsmodel uit hoofdstuk 4 wordt via een andere weg vergelijkbare informatie verkregen over de genoemde structurele herrangschikkingen. Het blijkt opnieuw dat herrangschikkingen gepaard gaan met een toename van de grofheid van de matrix (groei van compacte bouwstenen en gaten = locale verdichting) en dat verlaging van de pH deze herrangschikkingen versnelt. Deze overeenstemming met de resultaten van hoofdstuk 3, is een extra ondersteuning van de toepasbaarheid van het fractale schalingsmodel. Reologische metingen tonen aan dat gestremde caseïnegelen eerst steviger maar wel brokkeliger, en vervolgens slapper worden. Door analyse van reologische metingen aan de hand van het herrangschikkingsmodel, blijkt dat een van de belangrijkste types herrangschikkingen het langzaam samenvloeien van caseïnemicellen tot grotere deeltjes is. Waarschijnlijk is dit een belangrijke oorzaak van het optreden van twee van de andere drie genoemde herrangschikkingen. Het verklaart ook de toename in stevigheid en brokkeligheid. De afname van de stevigheid wordt veroorzaakt door het breken van (rechtgetrokken) strengen. Dit wordt indirect veroorzaakt door locale verdichting, en misschien dus ook gedeeltelijk door het samenvloeien van micellen. Het samenvloeien komt waarschijnlijk doordat de caseïnemicellen zélf bij lage pH enigszins vloeibaar zijn en dus langzaam kunnen vervormen.

Hoofdstuk 6 is de Engelstalige samenvatting. Deze is uitgebreider en gaat wat dieper op de resultaten per hoofdstuk in dan deze samenvatting.

Deze samenvatting is geschreven door:
Michel Mellema & Ivonne Amelia Moor.

List of publications

Articles in refereed journals (based on MSc theses)

- Bijsterbosch, H.D.; de Haan, V.O.; de Graaf, A.W.; Mellema, M.; Leermakers, F.A.M.; Cohen Stuart, M.A. and van Well, A.A., 'Tethered adsorbing chains: neutron reflectivity and surface pressure of spread diblock copolymer monolayers', *Langmuir*, 11 (11), 4467-4473 (1995).
- Mellema, M.; Clark, D.C.; Husband, F.A. and Mackie, A.R., 'Properties of β-casein at the air/water interface as supported by surface rheological measurements', *Langmuir*, 14 (7), 1753-1758 (1998).
- Mellema, M.; Leermakers, F.A.M. and de Kruif, C.G., 'Molecular mechanism of the renneting process of skim milk examined by viscosity and light scattering experiments and simulated by model SCF calculations', *Langmuir*, 15 (19), 6304-6313 (1999).

Articles in conference proceedings (based on PhD thesis)

- Mellema, M.; van Opheusden, J.H.J. and van Vliet, T., 'Brownian dynamics simulation of colloidal aggregation and gelation' in *Food Emulsions and Foams: Interfaces, Interactions and Stability*, Royal Society of Chemistry, Cambridge, 176-191 (1999).
- van Vliet, T. and Mellema, M., 'Structure and rheology of particle gels, a dynamic interplay' in *Proceedings of the 2nd ISFRS*, ETH Zürich, 33-39 (2000).
- Mellema, M.; van Vliet, T. and van Opheusden, J.H.J., 'Microstructural rearrangements affecting the rheology of rennet-induced casein gels' in *Proceedings of the 2nd ISFRS*, ETH Zürich, 181-185 (2000).

Articles in refereed journals (based on PhD thesis)

- **(Chapter 2)** Mellema, M.; van Opheusden, J.H.J. and van Vliet, T., 'Relating colloidal particle interactions to gel structure using Brownian dynamics simulations and the Fuchs stability ratio' *J Chem Phys*, 111 (13), 6129-6135 (1999).
- **(Chapter 3)** Mellema, M.; Heesakkers, J.W.M.; van Opheusden, J.H.J. and van Vliet, T., 'Structure and scaling behavior of aging rennet-induced casein gels examined by confocal microscopy and permeametry', *Langmuir*, 16 (17), 6847-6854 (2000)
- **(Chapter 4)** Mellema, M.; van Opheusden, J.H.J. and van Vliet, T., 'Categorization of rheological scaling models for particle gels, applied to rennet-induced casein particle gels', submitted.
- **(Chapter 5)** Mellema, M.; Walstra, P.; van Opheusden, J.H.J and van Vliet, T., 'Effects of structural rearrangements on the rheology of rennet-induced casein particle gels', in preparation.

Levensloop

De schrijver van dit proefschrift werd geboren te Losser op zaterdag 7 april 1973. Hij behaalde in juni 1991 zijn Atheneum diploma aan het Thijcollege te Oldenzaal, waarna hij met de studie Moleculaire Wetenschappen begon aan de Landbouwuniversiteit Wageningen. Hij studeerde in september 1996 af bij de vakgroep Fysische Chemie en Kolloïdkunde.

Van oktober 1996 tot en met juli 2000 was hij werkzaam als Assistent In Opleiding bij de leerstoel Fysica en Fysische Chemie van Levensmiddelen aan de (inmiddels) Wageningen Universiteit. Hieruit is dit proefschrift voortgekomen.

Sinds augustus 2000 is hij werkzaam bij Unilever Research Vlaardingen.

Dankwoord

Graag wil ik iedereen bedanken die mee heeft geholpen bij de totstandkoming van dit proefschrift. Allereerst gaat mijn dank uit aan de promotiecommissie: Pieter Walstra, Erik van der Linden, Joost van Opheusden en Ton van Vliet. Ton, je hebt belangrijke sturing gegeven aan de richting van mijn werk. Joost, de soms intense discussies met jou hebben erg bijgedragen aan de scherpte van mijn werk. Pieter, ik heb veel van je geleerd over de complexiteit van caseïnemicellen. Bovendien hebben je correcties veel bijgedragen aan de leesbaarheid van het proefschrift. Erik, bedankt voor je 'waar zijn wij nou helemaal mee bezig?'. Deze vraag wordt namelijk nog altijd te weinig gesteld bij promotieonderzoeken.

I would like to thank all those involved in the EU FAIR CT-1216 project. In particular I would like to acknowledge the cooperations with the scientists from Leeds (Eric Dickinson and coworkers), Gothenburg (Anne-Marie Hermansson and coworkers) and Ayr (David Horne and coworkers).

Ook de 'Nederlandse begeleidingscommissie' wil ik bedanken voor hun (vrijwillige) tijd en aandacht. Deze groep bestond naast mijn promotiecommissie uit: Wim Agterof, Leon Bremer, Martien Cohen Stuart en Dirk van den Ende.

Er is behoorlijk wat experimenteel werk verricht in het kader van mijn project. Dit is vooral uitgevoerd door drie mensen: Katja Grolle, Marijke Edelman en Jan-Willem Heesakkers. Katja, ik denk dat we een goed team vormden. Marijke, jij was mijn eerste en enige student en hebt een belangrijke rol gespeeld bij de eerste verkenningen van de reologie. Jan-Willem, de grote hoeveelheid aan confocale microscopieplaatjes die je bij me achter hebt gelaten, heeft ons uiteindelijk weer een publicatie opgeleverd.

Experimentele hulp heb ik verder gehad van Wim van Veenendaal (confocale microscopie), Johan Hazekamp (invriezen SEM samples), Adriaan van Aelst (cryo-SEM) en Erik ten Grotenhuis (DWS). Allemaal bedankt.

Op de vakgroep/sectie/leerstoel/divisie/lab heb ik een heel gezellige tijd gehad. Dit heb ik aan velen te danken; het is onmogelijk om iedereen bij naam te noemen. 'Het netwerk ligt weer plat', bioscoopfilms, botstests, koffie en alle andere belangrijke zaken des levens hebben de revue gepasseerd. Een speciale vermelding verdienen al mijn (oud-)kamergenoten, waarvan Arne het het langst heeft volgehouden.

Rest mij mijn directe familie en vrienden te bedanken voor hun belangrijke morele steun op de achtergrond. Ik kon altijd bij ze terecht om te vertellen dat ik een succesje had of om wat te klagen als het minder ging. Enkele namen wil ik speciaal noemen: Jorrit, misschien komt het allemaal wel door jou. Sophie, door jouw kaft is mijn boekje ook een beetje een kunstwerk geworden. Stefan, binnenkort ben ik uiteraard bij jouw promotie.

Tot slot: lieve Ivonne, bedankt dat je trots op me bent. Hierdoor kan ik terugkijken én vooruitkijken op een prachtige tijd.

Michel.